3-14-2007

Damage Detection Using Lamb Waves for Structural Health Monitoring

Jeffrey S. Crider II

DAMAGE DETECTION USING LAMB WAVES FOR STRUCTURAL HEALTH MONITORING

THESIS

Jeffrey Stevan Crider II, Captain, USAF

AFIT/GA/ENY/07-M05

AFIT/GA/ENY/07-M05

DAMAGE DETECTION USING LAMB WAVES FOR STRUCTURAL HEALTH MONITORING

THESIS

Presented to the Faculty

Department of Aeronautics and Astronautics

Graduate School of Engineering and Management

Air Force Institute of Technology

Air University

Air Education and Training Command

in Partial Fulfillment of the Requirements for the

Degree of Master of Science in Astronautical Engineering

Jeffrey Stevan Crider II, BS

Captain, USAF

March 2007
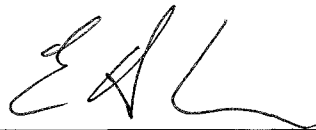
DAMAGE DETECTION USING LAMB WAVES FOR

STRUCTURAL HEALTH MONITORING

Jeffrey Stevan Crider II, BS

Captain, USAF

Approved:

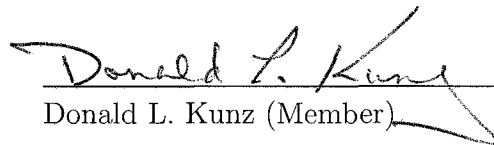_____   /4 Mar 07
Eric D. Swenson (Chairman)   Date

_____   March 14, 2007
Martin P. DeSimio (Member)   Date

_____   14 March 2007
Donald L. Kunz (Member)   Date

AFIT/GA/ENY/07-M05

Abstract

Nondestructive structural health monitoring (SHM) is an evolving technology being developed for monitoring air and space systems. The information gathered on a system's structural integrity through SHM detection methods may result in reduced costly maintenance inspections, enhanced safety, and system failure predictions. This study evaluates Lamb wave approaches used to detect simulated cracks in laboratory experiments on thin plates to detect realistic damage in a test article representing the complex geometry of an existing aircraft bulkhead. We take a "hot-spot" monitoring approach, where we monitor an area of the structure known to fail. In our experiments, we evaluated the use of piezoelectric generated tuned Lamb waves for crack detection. The use of Lamb waves, guided elastic waves in a plate, has shown promise in detecting highly localized damage due to the relatively short wavelengths of the propagating waves. We evaluated both pitch-catch and pulse-echo approaches for Lamb wave excitation and measurement. Crack detection is accomplished by comparing the responses from the damaged test article to the responses of the healthy test article.

Acknowledgements

I would like to express my appreciation to my thesis advisor, Maj Eric Swenson, for his guidance through the many stages of this project and to Dr. Kunz for the helpful comments and inputs as a member of my committee. I would also like to thank the team at AFRL: Dr. Marty DeSimio, Dr. Steve Olson, and Mr. Todd Bussey for the assistance and insights into the world of structural health monitoring and to Mark Derisso for financial support. Thanks to Jason Vangel and Daniel Ryan at the AFIT model fabrication shop for facilitating the fabrication of the F-15 test specimen. Special thanks to Dr. Soni for the acquisition and financial support of the F-15 bulkhead.

Most importantly, I would like to thank my beloved wife for her continuous support and heartfelt encouragement while concurrently obtaining her master's degree at AFIT. We had a great time together and, once again, grown even closer.

Jeffrey Stevan Crider II

Table of Contents

List of Figures

List of Tables

List of Symbols

List of Abbreviations

DAMAGE DETECTION USING LAMB WAVES FOR STRUCTURAL HEALTH MONITORING

I. Introduction and Background

1.1 Motivation: Structural Health Monitoring

Knowledge of a system's structural integrity is of vital importance in determining the operational status of a system, like an aircraft. The structural integrity status is usually obtained through scheduled maintenance inspections; which are time consuming and expensive because they usually require disassembly of a structure so visual, or other non-destructive inspection types can be made. If visual inspections are used to determine the current working condition of a structure, the disassembly procedure can inflict unnecessary damage to a healthy structure. Often working with mature aircraft, parts are broken during an inspection. By performing condition based maintenance, maintenance operations are only performed when known problems exist, costly unnecessary scheduled inspections would be reduced. According to Mal, over 25% of an aircraft's life cycle cost is due to maintenance and inspections of the airframe [10].

The implementation of a Structural Health Monitoring (SHM) system can alleviate issues associated with regular maintenance inspections. SHM is defined as "an emerging technology that can be defined as continuous, autonomous, real time, in-service monitoring of the physical condition of a structure by means of embedded or attached sensors with minimum manual intervention" [10]. Simply put, SHM provides the ability of a system to detect adverse changes within a system's structure to enhance reliability and reduce maintenance costs [6].

1.1.1 Relevance to the USAF. The United States Air Force (USAF) has an aging aircraft fleet with high operational demands and requires mission success in all environmental conditions. The USAF has increased its demand of sustainment for aging aircraft (over 25 years) in service [10]. An increased workload expected from the USAF aging fleet results in an increase of in-depth maintenance inspections. An automated accurate assessment of a system's structural integrity could reduce unnecessary maintenance, resulting in maintenance savings which could be directed towards operational costs.

The USAF seeks the benefits of implementing SHM into its fleet, which is demonstrated by the SHM methods currently being researched by the Air Force Research Lab (AFRL). The research objectives of this thesis were driven by AFRL research needs.

1.2 Research Objectives

Our research goals focused on two objectives. The first objective was to determine the applicability of a SHM sensor provided to AFRL through an Air Force Office of Scientific Research Small Business Technology Transfer Phase II contract (FA9550-05-C-0024). The SHM sensor was the Monitoring & Evaluation Technology Integration (M.E.T.I.) Disk 3 sensors created by Metis Design Corporation (MDC) [2].

The second objective focused on implementation of the Lamb wave SHM method into a realistic USAF SHM issue, and show that Lamb waves can be used to detect damage on actual aircraft parts. Ultimately, we want to bridge the gap between detecting damage in lab experiments and a realistic damage on actual aircraft parts. Within the USAF, we located three possible candidates for Lamb wave implementation. The three issues involved localized "hot-spot" monitoring of cracks, meaning we monitor an area of the structure known to fail. Two SHM issues were provided by Hill Air Force Base (AFB) and one from Robins AFB. Robins AFB's SHM issue, a cracked F-15 titanium alloy bulkhead, was chosen due to the avail-

ability of a specimen. Figure 1.1 shows the damaged F-15 bulkhead in the aircraft. Although not visible in Figure 1.1, a crack is present in the lower portion of the bulkhead. The bulkhead crack can be seen in Figures 1.2 and 1.3. Also, Robins AFB provided AFIT with an undamaged bulkhead for experimentation (Figure 1.4) and experiments were designed and conducted on an fabricated bulkhead section.
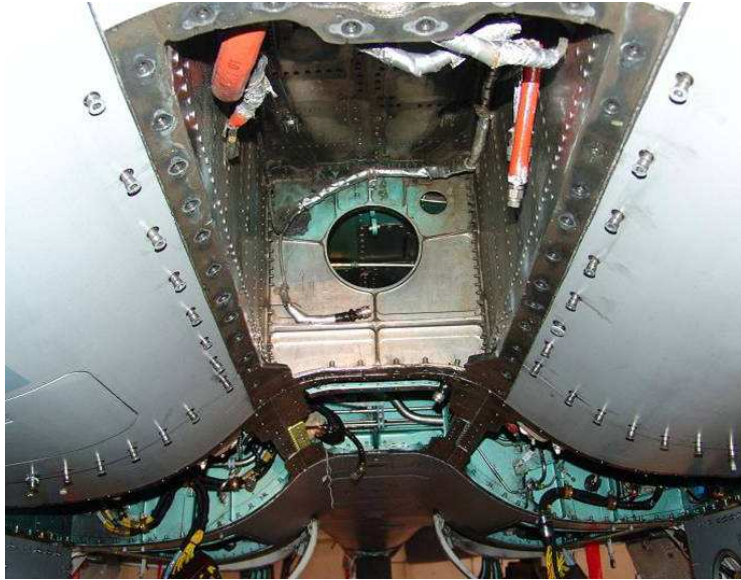
Figure 1.1   F-15 bulkhead: location of damaged bulkhead in F-15
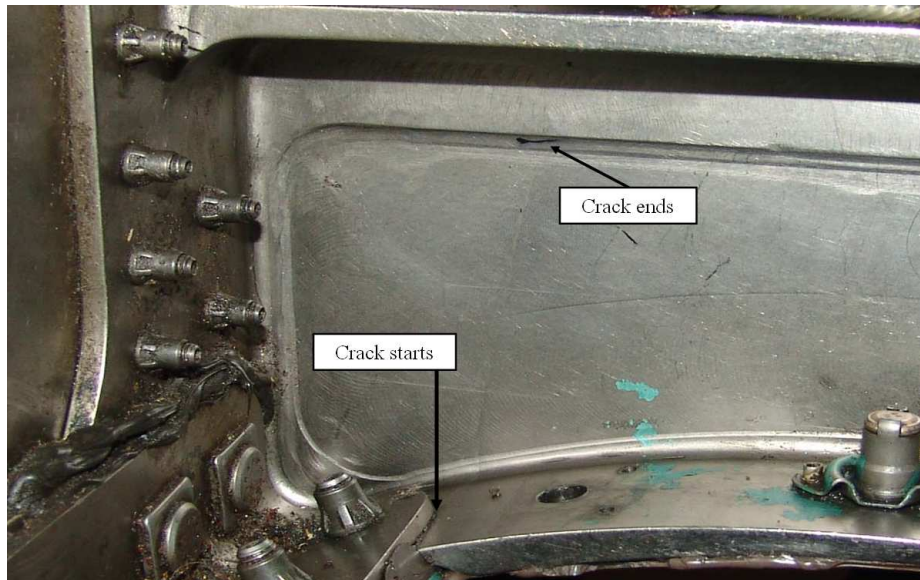
Figure 1.2   F-15 bulkhead: front view of cracked bulkhead section
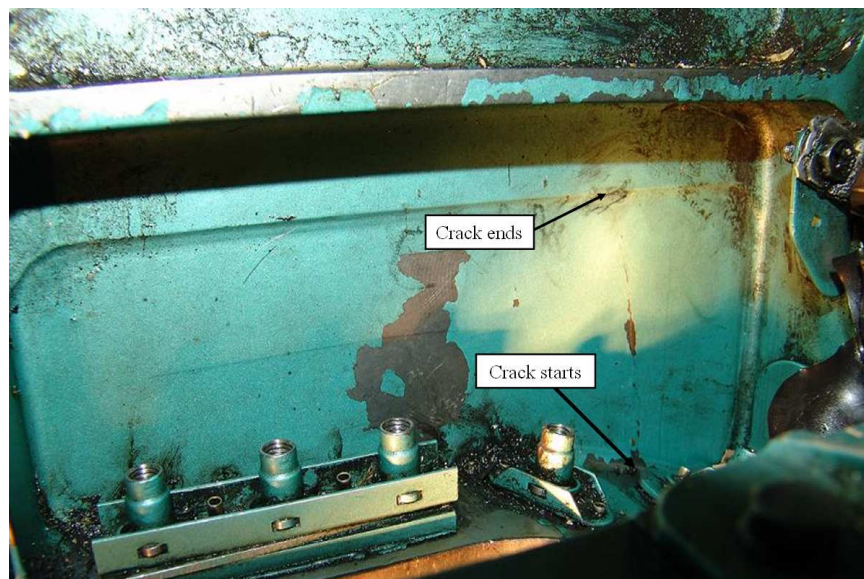
Figure 1.3   F-15 bulkhead: aft view of cracked bulkhead section

Figure 1.4   F-15 bulkhead: undamaged bulkhead provided to AFIT

1.3 Background

1.3.1 Lamb Wave Theory. Sir Horace Lamb first introduced his theory on Lamb waves (ultrasonic guided waves in flat plates) in 1917 [9]. Lamb waves occur when the thickness of the test material is on the order of a few wavelengths of the guided wave and where the test specimen is of uniform thickness [3]. Lamb waves have the important property that they stay confined inside walls of thin-walled structures and propagate over large distances (several meters) along the major axis of the structure. In addition, guided waves can also travel inside curved walls and allow for fast measurement of large areas of a structure [5]. The basic wave equations are:

$$\frac{\partial^2 \phi}{\partial x^2} + \frac{\partial^2 \phi}{\partial y^2} + \frac{\omega^2}{c_L^2} \phi = 0 \tag{1.1}$$

$$\frac{\partial^2 \psi}{\partial x^2} + \frac{\partial^2 \psi}{\partial y^2} + \frac{\omega^2}{c_T^2} \psi = 0 \tag{1.2}$$

where ϕ and ψ are two potential functions, and c_L and c_T are the longitudinal (pressure) and transverse (shear) wave speeds in the material. The longitudinal and transverse wave speeds are defined as:

$$c_L = \sqrt{\frac{\lambda + 2\mu}{\rho}} \tag{1.3}$$

$$c_T = \sqrt{\frac{\mu}{\rho}} \tag{1.4}$$

where λ and μ are the Lamé constants [9], and ρ is the mass density. For an isotropic material, the Lamé constants can be defined as [6]:

$$\mu = \frac{E}{2(1+\nu)} \tag{1.5}$$

$$\lambda = \frac{E\nu}{(1-2\nu)(1+\nu)} \tag{1.6}$$

where E is the Young's Modulus in the direction of the propagation direction and ν is Poisson's Ratio.

The general solutions to Equations 1.1 and 1.2 are:

$$\phi = [A_1 sin(py) + A_2 cos(py)]e^{i(kx-\omega t)} \tag{1.7}$$

$$\psi = [B_1 sin(qy) + B_2 cos(qy)]e^{i(kx-\omega t)} \tag{1.8}$$

where k is the wavenumber (equal to $2\pi/wavelength$) and:

$$p = \sqrt{\frac{\omega^2}{c_L^2} - k^2} \tag{1.9}$$

$$q = \sqrt{\frac{\omega^2}{c_T^2} - k^2} \tag{1.10}$$

and x is the coordinate in the direction of the wave propagation and y is the coordinate in the direction through the plate thickness. The four arbitrary constants: A_1, A_2, B_1, and B_2, are determined by applying boundary conditions. Using the solutions to the basic wave equations, Equation 1.7 and 1.8, and assuming the boundary conditions correspond to traction free surfaces, we obtain the Rayleigh-Lamb frequency relations (known as the dispersion equations) for Lamb waves:

$$\frac{tan(0.5qd)}{tan(0.5pd)} = -\frac{4k^2 \ pq}{(q^2 - k^2)^2} \tag{1.11}$$

$$\frac{tan(0.5qd)}{tan(0.5pd)} = -\frac{(q^2 - k^2)^2}{4k^2 \ pq} \tag{1.12}$$

where d is the plate thickness. Equation 1.11 is the solution for symmetric Lamb wave motion and Equation 1.12 is the antisymmetric Lamb wave motion solution.

Figure 1.5 illustrates the symmetric motion of Lamb waves. Viewing the illustration from the exterior boundaries, notice the wave crests on the upper and lower surfaces coincide for the symmetric motion. The antisymmetric motion is illustrated in Figure 1.6 where the crest on one side coincides with a trough on the other, when viewed from the exterior of the plate's surface [3].
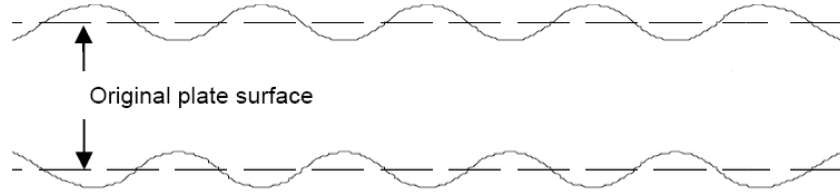
Figure 1.5   Illustration of a symmetric Lamb wave [3]
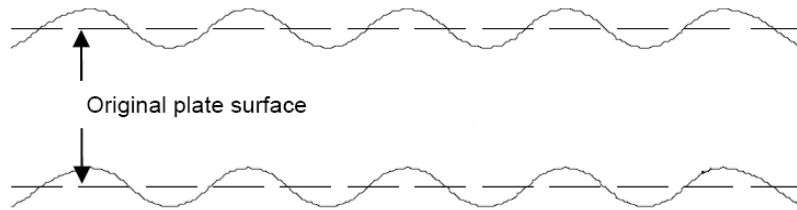
Figure 1.6   Illustration of an antisymmetric Lamb wave [3]

1.3.2   Dispersion.   If media is dispersive then the guided wave speeds through the medium vary with frequency, and a wave propagating in such a medium

is called a dispersive wave. It is common to characterize such behavior by expressing the angular frequency, ω, as a function of wavenumber, k, where:

$$k = \frac{\omega}{c} \qquad (1.13)$$

and $\omega = 2\pi f$, where c is the speed of light and f is the linear frequency (cycles per second). This relationship is called the dispersion relation [13].

There are many solutions to Equations 1.11 and 1.12 since for each solution the wave speed is a different function of frequency. The many solutions correspond to Lamb mode shapes of the symmetric and antisymmetric motion and are designated S_0, S_1, S_2, etc. and A_0, A_1, A_2, etc., respectively. The wave speed (or phase velocity v_p) is given by:

$$v_p = \frac{\omega}{k} \qquad (1.14)$$

Wave speed is not only affected by the frequency f, but by the plate thickness d. The product of the frequency and thickness fd is often used as the independent variable for representing wave speeds. Figure 1.7 is a plot of phase velocity for versus frequency-thickness product typical aluminum. Different wave modes may exist for a given frequency-thickness product including both symmetric and antisymmetric wave modes [12].

The phase velocity is the speed at which the crests and troughs of the wave move in the propagation direction. However, if we modulate the wave, it is the modulation that carries the information. We therefore need to know the speed at which the modulating wave packet travels. The velocity of the wave packet is the group velocity v_g where:

$$v_g = \frac{d\omega}{dk} \qquad (1.15)$$

1-9

Figure 1.8 shows a plot of both symmetric and antisymmetric waves group velocity versus frequency-thickness product fd for a typical aluminum alloy. The phase and group velocity dispersion curves were computed from Equations 1.11 and 1.12 using numerical methods outlined by Rose [14].

When considering SHM using Lamb waves, choosing the correct frequency-thickness product is paramount. For a given test article of constant thickness, the testing frequency is the independent variable for Lamb wave analysis. In general, low frequency selection yields larger antisymmetric wave responses, whereas higher frequencies yield larger symmetric wave responses, as shown in Figure 1.9. Wave selection based on frequency and signal response is referred to as tuning [4].

Because the experiments presented in this paper used a variety of aluminum alloys for each experiment, we were interested in how the dispersion curves varied for different aluminum alloys whose material properties were different. Table 1.1 shows the range of aluminum properties used to calculate the dispersion curves. We also considered titanium to determine if aluminum has very similar dispersive properties since our goal is to show proof of concept that the Lamb wave SHM method will work when applied to a titanium structure. From Figures 1.11 and 1.12, one can see that the dispersive properties are very similar for aluminum and titanium. Therefore, it is assumed that methods can be developed and demonstrated on an aluminum structure, then applied to a titanium structure, possibly requiring a change in operating frequency.

Table 1.1   Dispersion Curve Material Properties

Material	Modulus of Elasticity	Mass Density	Poisson's Ratio
Al I	10,000 ksi	2800 kg/m^3	0.33
Al II	11,400 ksi	2600 kg/m^3	0.33
Ti	15,500 ksi	4500 kg/m^3	0.33
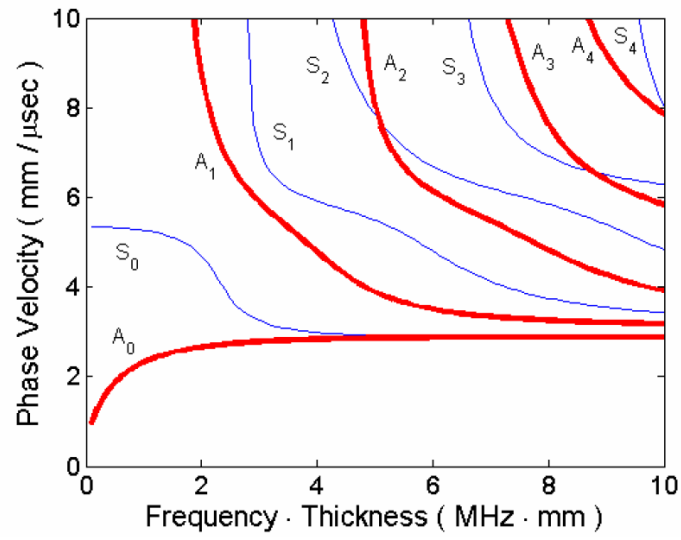
Figure 1.7   Phase velocity dispersion curves for aluminum [12]
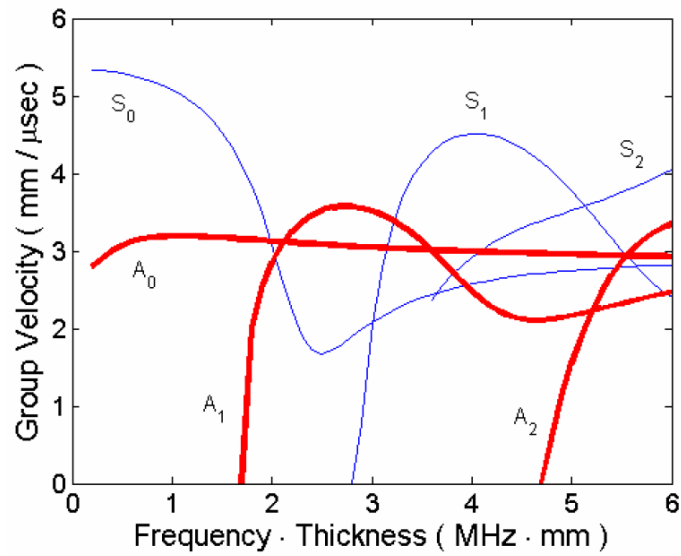
Figure 1.8   Group velocity dispersion curves for aluminum [12]
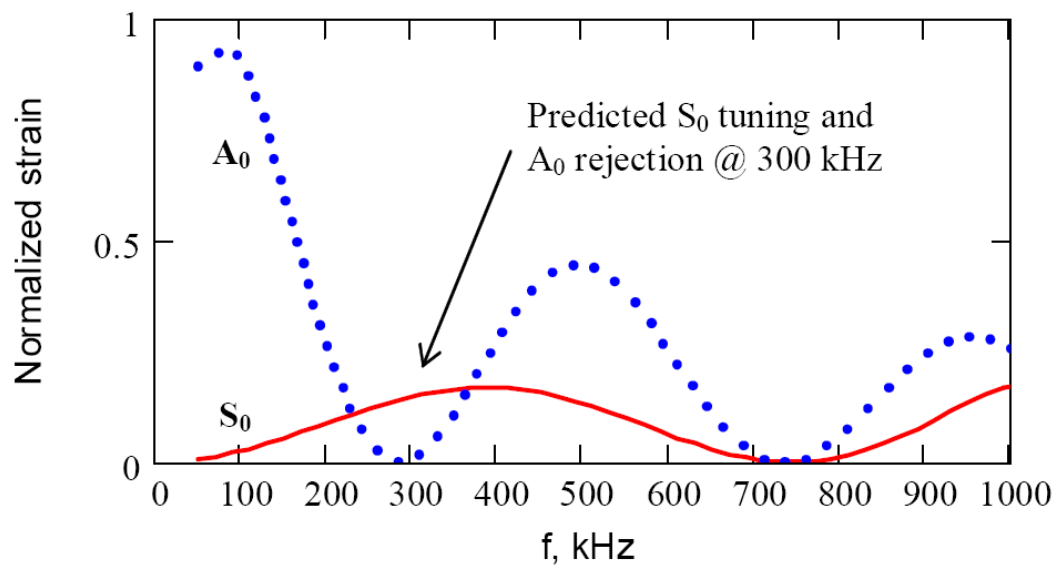
Figure 1.9   Theoretical Lamb wave response of a 1.6 mm aluminum plate [4]
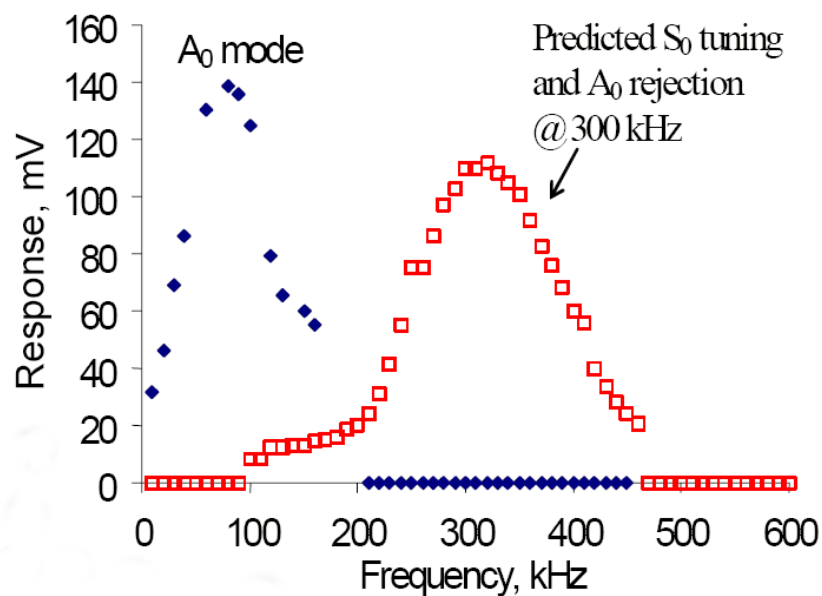
Figure 1.10   Measured Lamb wave response of a 1.6 mm aluminum plate [4]
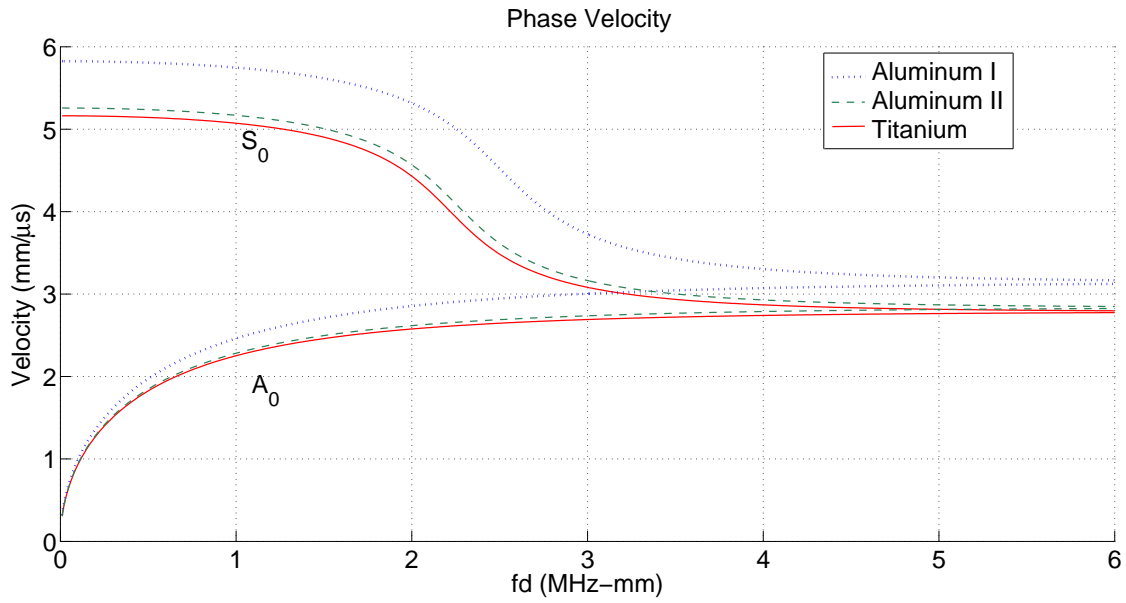
Figure 1.11   Phase velocity dispersion curves based on material properties from Table 1.1
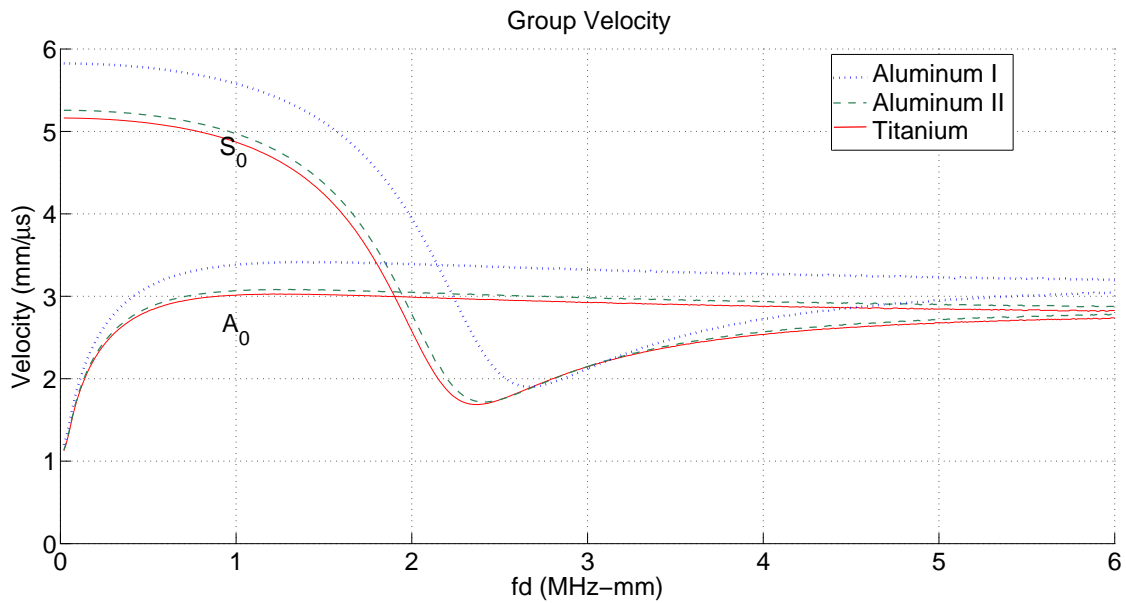
Figure 1.12   Group velocity dispersion curves based on material properties from Table 1.1

1.3.3   Detection Methods.   For Lamb waves, the most common ultrasonic methods for Non-Destructive Evaluation (NDE) used are the pitch-catch and pulse-echo techniques. The pitch-catch technique uses two transducers, one to excite the structure and the other to measure the received response. Damage is determined by characterizing the change in the response. However, to locate the damage multiple pitch-catch sensors may be required.

The pulse-echo technique uses one transducer to both excite the structure and to detect the returns, or echoes, from the excitation. The signal returns can aide in determining and locating material defects [5]. The returned signal's time-of-flight can be analyzed to determine the distance between the transducer and the damage while the amplitude can be used to assess the severity of damage.

1.4   Thesis Overview

This research explores the use of piezoelectric sensors as a means to detect damage in metallic structures. In Chapter 2, the four experimental aluminum setups are covered in detail. Chapter 3 discusses the results obtained from the M.E.T.I.-Disk 3 sensors using the pulse-echo technique implemented in two thin aluminum plates. Chapter 4 discusses the results obtained using piezoelectric sensors in a pitch-catch technique for a thin aluminum plate and an aluminum test article fabricated to represent an F-15 bulkhead. Finally, in Chapter 5, the results of the experiments are summarized and conclusions are drawn.

II. Methodology

In this chapter, the experimental setup and methodology is discussed for four experiments. The four experiments were required to determine the applicability of the M.E.T.I-Disk 3 and implementation of the Lamb wave method in a realistic SHM application. The initial experiments were required to develop our Lamb wave technique for finial implementation into a fabricated F-15 test specimen.

2.1 Small Aluminum Plate

The initial step was to determine the limitations and applicability of the M.E.T.I.-Disk 3 sensors for future consideration in an identified USAF SHM issue. Along with the M.E.T.I. sensors, AFRL also provided an aluminum plate with two sensors attached, shown in Figure 2.1, and the MDC software needed to instrument the M.E.T.I. sensor.

Figure 2.1   Small plate: aluminum plate with attached sensors

2.1.1 Equipment.   The aluminum plate provided by AFRL was 608 mm long by 102 mm wide by 1.6 mm thick. A M.E.T.I.-Disk 3 sensor and an American Piezo Ceramics (APC) 850 piezoelectric transducer (Piezo) are glued to one end of the plate shown in Figure 2.1. The two sensors were attached to the aluminum plate using M-Bond 200, a general-purpose strain gauge adhesive. Figure 2.2 shows a closeup of the two attached sensors. The 6.5 mm diameter APC 850 piezo was

centered 51 mm from the plate's left edge and a 25.4 mm M.E.T.I.-Disk 3 was centered 88 mm in length from the plate's left.

Figure 2.2   Small plate: closeup of attached APC 850 and M.E.T.I.-Disk 3 sensors

The key advantage of using the MDC M.E.T.I. sensor is the reduction in required testing equipment. The only additional hardware requirements for SHM testing is a computer with an available Universal Serial Bus (USB) port for connecting the M.E.T.I. sensor. The computer provides the power to the M.E.T.I.-Disk 3 sensor through the mini-USB connector. The on-board electronics of the sensor serves as the excitation function generator. An exploded view of the M.E.T.I.-Disk 3 is shown in Figure 2.3. The M.E.T.I.-Disk 3 sensor has two piezo disks of which the inner disk serves as the sensor while the outer disk is the actuator. The APC 850 sensor was connected to an oscilloscope for the sole purpose of ensuring the MDC sensor was exciting the test specimen as instructed by the MDC software.

2.1.2   Software.   MDC provides software required for operation of the M.E.T.I.-Disk 3 sensors. The software provided to Air Force Institute of Technology (AFIT) consisted of two MDC programs: 'MD3 Demo version 2' and 'MD3 Testing version 1.6.' Both programs are LabVIEW based and allow control of the sensor. The MD3 Demo program only allows for one experimental test collection, while the MD3 Test program can be pre-programmed for multiple test collections. The collected response data is stored by the MDC software in a tab-delimited file for-
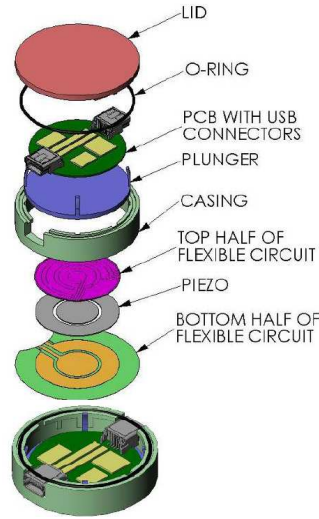
Figure 2.3   M.E.T.I.-Disk 3: exploded view [7]

mat. We wrote MATLAB codes for post-processing of the collected data to compare with the Lamb wave theory presented in Chapter 1.

2.1.3 Experimentation.   We used the M.E.T.I.-Disk 3 sensor in a pulse-echo testing configuration. To simulate structural damage, a mass was placed on the plate to simulate damage by increasing the stiffness. The mass was a 0.05 kg aluminum bar measuring 100 mm long by 14 mm wide by 12 mm thick. Sonotech Shear Gel was applied to the mass to ensure coupling with the plate. Commonly, damage detection using Lamb waves is accomplished by detecting a local change in the stiffness (or density) of the structure resulting in a reflected wave. The method of adding mass to change the local stiffness of a specimen is referred to as the inverse-damage approach [8]. Similar experiments have been reported by Seth Kessler [8].

2.2 Large Aluminum Plate

The second experiment included a 2024-0 aluminum plate with dimensions of 758 mm long by 735 mm wide by 1.6 mm thick. The same MDC software and experimentation used for the small plate was used with the large aluminum plate. The large plate was raised from the table surface using wood supports at the corner's to

2-3

prevent interference of the Lamb wave with the table. A M.E.T.I.-Disk 3 sensor was attached to the center of the plate, see Figure 2.4, using Hysol 608 epoxy adhesive, a strain-gage adhesive.

MDC provides AE-10 epoxy with the M.E.T.I.-Disk 3, but the epoxy was within 22 days of expiration. According to the manufacture, the adhesive's shelf life is 12 months when stored at 75°F and 18 months at 20°F [15]. This was an area of concern since we had a limited supply of sensors. MDC tested a sample of their AE-10 with the same expiration date and found the epoxy sample would not cure completely. Therefore, we decided to use a different adhesive to ensure proper coupling with the specimen.
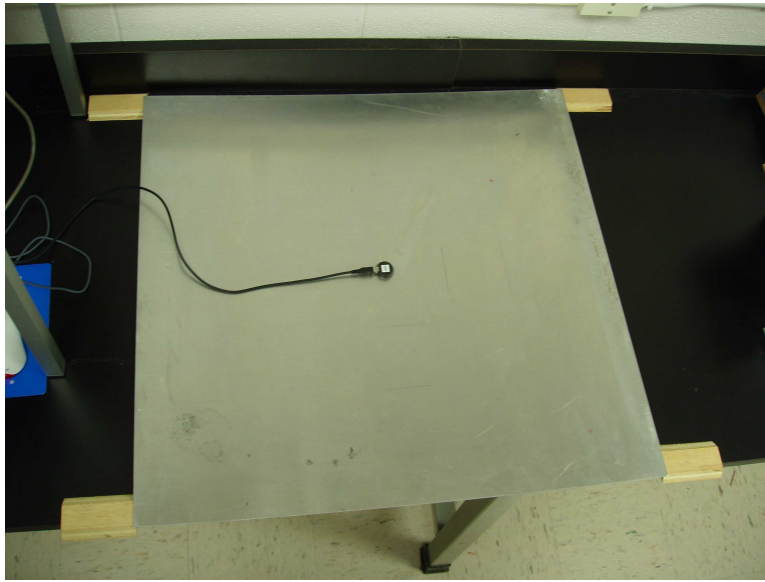
Figure 2.4   Large plate: aluminum plate with sensor

2.3   Multi-Purpose Panel Aluminum Plate

The third plate was a 2024-T3 aluminum specimen that was constructed by AFRL, see Figure 2.5. The plate is referred to as the multi-purpose panel (MPP) due to the variety of experiments intended for the plate. Figure 2.6 shows a schematic of the MPP measuring 1220 mm long by 610 mm wide by 1 mm thick. The plate

is separated into a healthy region (top half) and a damaged region (bottom half). The healthy region was used to establish a baseline. Simulated damage was created on the lower half of the plate prior to bonding the APC 850 piezos.

The damaged region consisted of simulated cracks and corrosion. The cracks were simulated by cutting a cut into the plate using an electrical discharge machining (EDM) machine. The EDM machine used a 0.01 in wire to make three 0.012 in cuts, each 18 mm in length, see Figure 2.7. The plate was also machined to simulated corrosion by milling a 18 mm in diameter bore that removed half the thickness of the plate. However, for our experiment corrosion was not evaluated.

A total of 26 APC 850 piezos were attached to the MPP. Eight piezos were attached in the center of the MPP and nine were attached in each of the two regions (Figures 2.8 and 2.9). The piezos were attached using M-Bond 200 adhesive.
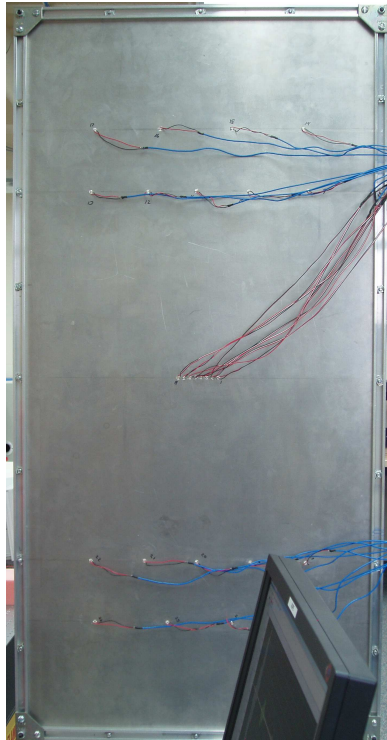
(a)   (b)

Figure 2.5   MPP: (a) front (b) back
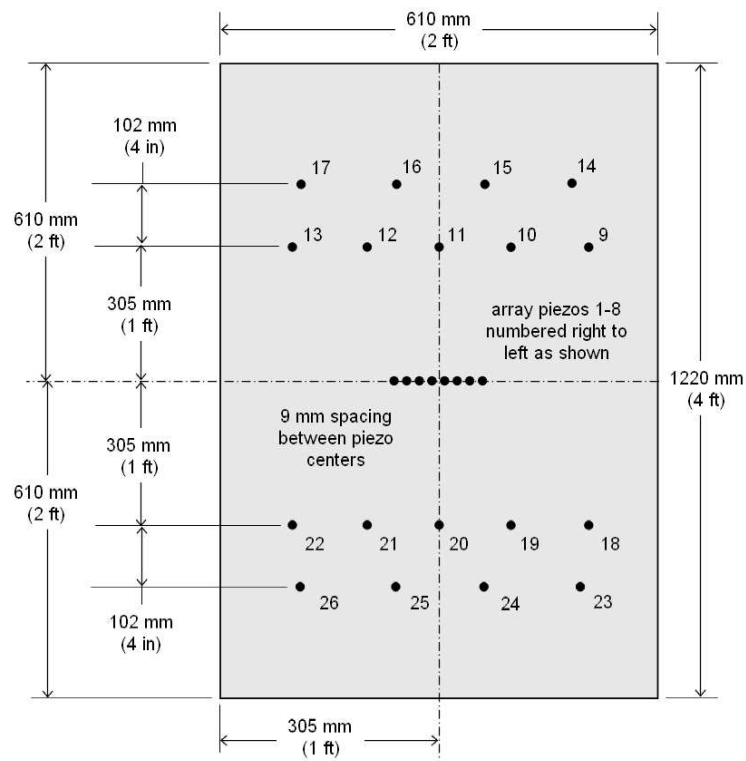
Figure 2.6   MPP: layout and dimensions
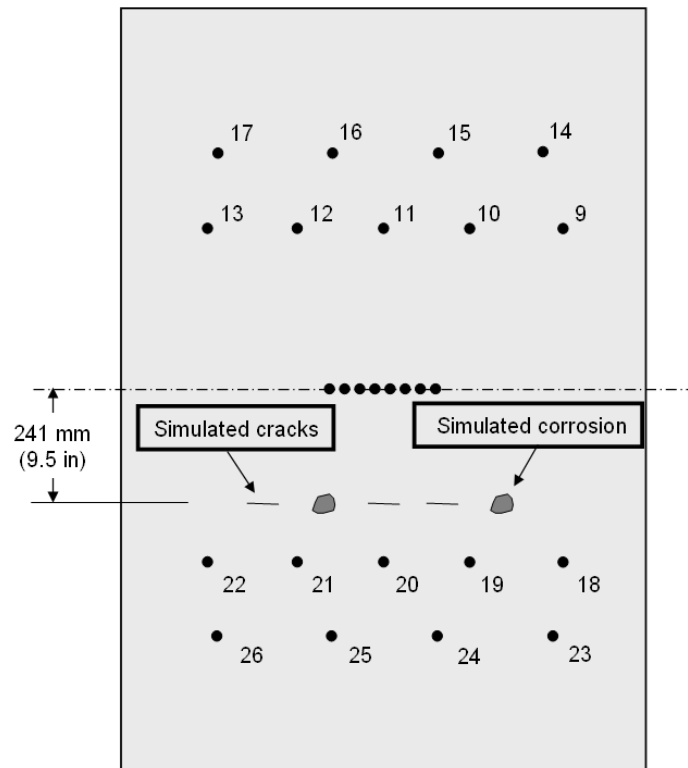
Figure 2.7   MPP: damage locations
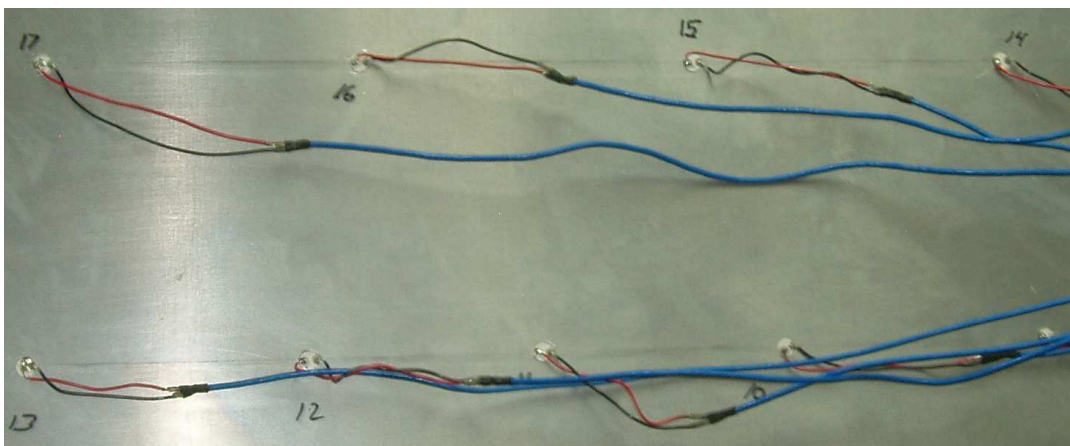
Figure 2.8   MPP: array of top APC 850 piezos
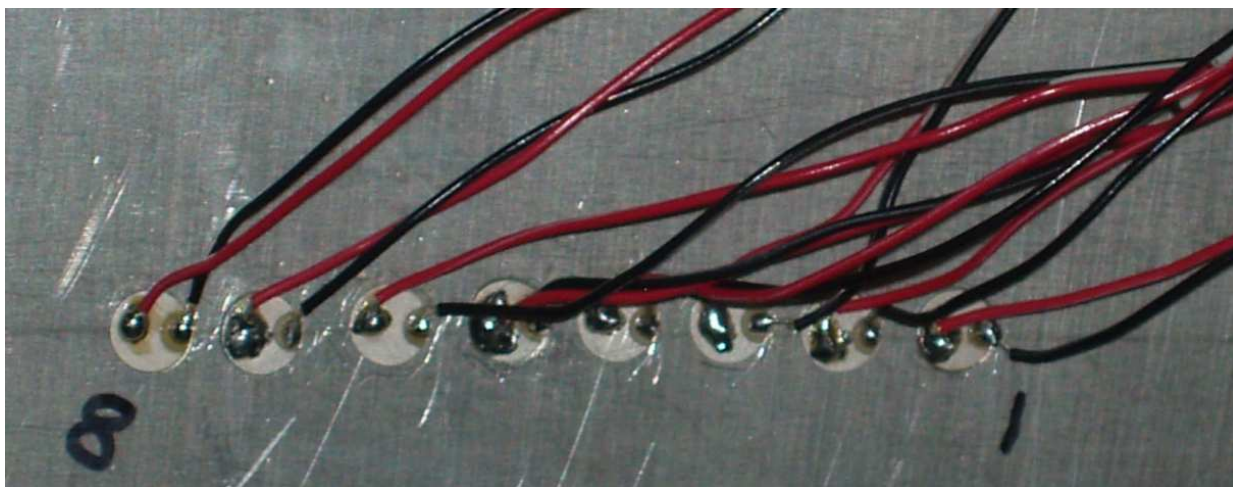
Figure 2.9   MPP: array of middle APC 850 piezos

2.3.1 Equipment. The MPP equipment setup is shown in Figure 2.10. The setup included an Agilent 33250A function generator, LeCroy WaveSurfer 454 oscilloscope, voltage divider, National Instruments (NI) BNC-2110 junction connector, and a data acquisition computer with an embedded NI PXI-8187 high-performance real-time controller. The equipment, and instruction on using the equipment, was provided to us by AFRL.
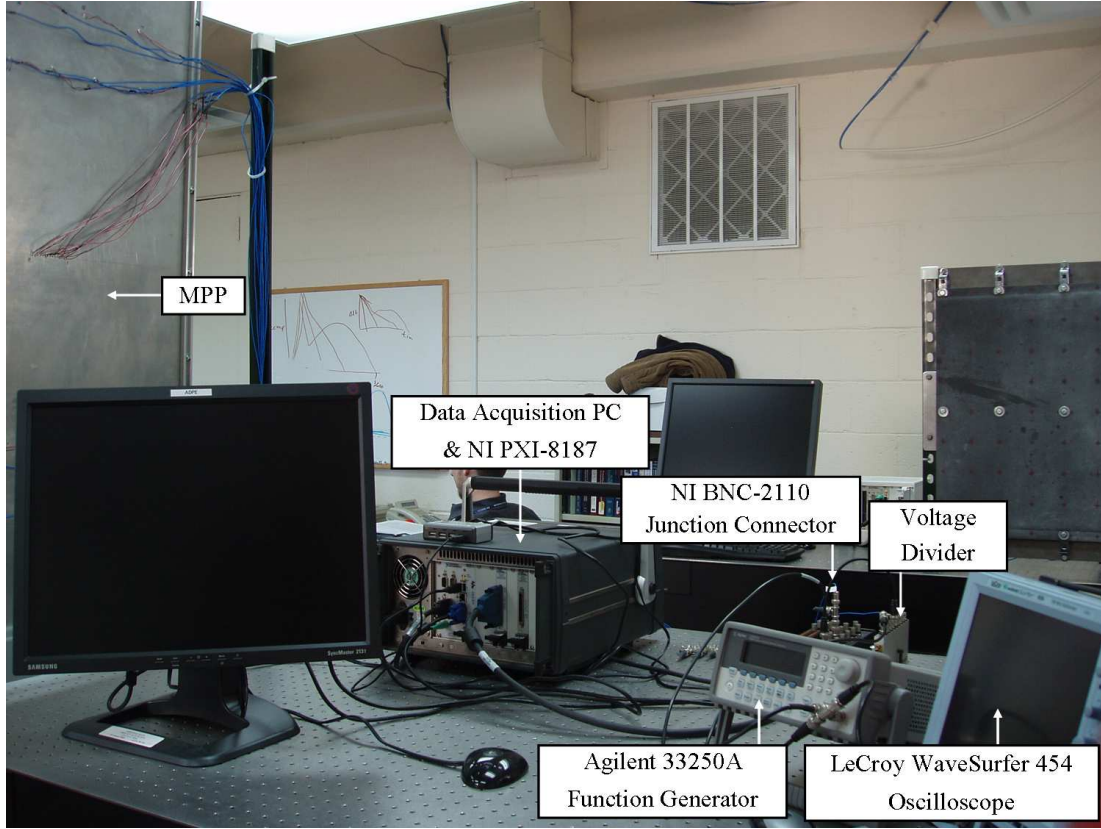
Figure 2.10   MPP: experimental setup

2.3.2 Software. A LabVIEW program that controls the MPP equipment and collects the response data was provided by AFRL. We set the program collection constraints to a 1,000 samples with a sampling rate of 2.5 MHz, yielding a total testing time of 400 μs. A $5\frac{1}{2}$ cycle Hanning-windowed sine wave excitation signal with a frequency range of 50 kHz to 500 kHz in increments of 5 kHz was used for

exciting the structure. Each recorded response is the average of 10 responses to repeated excitation signals.

   2.3.3 Experimentation. Using a pitch-catch technique, the structure was excited at piezo 5, and the response was collected at piezos 11 and 20. The excitation signal propagating to piezo 20 was disrupted by the EDM simulated crack. We used a change detection approach, i.e., comparing the healthy response of piezo 11 to the damaged response of piezo 20, to determine if damage occurred in the structure. The change detection approach only determines if damage occurred, not where the damage is within the structure.

2.4 F-15 Simulated Bulkhead

   The final experiment implemented the testing procedures developed using the MPP on a realistic SHM issue. Recall from Chapter 1, the SHM problem chosen was a F-15 bulkhead provided to AFIT by Robins AFB (see Figures 1.1 through 1.4). It is not acceptable to damage the actual bulkhead; therefore, a test article was milled out of aluminum based on dimensions from the undamaged bulkhead. We instrumented the test article using the same procedures as the MPP. A series of EDM cuts were made to simulate a crack representative to the actual damage. Differences in pitch-catch measurements characterize healthy and damaged states.

   2.4.1 Milling Process. The F-15 bulkhead is made of a titanium alloy, but we choose aluminum due to similar dispersive properties (Figures 1.11 and 1.12), availability, and cost. Figure 2.11 shows the dimensions of the scaled F-15 drawing that was provided to AFIT's model fabrication shop for the milling. Sensor 3 through 6 were placed as shown. A closeup of the F-15 section is shown in Figure 2.12. Three test articles were milled from Al 6061-T6 using a Fryer MB-10 CNC Mill, see Figure 2.13.
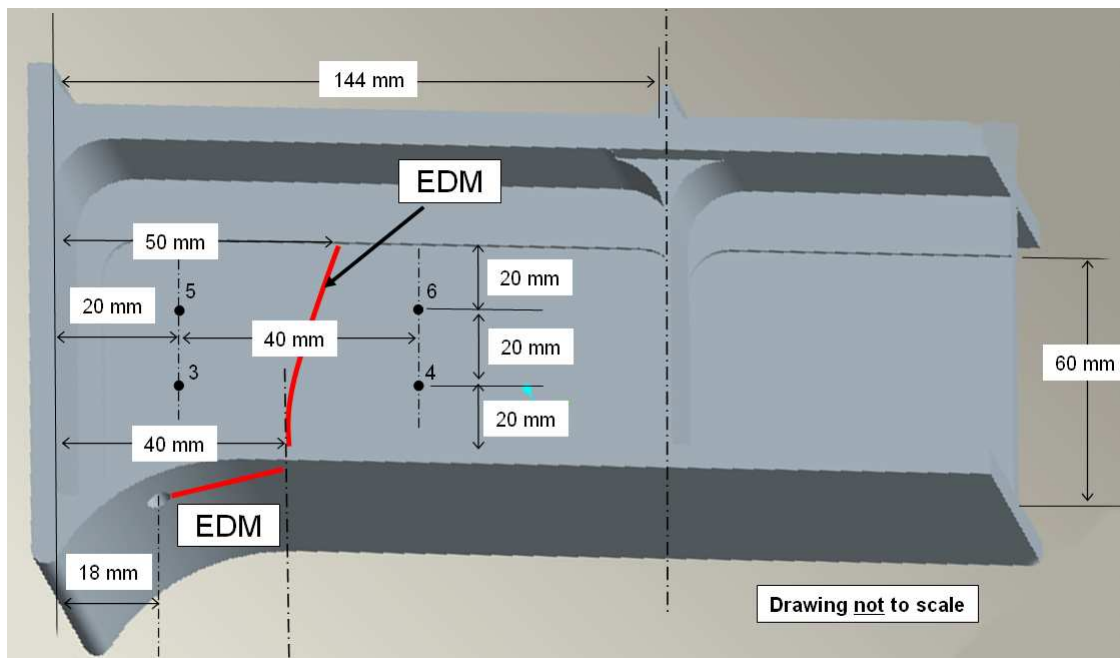
Figure 2.11   F-15: schematic of aluminum F-15 specimen and sensor placement

Figure 2.12   F-15 bulkhead: closeup of undamaged bulkhead where damage occurred

Figure 2.13   F-15: milling using Fryer MB-10

2.4.2 Sensor Attachment Process. Six APC 850 piezos were bonded to the test specimen using M-Bond 200 adhesive as shown in Figure 2.14. Two piezos were attached on the 6 mm thick lower horizontal stiffener. The stiffener is 24 mm wide and the hole from which the crack initiates is 6 mm in diameter and centered on the stiffener. This leaves a span of 9 mm between the hole and the bulkhead wall. The APC 850 piezos are 6.5 mm in diameter and are centered on the 9 mm span and placed across from each other with the stiffener crack running between piezo 1 and piezo 2, the two piezos on the stiffener. Piezo 1 is centered at 18 mm from the left stiffener and 4.5 mm from the bulkhead wall. piezo 2 is centered at 60 mm from the left vertical stiffener and 4.5 mm from the bulkhead wall. The remaining four piezos are attached on the 3 mm thick bulkhead wall at the dimensions shown in Figure 2.11, and labeled three through six.
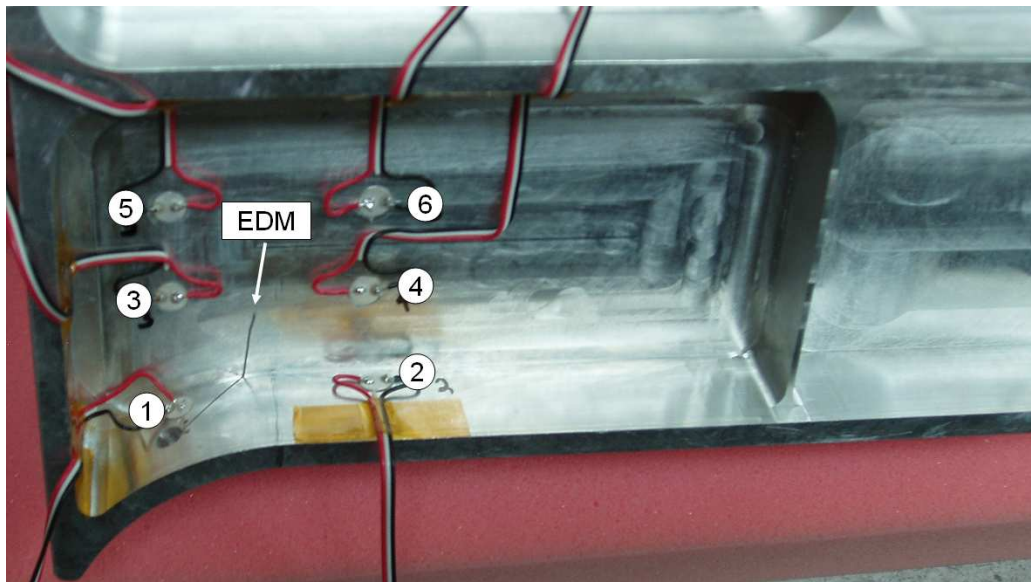
Figure 2.14   F-15: sensor locations for APC 850 piezos 1 through 6 with first EDM cut

2.4.3 EDM Process. The next phase was the introduction of damage using the EDM machine. The EDM cut is intended to replicate the crack seen in Figures 1.2 and 1.3. The overall EDM process began at the lower horizontal

stiffener hole and terminated at the bulkhead wall thickness change 50 mm from the left vertical stiffener, see Figure 2.11. The cut was accomplished over three EDM intervals with data collection at each interval. The EDM machine used a 0.01 in wire, resulting in a 0.012 in wide cut. The specimen was notched at AFIT's model fabrication shop with the EDM machine, then taken to AFRL for data collection and analysis.

The first EDM cut began at the lower horizontal stiffener hole and ended 15 mm from lower vertical stiffener by 37 mm from left horizontal stiffener (Figure 2.14). The cut made a direct line from the hole to the intersection, 37 mm from the left horizontal stiffener. The EDM wire was not allowed to come into contact with the surface before cutting began. Therefore, each cut required a drilled 0.043 in (#57 bit) hole before beginning the next cut. The first cut did not require a drilled hole since the cut started inside the stiffener hole.

The second and third EDM cuts are shown in Figure 2.15. The second cut began at 35 mm from the left vertical stiffener by 5 mm from the lower horizontal stiffener and ended 43 mm from the left vertical stiffener by 30 mm from the lower vertical stiffener. The second cut did not initiate at the ending location of the first cut since the first cut was made at an angle. The specimen was angled in the EDM machine for the first cut, see Figure 2.16, which resulted in an angled cut through the specimen. The upper surface cut ending 15 mm from lower vertical stiffener, 37 mm from left horizontal stiffener, while the lower surface cut ended 8 mm from lower vertical stiffener, 39 mm from left horizontal stiffener. For the second cut, an EDM wire clearance hole was drilled at a location to ensure the second cut was tied into the first cut. The third cut continued where the second cut ended and terminated at the intersection of the thicker wall, 50 mm from the left stiffener. Figure 2.18 shows the position of the F-15 specimen inside the EDM machine for cutting the second and third cut.
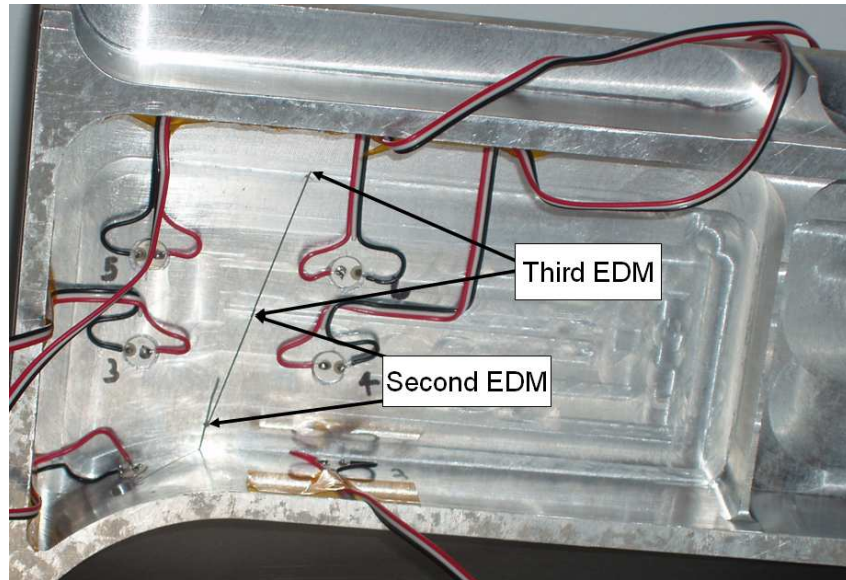
Figure 2.15   F-15: second and third EDM notches

Figure 2.16   F-15: arrangement of F-15 specimen in EDM machine for first cut
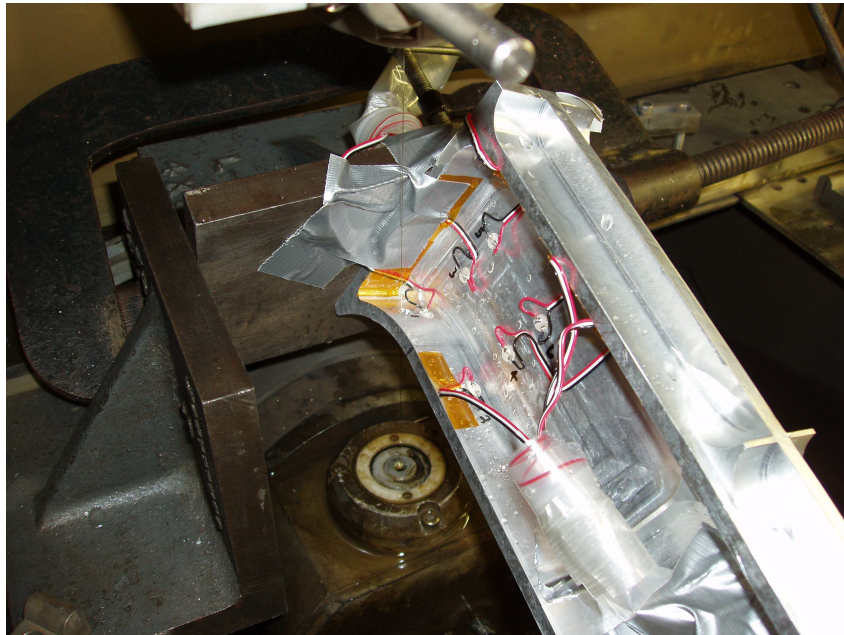
Figure 2.17   F-15: arrangement of F-15 specimen in EDM machine for first cut
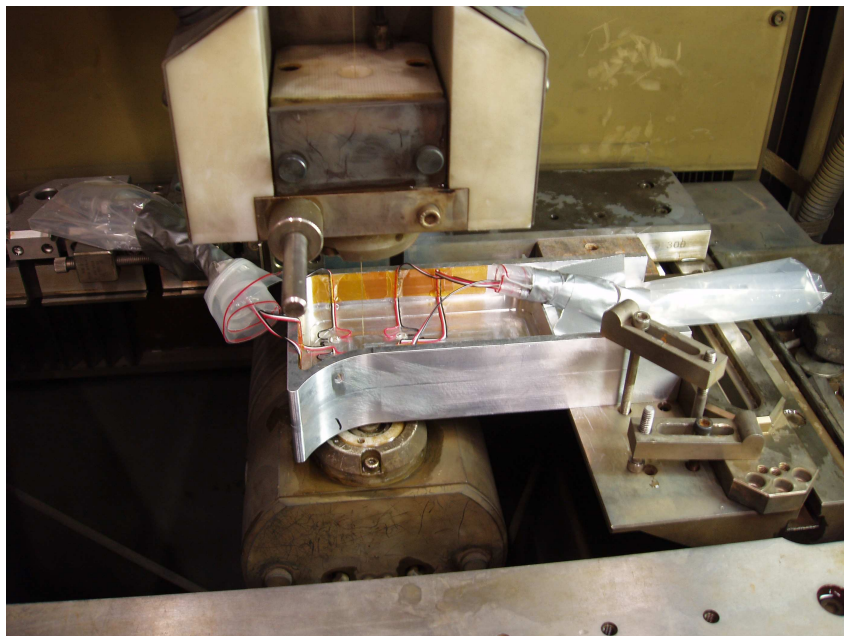
Figure 2.18   F-15: arrangement of F-15 specimen in EDM machine for second cut

2.4.4 Experimentation. The same LabVIEW program used for the MPP was used for the F-15 test specimen, see Section 2.3.2. We used an excitation signal frequency range of 50 kHz to 800 kHz, incrementing by 10 kHz for the F-15 experiment. Prior to introduction of the EDM cuts, a healthy baseline was established for the F-15 specimen. The F-15 tests involved exciting the structure with one sensor and recording the responses at each of the remaining five piezos; thus, utilizing the pitch-catch method. A complete sweep, exciting from all six piezos individually and collecting from the remaining five, was completed. The F-15 specimen rested on soft foam during all testing of the structure. We did accomplish one test without the foam by placing it directly on the lab table to see if the resting media affected our Lamb wave results.

After collection of the healthy data set, we used the EDM machine to cut the F-15 specimen. After each cut, the specimen was tested using the same method as the healthy, i.e., exciting from each sensor individually and collecting from the remaining five. The cutting-testing process was repeated after all three EDM cuts.

2.5 Methodology Summary

Chapter 2 discussed the methodology developed and implemented for the different experiments leading up to the final experiment on the fabricated F-15 test specimen. The first two experiments used the pulse-echo technique with M.E.T.I.-Disk 3, and the last two experiments used the pitch-catch technique with APC 850 piezos. The results from the pulse-echo experiments are presented in Chapter 3. Chapter 4 presents the results from the pitch-catch experiments.

III. Results and Analysis: Pulse-Echo

This chapter presents the results of the experiments described in Chapter 2 and compares the results to theoretical calculations. Our goals for this study encompassed two aspects: determining functionality of the MDC sensors and determining if damage can be located in a more realistic test specimen. The pulse-echo technique was conducted on the first two experiments and the pitch-catch technique was used on the last two experiments. The first three specimens were thin aluminum plates used to validate and refine experimental methods for the final experiment, the fabricated F-15 specimen. The results and analysis of the last two experiments are presented in the next chapter.

3.1 Small Aluminum Plate

The purpose of the small aluminum plate experiment was to determine the functionality of the MDC M.E.T.I.-Disk 3 sensors and use the MDC sensor along with SHM pulse-echo theory to locate damage in the plate. The M.E.T.I.-Disk 3 sensors used in this experiment operate only in a pulse-echo method. To use the MDC sensors, we used either the MD3 Demo or the MD3 Testing programs for instrumentation. The MD3 Demo program was straight forward and was used to gain an understanding of SHM using Lamb waves.

The MD3 Demo program allows for one test collection, defined as a single excitation and a single collection of the response generated from the excitation. Figure 3.1 shows the experiment settings, which were: a 100 kHz $5\frac{1}{2}$ cycle Hanning-windowed sine wave excitation signal, 20 Volts peak-to-peak (V_{pp}) excitation amplitude, collecting 1,000 samples with a sampling frequency of 1000 kHz (1 MHz); thus yielding a total testing time for one test of 1,000 μs. The excitation signal and response are plotted in the MD3 Demo program shown in Figure 3.1. Looking at the excitation signal plotted in the top window of the MD3 Demo program (Figure 3.1),

we noticed that our excitation signal was not producing the 20 V_{pp} selected, but was producing approximately 6 V_{pp}, shown in Figure 3.2.

Our first focus was on verifying the response (A_0 and S_0 waves) with theoretical calculations. Initially we chose an excitation frequency of 100 kHz for the purpose of exciting with the Lamb waves dominated by the A_0 wave. According to the tuning and measured response curves, Figures 1.9 and 1.10, the response for a 1.6 mm thick plate excited with a frequency below 100 kHz produces a response consisting mainly of the A_0 wave. At 100 kHz, the response appears to be void of the S_0 wave.

Trying to locate the A_0 and S_0 waves based on theoretical calculations from Lamb wave theory was a difficult task considering the short distances between the MDC sensor and the boundary conditions. Operating at 100 kHz meant the frequency-thickness product, fd ($0.1\ MHz \times 1.6\ mm$), was 0.16 MHz-mm. According to the theoretical dispersion curves, see Figure 1.8, our A_0 and S_0 waves' group velocities v_g were 2.1 $mm/\mu s$ and 5.3 $mm/\mu s$, respectively. The calculated theoretical A_0 and S_0 waves time-of-flight ($2 \times distance\ /\ v_g$) for the excitation response to return from the first boundary was 48.6 μs and 19.2 μs, but we expect a very minimal amplitude contribution from the S_0 wave. Figures 3.3 and 3.4 show where the predicted time-of-flight returns from the closest boundary (plate edge) should occur throughout the entire response. Theoretically, the first A_0 return occurs before the excitation is completed, but the second A_0 return (approximately 140 μs) appears to coincide with the theoretical calculations. However, there is a theoretical S_0 wave that corresponds to the same 140 μs return. Also, Figures 3.3 and 3.4 only shows the theoretical returns from two edges not all four edges. A larger test specimen is needed to accurately distinguish the A_0 and S_0 waves.
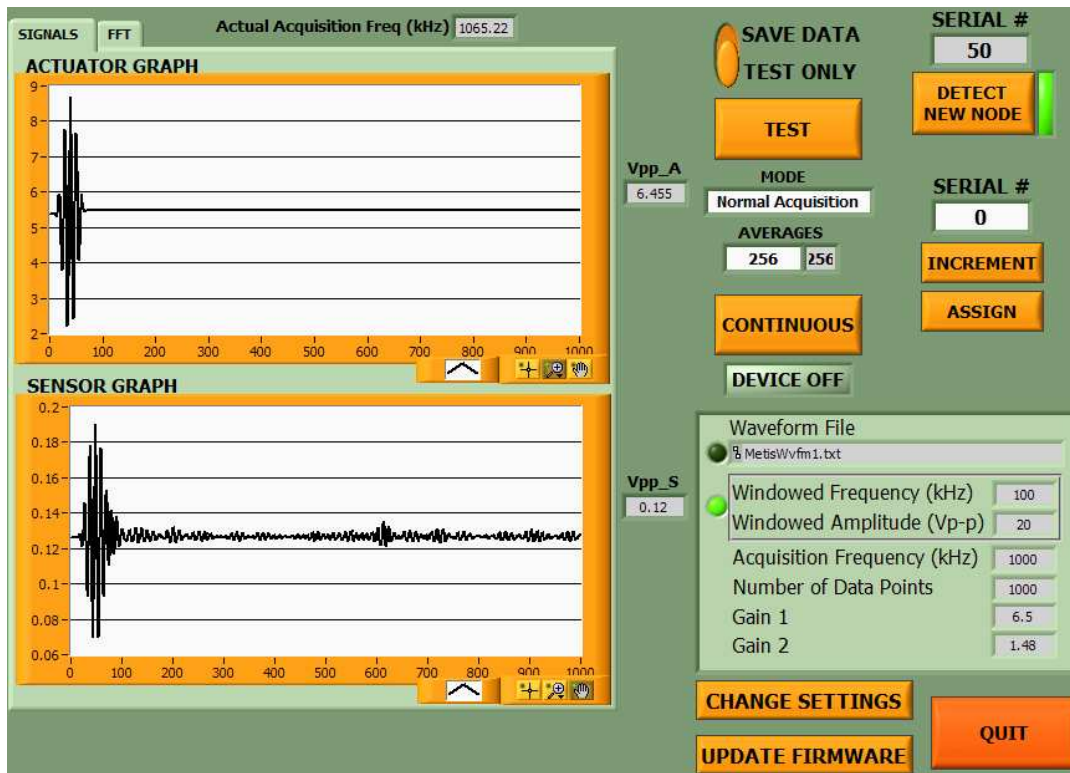
Figure 3.1   Small plate: MD3 Demo program with excitation of 100 kHz
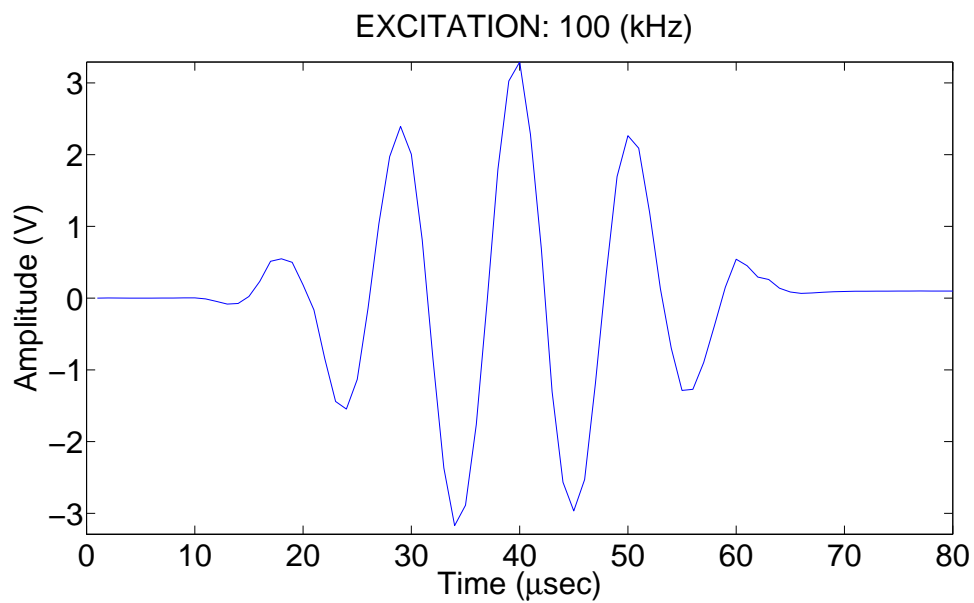

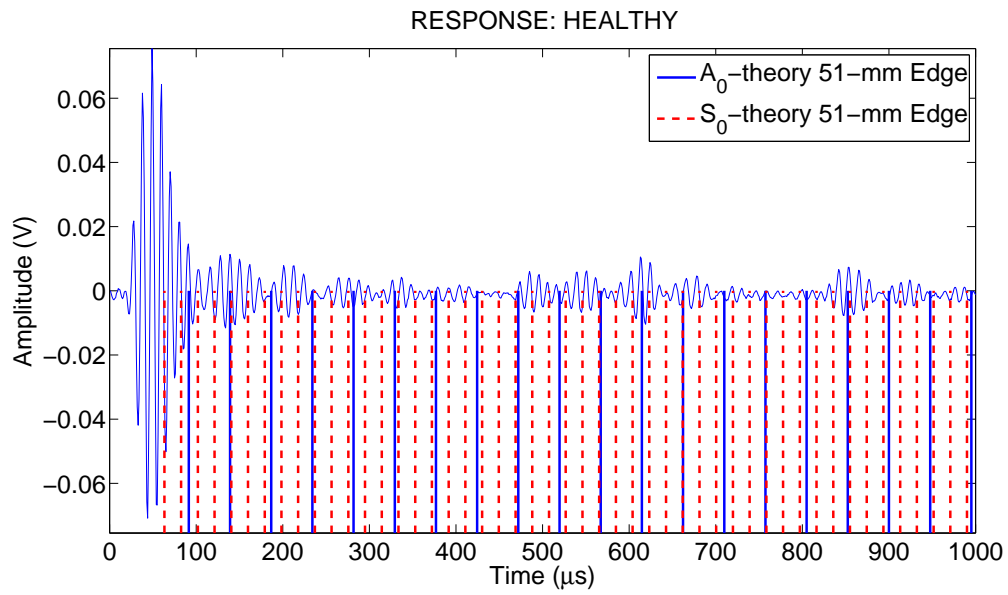Figure 3.2   Small plate: 100 kHz excitation from MD3 Demo program

Figure 3.3   Small plate: 100 kHz response over entire sampling total time window
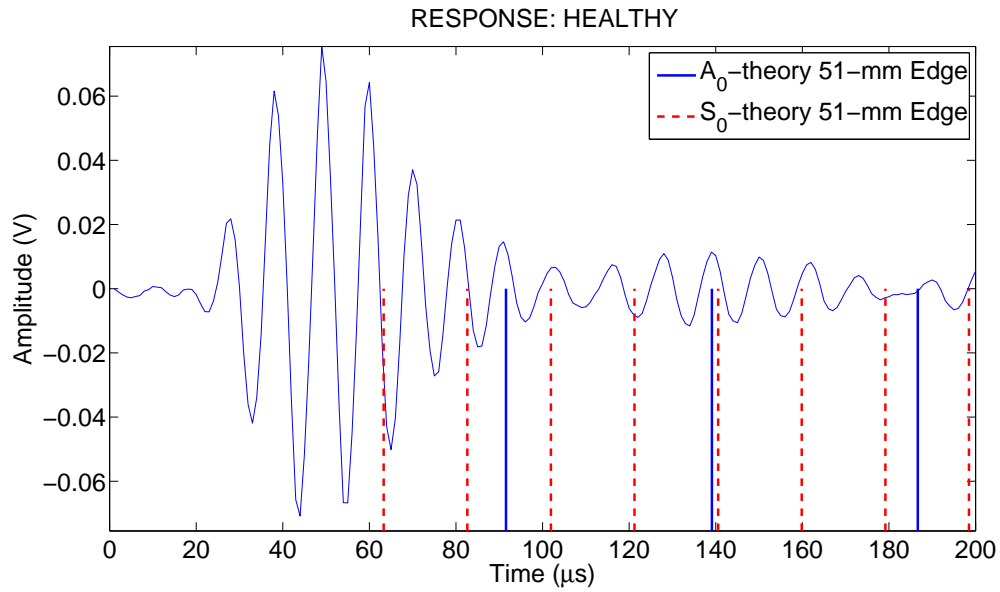

Figure 3.4   Small plate: closeup of 100 kHz response

3-4

We did use the MD3 Testing program on the small plate. The MD3 Testing program was a more capable program. The MD3 Testing program allowed for programming multiple test runs which significantly reduced the testing time. Figure 3.5 shows the layout of the program. The differences between the MD3 Demo and MD3 Testing programs included a reduction in collection samples (800 instead of the 1,000), ability to control time between data set collections, and number of data sets to acquire.
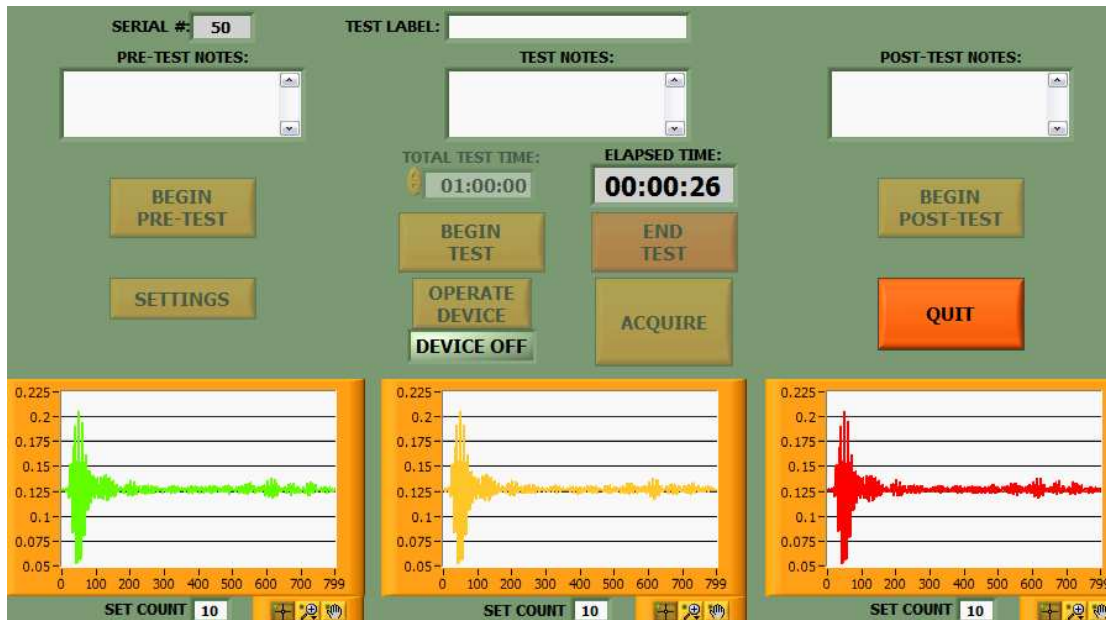
Figure 3.5   Small plate: MD3 Testing program screen capture of small plate at 95 kHz

With the MD3 Demo program, only one data set could be collected. Thus, if the user wanted to collect a thousand healthy data sets to build a healthy data library (for example to use with a pattern recognition algorithm), the user must run every test individually. Another benefit of the MD3 Testing program was the ability to collect pre-test (baseline) responses, testing responses, and post-test responses while displaying these responses graphically to the user, within in the same test. For example, the user can collect a healthy baseline, then collect the response from induced damage in the structure (for example increasing the plate stiffness using

added mass, discussed in Section 2.1.3), and lastly collect the response once the damage was removed to see what affects the damage left in baseline structure.

For both MDC programs, the user has the option to select the number of averages to collect for a given test. Preliminary tests were conducted to determine the number of averages. The tradeoff of the averaging is between testing time and signal-to-noise (SNR). More averaging provides higher SNR, but takes more time. The MD3 Testing program has a maximum averaging value of 255 and the MD3 Demo maximum averaging is 256. We chose 64 averages for our MDC experiments. Figures 3.6 and 3.7 shows the 64 averages plots of the small aluminum plate from both MDC programs. Notice that even between the two programs, the received response amplitudes are different between 300 to 600 μs.

From the small plate we learned that the excessive returns from the boundaries prevented positive identification of the A_0 and S_0 waves. The test results were too complex for initial learning of SHM Lamb wave applications and the damage was not apparent in the measurements. However, the plate did serve as a learning tool for the MDC software and how to apply tuning and dispersion curves to an aluminum test specimen. A larger specimen is required to gain a better understanding of which Lamb wave modes are occurring and if the M.E.T.I.-Disk 3 sensors are producing results predicted by theory.
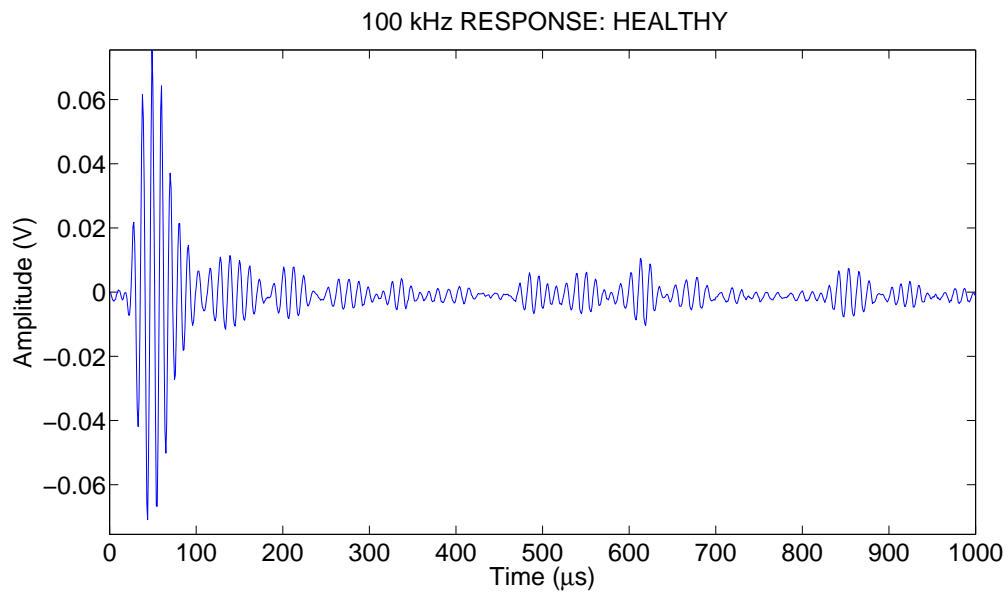
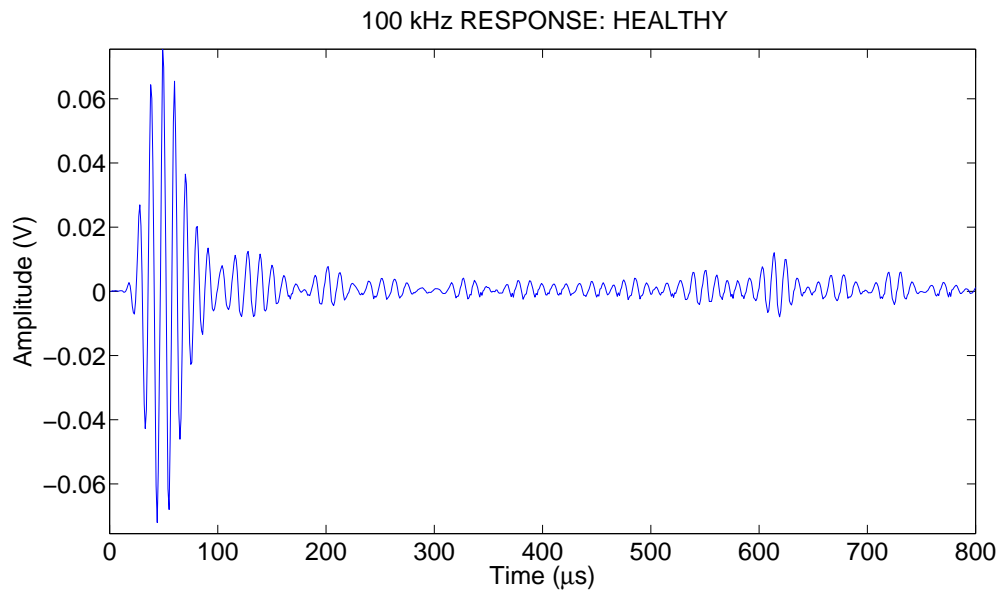Figure 3.6   Small plate: MD3 Demo plot with 64 averages

Figure 3.7   Small plate: MD3 Testing plot with 64 averages

The large aluminum plate specimen is the same thickness as the small plate, but has a M.E.T.I.-Disk 3 sensor attached in the center. The goals are the same as with the first experiment: determine MDC sensor functionality and use the MDC sensor to locate damage in the plate. The larger plate was chosen because we needed an adequate distance between the boundaries so we could distinguish the A_0 from S_0 waves by their arrival times after reflecting off the boundaries or damage. To utilize the pulse-echo technique, dispersion theory must be applied correctly which requires correct identification of the A_0 and S_0 waves. Also, we needed sufficient separation between the sensor and the boundaries to differentiate the signal returns from the damage from the boundary returns. Figure 3.8 shows the healthy response with the theoretical A_0 and S_0 waves plotted for a distance of 380 mm from the sensor, approximately averaged distance between sensor and edges. Recall from the previous chapter that our plate is not square and adjacent edges differed by 23 mm.

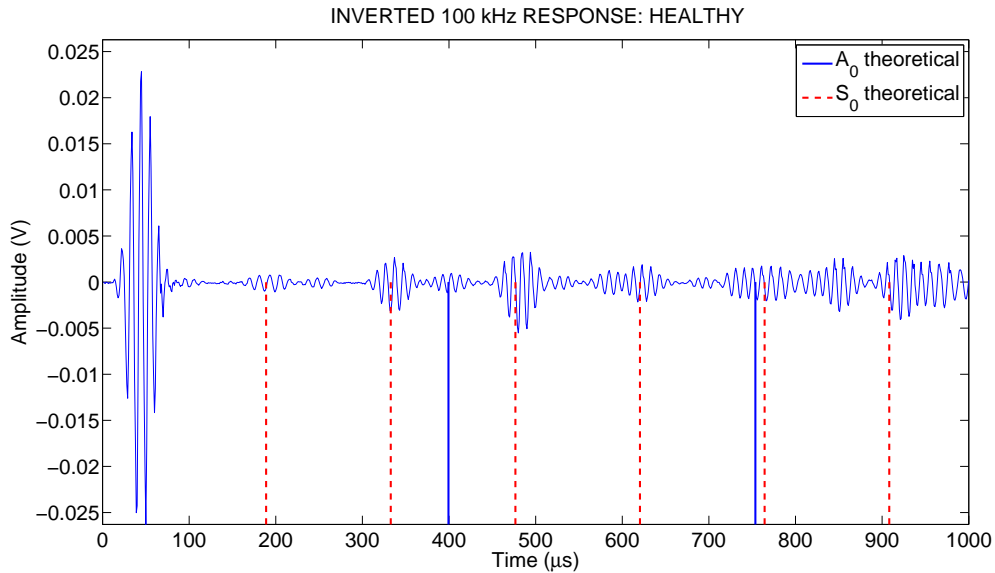Figure 3.8   Large plate: healthy response with predicted A_0 and S_0 waves

We were able to clearly identify the A_0 and S_0 waves in the healthy response from the edge reflections. However, according to the tuning curves, Figure 1.9, at

100 kHz the A_0 wave amplitude should be greater than the S_0 wave amplitude, but this is not the case as shown in Figure 3.8. The first measured A_0 and S_0 wave amplitudes are approximately the same; whereas, the second measured S_0 wave amplitude is much greater than either of the first A_0 and S_0 wave amplitudes. Since our tuning results were not what we expected for the A_0 wave, we moved to testing the specimen at a higher frequency to compare the S_0 wave amplitude.

The next step was to focus on tuning our experiment to excite the S_0 wave. As shown in Figure 1.9, the desired frequency for exciting primarily the S_0 wave is 300 kHz. The sensors are limited to a maximum excitation signal of approximately 250 kHz. Based on our tests, we were only able to generate a useful excitation signal up to 200 kHz, see Figures 3.9 through 3.11. In a piratical sense, the restriction of operating below 200 kHz keeps us focused on using the A_0 wave.

We decided to look at damage detection focusing on tuning with the A_0 wave using a 95 kHz exciting signal. The damage was simulated by placing a 0.05 kg aluminum bar on top of the plate. The aluminum bar measured 100 mm long by 14 mm wide by 12 mm thick. Sonotech Shear Gel was applied to the aluminum bar to ensure coupling with the plate. The front edge of the bar was placed 100 mm from the center of the MDC sensor, aligned length-wise in front of the sensor. Figure 3.12 shows the plot of the healthy versus damaged response. There are differences in the two signals, but nothing of significant magnitude that allowed a positive identification that damage had occurred. Comparing the two signals in Figure 3.12, the A_0 response, located at 400 μs, is clearly seen in the healthy case, but not clear in the damaged case. An edge reflection is masked.

By this time in the study we had narrowed our search for an actual USAF SHM issue to the F-15 bulkhead. A common thread among the different USAF structural issues dealt with small, geometrically complex, areas of varying stiffness and thickness. Because the pulse-echo technique using the MDC sensors was limited, and due to the complex and constrained geometry of the F-15 specimen, we started
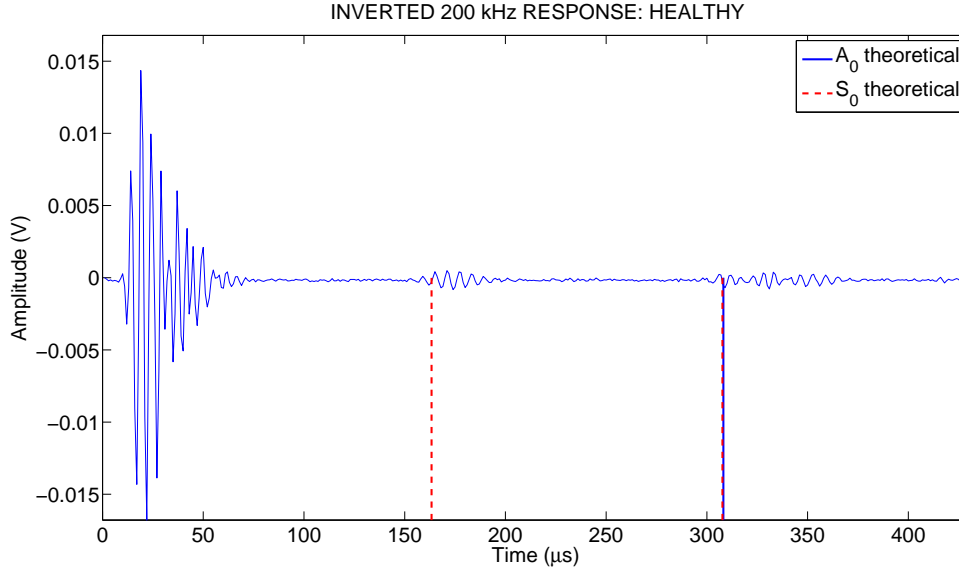
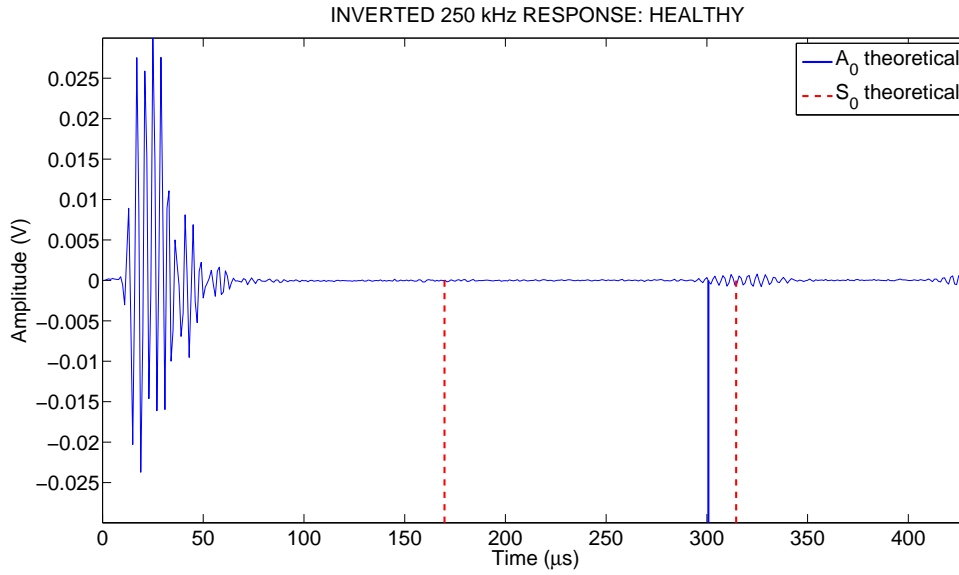Figure 3.9   Large plate: response of a 200 kHz excitation

Figure 3.10   Large plate: response of a 250 kHz excitation

using standard piezos in a pitch-catch technique. We decided to use a pre-existing experimental setup to learn how to implement the pitch-catch technique in our final experiment, the fabricated F-15 specimen. The results from the two pitch-catch experiments are presented in Chapter 4.
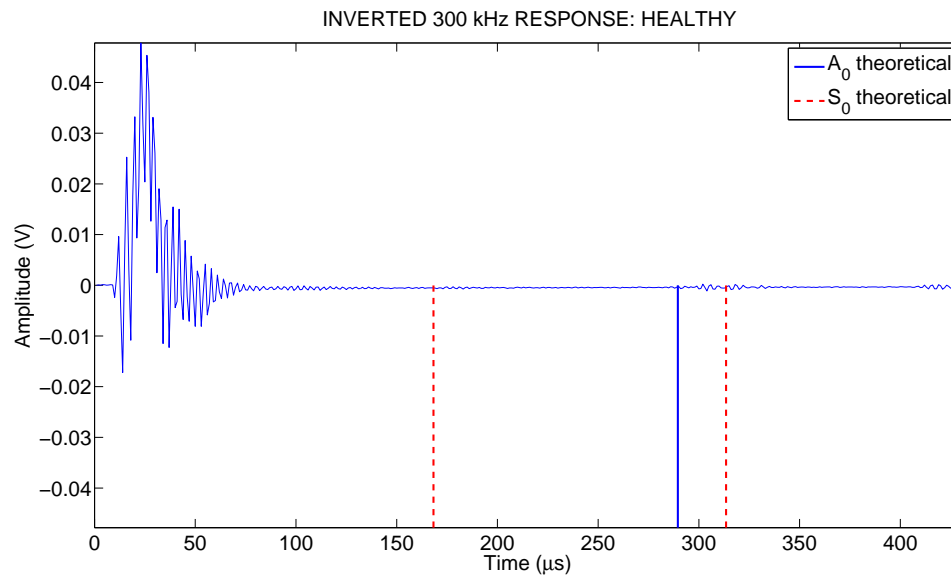
3-10

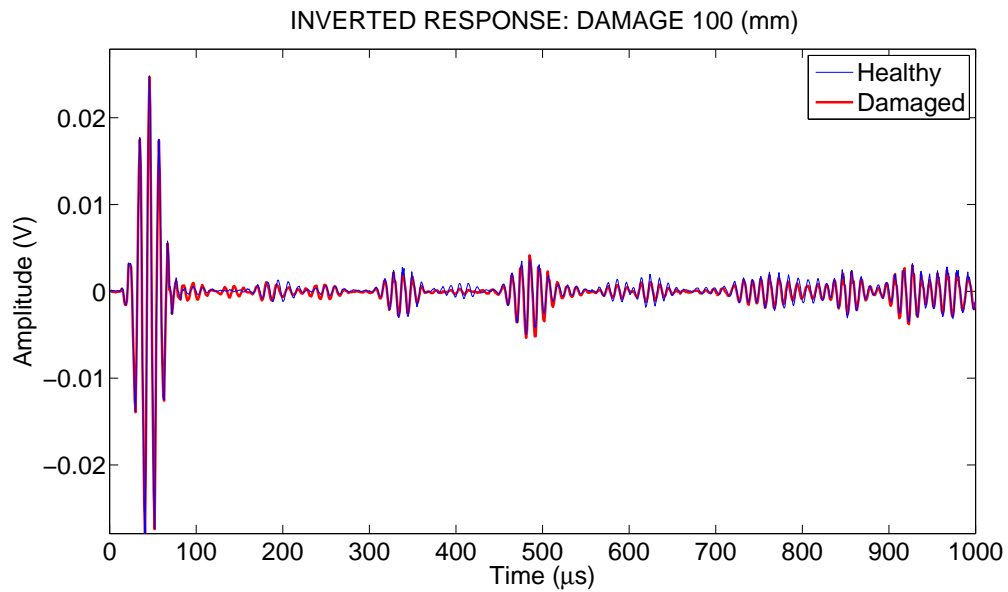Figure 3.11   Large plate: response of a 300 kHz excitation

Figure 3.12   Large plate: healthy versus damaged response of a 95 kHz excitation

3-11

IV. Results and Analysis: Pitch-Catch

This chapter presents the results of the Lamb wave experiments using the pitch-catch techniques and compares the results to theoretical calculations. Also, this chapter focuses on our goal to determine if damage can be located in a more realistic test specimen. The pitch-catch experiments were conducted using two different test specimens. The first specimen was a thin aluminum plate used to validate and refine experimental pitch-catch methods for final experimentation, the fabricated aluminum F-15 specimen.

4.1 Multi-Purpose Panel (MPP) Aluminum Plate

The purpose of this experiment was to learn and validate the SHM Lamb wave technique of pitch-catch for detecting a crack. We collected responses from both the healthy (upper half) and damaged (lower half) section of the MPP. In the experiment, we used an excitation frequency range of 50 kHz to 500 kHz in increments of 5 kHz. The processing of the data, i.e., comparing experimental results to theocratical calculations, was accomplished using MATLAB. Figures 4.1 and 4.2 show the healthy and damaged experimentally measured A_0 and S_0 wave dispersion curves compared to theoretical dispersion curves. Recall that the structure was excited at piezo 5, and the responses was collected at piezos 11 and 20. The locations for piezos 11 and 20 were, respectively, in the healthy and damaged regions of the MPP. The measured A_0 wave dispersion for the healthy region more closely matches the theoretical curve than the damaged region's measured results. However, the measured S_0 wave for both regions (healthy and damaged) appears equally distributed about the theoretical dispersion curves.

The A_0 and S_0 waves were confirmed by locating the maximum peak amplitude within in a bounded region of the response coinciding with the theoretical calculations for the group velocities (Figures 4.3 and 4.4). The measured time associated

with the peak amplitude is used to calculate the experimental group velocity using the distances between the fixed APC 850 piezo locations (the pitch and catch sensor). The small circle on the peak responses in Figures 4.3 and 4.4 correspond to the maximum values within the bounded regions. The maximum amplitude values of the measured A_0 and S_0 wave are plotted in Figures 4.5 and 4.6 for the frequency range of the MPP experiment. Comparing Figures 4.5 and 4.6, we can see significant changes in peak amplitudes for the A_0 wave between 125 kHz to 250 kHz and the S_0 wave between 150 kHz to 500 kHz. The best frequency for crack damage detection, based on the maximum decrease in peak frequency, corresponds to the S_0 wave at 410 kHz.

Figures 4.7 through 4.9 show the comparison between collected healthy and damaged responses for three frequencies (55 kHz, 150 kHz, and 410 kHz). The 55 kHz response was chosen to show the slight differences between the healthy and damaged responses for a low frequency-thickness product of 55 kHz-mm; thus, revealing that this low frequency is not a good choice for crack damage detection. The 150 kHz and 410 kHz responses was selected to show the substantial difference in signal responses for the A_0 and S_0 waves.
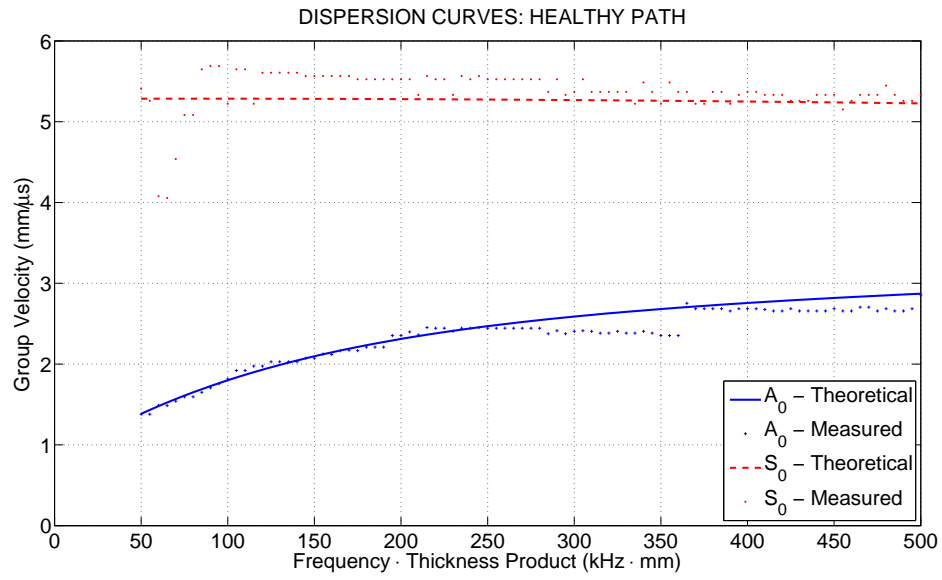
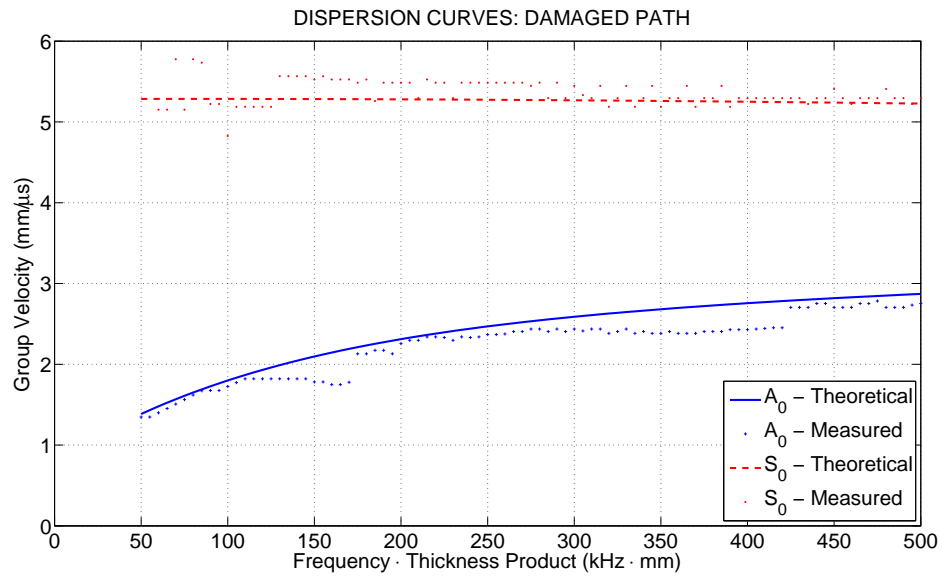Figure 4.1   MPP: healthy dispersion curves

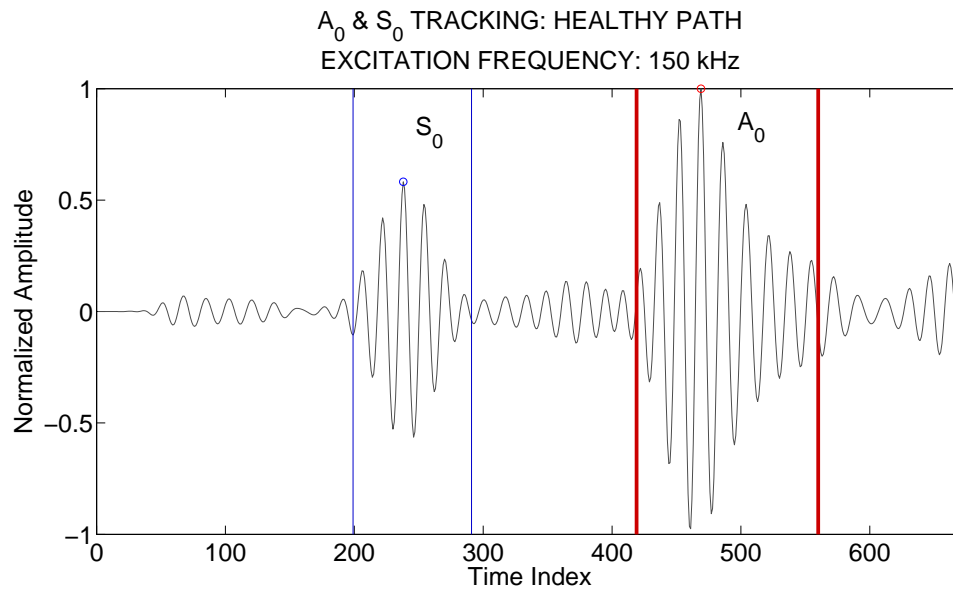Figure 4.2   MPP: damaged dispersion curves

Figure 4.3   MPP: healthy tracking plot of 150 kHz response at piezo 11
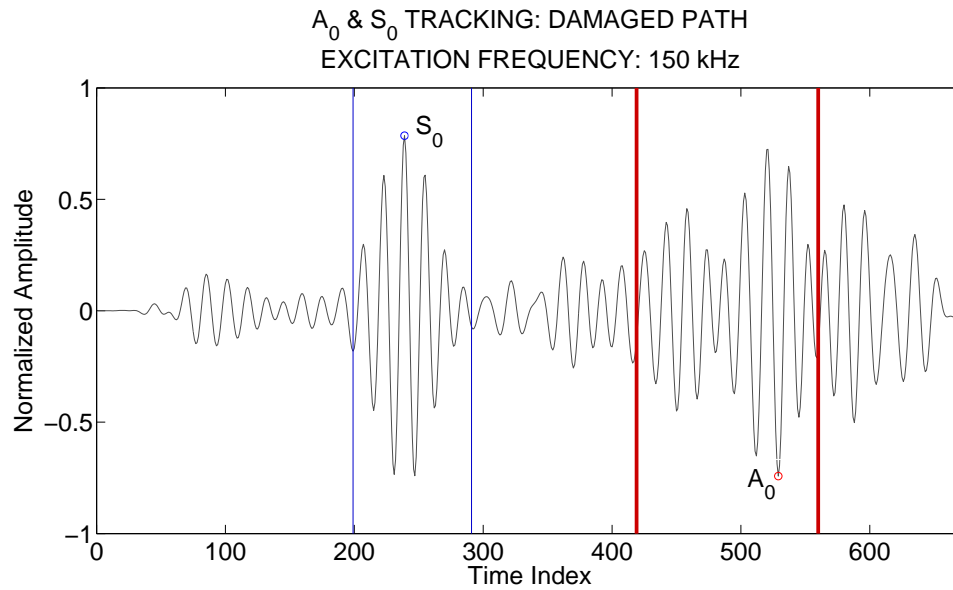

Figure 4.4   MPP: damaged tracking plot of 150 kHz response at piezo 20
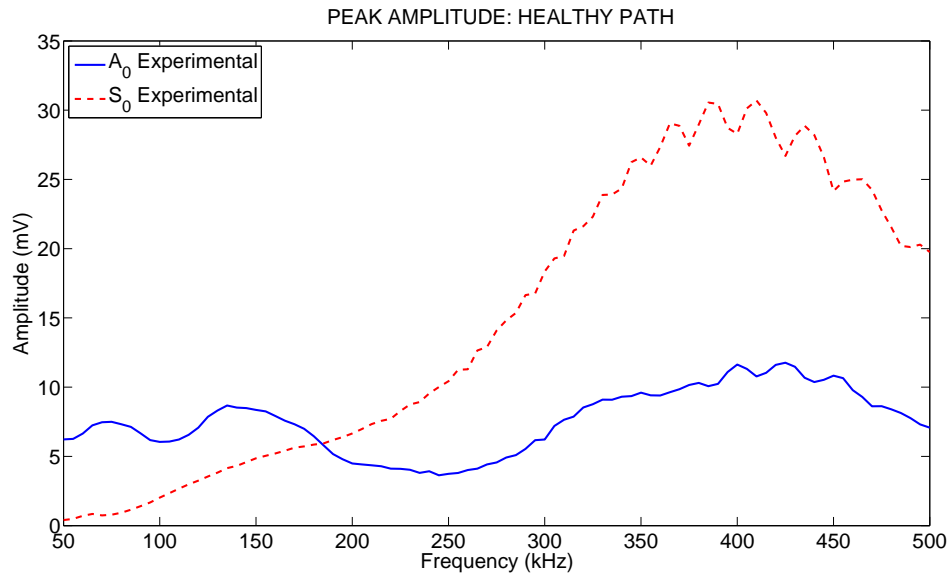
Figure 4.5   MPP: healthy peak amplitudes measured at piezo 11
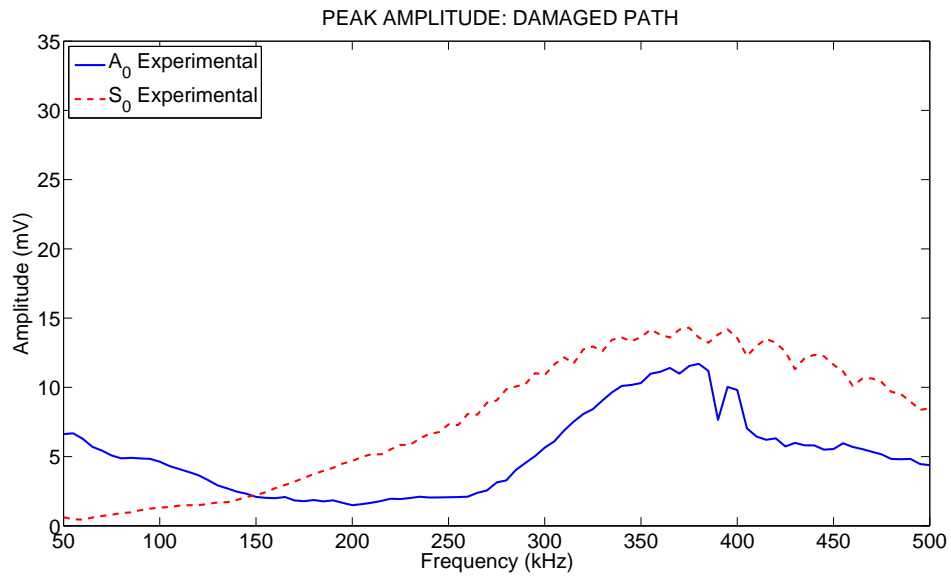

Figure 4.6   MPP: damaged response peak amplitudes measured at piezo 20
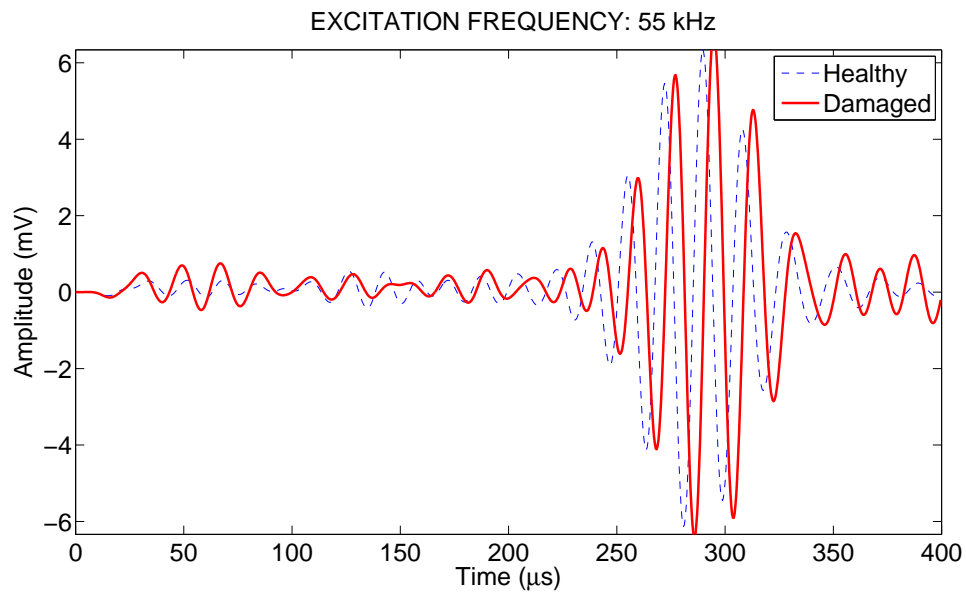
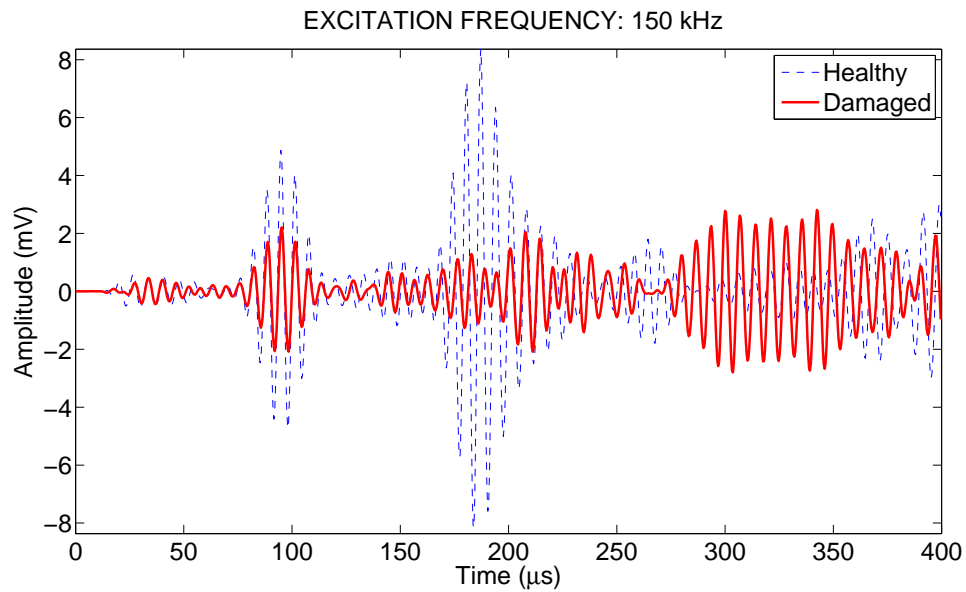Figure 4.7   MPP: healthy vs. damaged response at 55 kHz excitation

Figure 4.8   MPP: healthy vs. damaged response at 150 kHz excitation
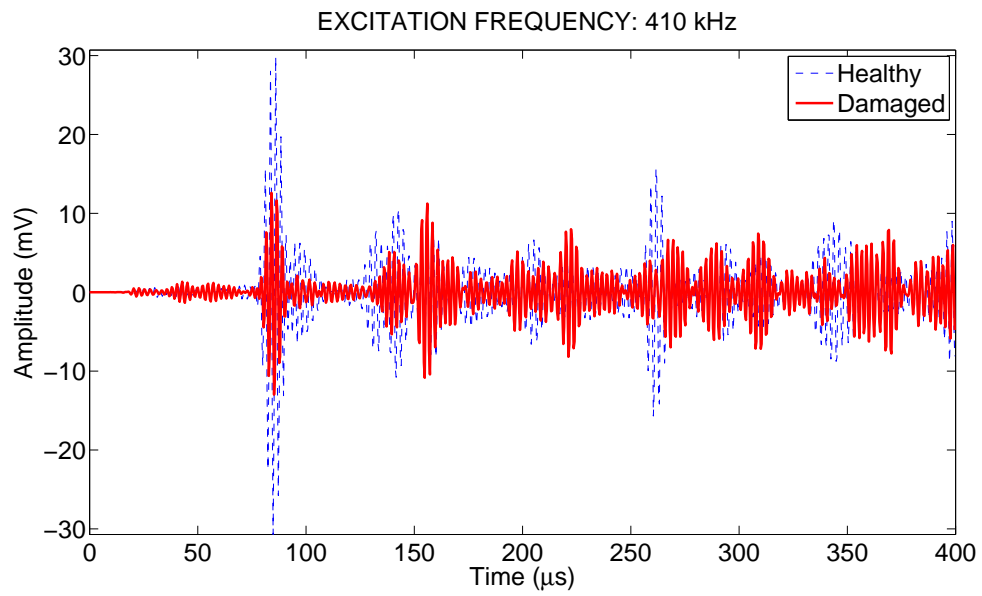
Figure 4.9   MPP: healthy vs. damaged response at 410 kHz excitation

4.2   F-15 Simulated Bulkhead

Our final experiment was designed to achieve the goal of implementing a SHM technique for a realistic USAF application. The experimental procedures followed the techniques developed in the MPP experiment. The experiment involved four phases, which included a healthy collection phase and three damage collection phases. The three damage collection phases correlated to the three incremental EDM cuts.

The first phase tested the simulated bulkhead in its healthy state. We repeated the healthy test collection to ensure the experiment was producing similar results; however, our first attempts at ensuring the test was repeatable was unsuccessful, see Figure 4.10. We isolated the cause to the RG-58/U coaxial cables connecting the F-15 specimen to the voltage divider and junction connector. We corrected the faulty cabling by exchanging the general purpose RG-58/U coaxial cables for a low-noise PCB Piezotronics cable assembly, Model 003D20.
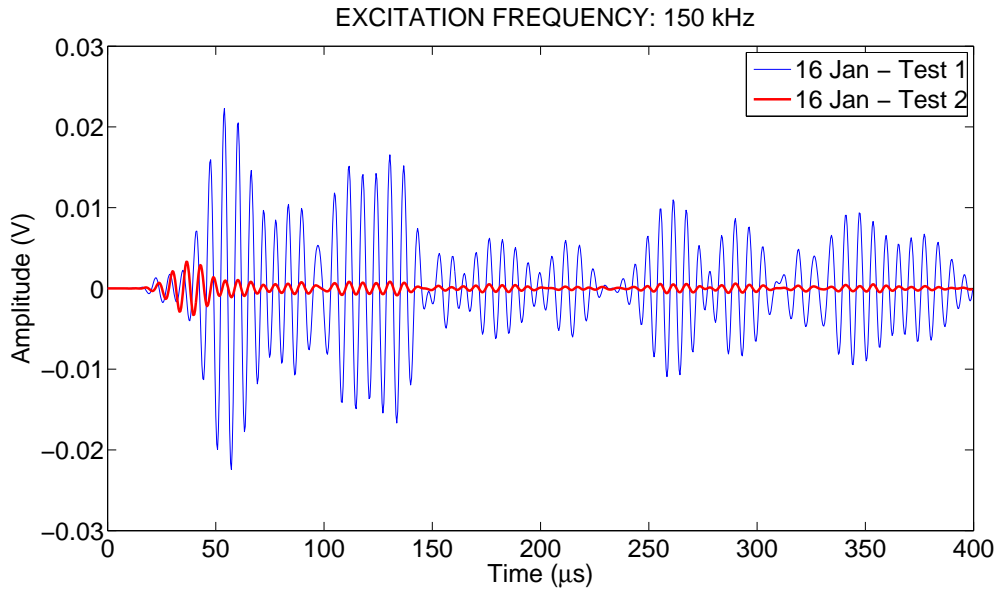

Figure 4.10   F-15: unsuccessful healthy responses repeatability at piezo 4 from piezo 3 excitation

Once the faulty cabling was corrected, we started our healthy baseline response collection. We collected three healthy responses for the frequency range of 50 kHz to

800 kHz in increments of 10 kHz for the healthy response baseline. During the experiment, we wanted to know if the surface the specimen rested on affected the results. Two responses were collected with the simulated bulkhead resting on soft foam, and then compared to a response with the specimen resting directly on the metal lab table. Figure 4.11 shows the comparison plot between the responses collected with the specimen on the lab table and on the foam. There are differences in the signal responses, but the differences were only slight sporadic changes in amplitude. We concluded that the surface which the specimen rests upon appears not to have a direct affect on the response.
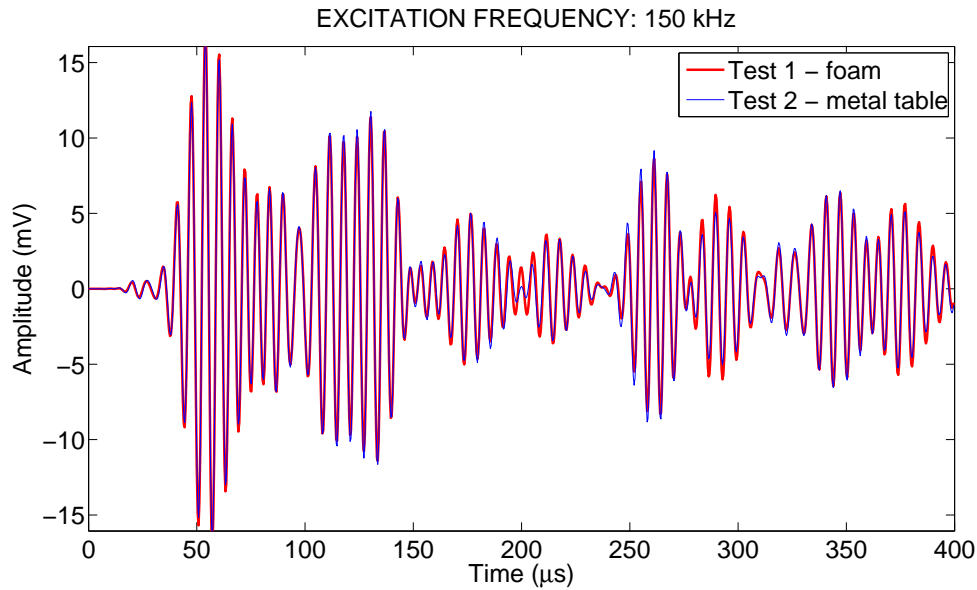

Figure 4.11   F-15: comparison of healthy responses of piezo 4 from piezo 3 excitation

Once we were confident in our healthy baseline results, we moved on to the second phase of the experiment, the first EDM cut. Since an EDM machine uses pressurized distilled water during cutting and our six attached piezos were going to be exposed to this water environment, we measured the impedance of the six piezos before the first cut. After each EDM cutting phase, we tested the piezos for impedance changes. Based on the impedance measurements as well as the wave

propagation signals, we concluded that the exposure to water did not appear to have any significant adverse affects on the six piezos during all three cutting phases.

Figure A.1 shows the peak amplitude responses received at piezo 2 from piezo 1 excitation for all four phases (healthy and the three cuts). Notice the drop in peak amplitude between the healthy state and the three cuts. We would expect all three post cut responses to be the same since the first cut was made between piezo 1 and piezo 2. The peak amplitude response curves were created by finding the peak amplitude in the entire response. We did not use a widow as in the MPP experiment.

Figures 4.12 through 4.14 compare the 100 kHz healthy and damaged responses from piezo 2 and shows how the response changed. The 100 kHz excitation frequency was chosen for its separation between pre-cut and cut responses (Figure A.1) and to avoid analysis of a response where many dispersion modes exists. Piezo 1 and piezo 2 are bonded to the 6 mm lower horizontal stiffener; thus, the range of frequency-thickness products for the excitation frequencies of 50 kHz to 800 kHz was 300 kHz-mm to 4800 kHz-mm (0.3 MHz-mm - 4.8 MHz-mm).
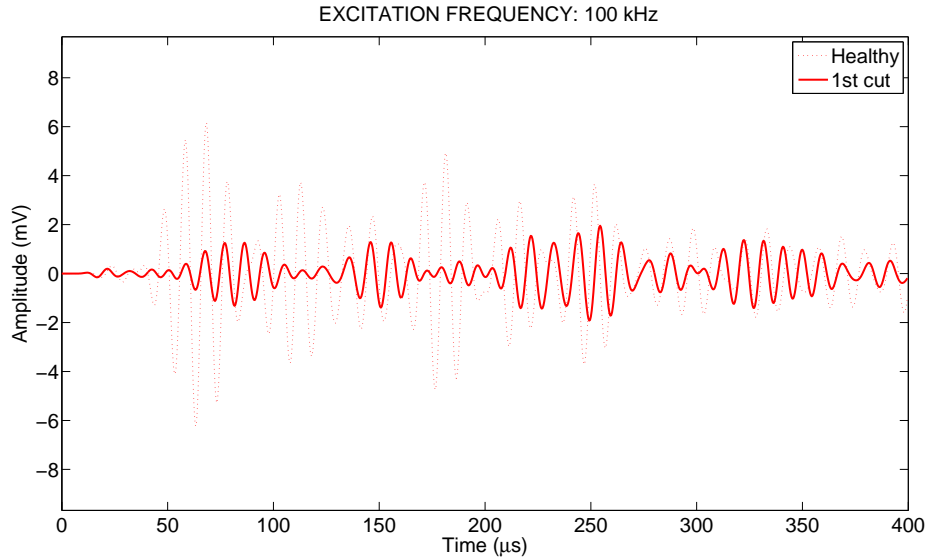

Figure 4.12   F-15: healthy compared with 1st cut of piezo 2 response from piezo 1 excitation
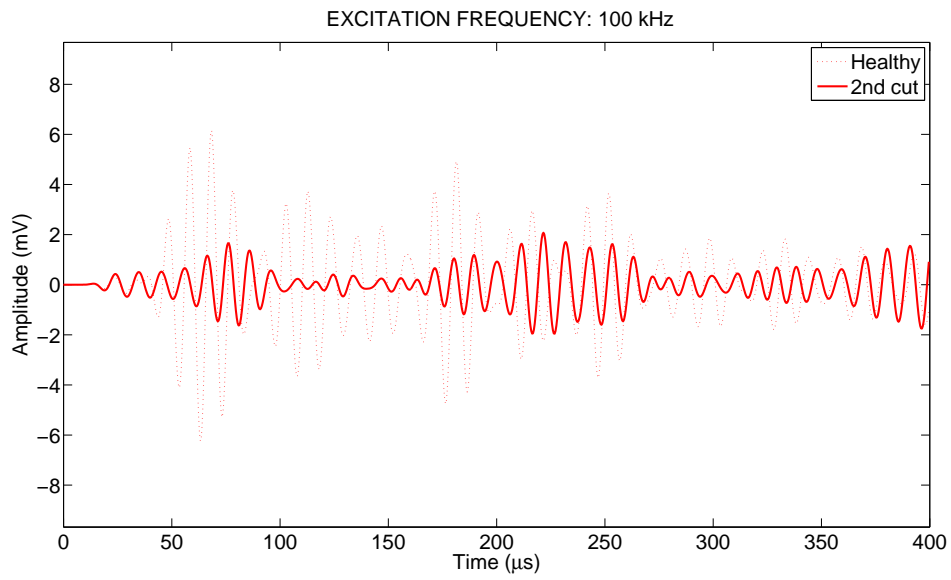
Figure 4.13   F-15: healthy compared with 2nd cut of piezo 2 response from piezo 1 excitation
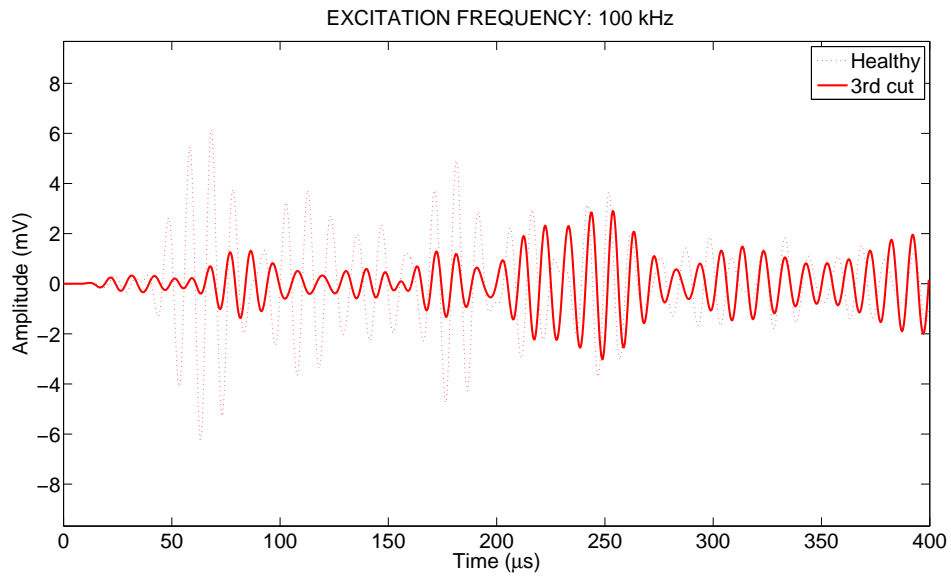

Figure 4.14   F-15: healthy compared with 3rd cut of piezo 2 response from piezo 1 excitation

Figure A.13 shows the peak amplitude responses received at piezo 4 from exciting piezo 3 for all four phases. Based on the decrease in peak amplitude shown in Figure A.1, we expected a drop in peak amplitude after the second cut was made. In Figure A.13, the peak signal response did drop for the second and third EDM cut, but not the first cut. Also, there is even a further drop in the signal response between the second and third cut. This makes sense that a drop in signal response was detected once the cut was made between the pitch-catch path of piezos 3 and 4.

Figures 4.15 through 4.17 compare the 150 kHz healthy and damaged responses from piezo 4 and shows how the entire response changed. Choosing a low frequency with reasonable separation is still good practice when working with Lamb waves. The 150 kHz response was chosen, instead of the 100 kHz, for its separation between pre-cut and cut responses (Figure A.13). We are now operating in the 3 mm bulkhead section; thus, our frequency-thickness product range is 150 kHz-mm - 2400 kHz-mm (0.15 MHz-mm - 2.4 MHz-mm).
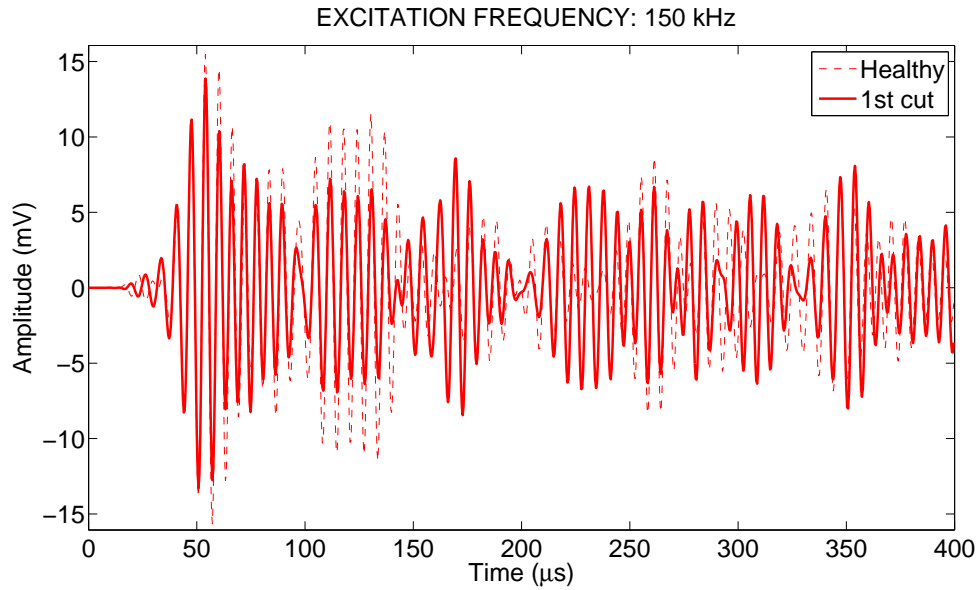

Figure 4.15   F-15: healthy compared with 1st cut of piezo 4 response from piezo 3 excitation
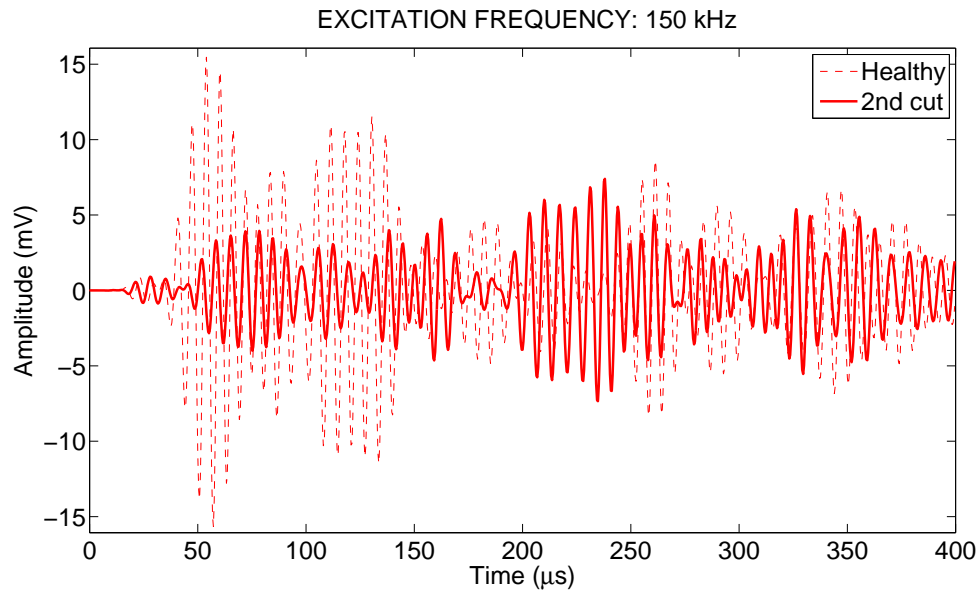
Figure 4.16   F-15: healthy compared with 2nd cut of piezo 4 response from piezo 3 excitation
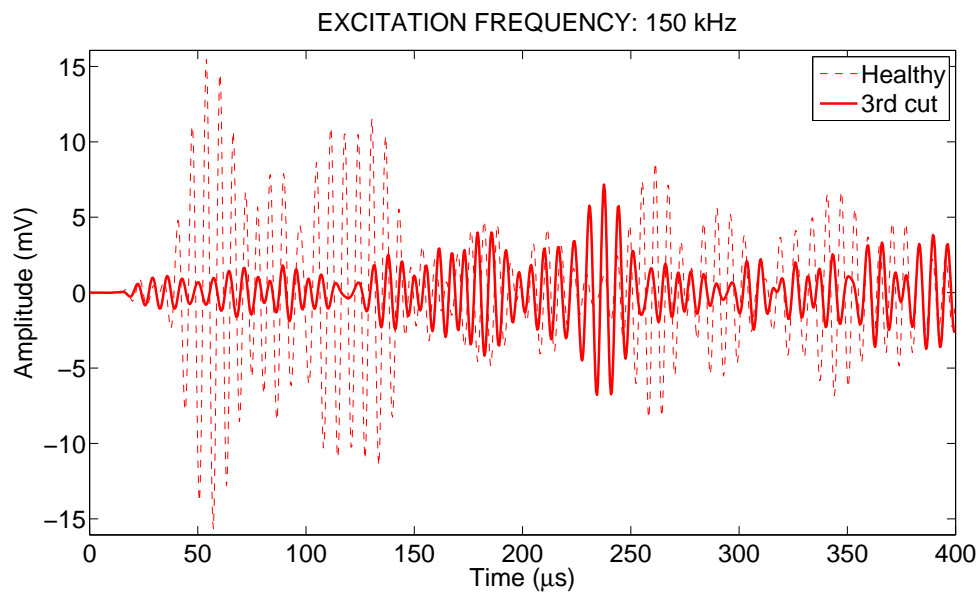

Figure 4.17   F-15: healthy compared with 3rd cut of piezo 4 response from piezo 3 excitation

Our last trial compares the responses of piezo 6 from exciting piezo 5. Once again, based on what we observed before, we expected to see a strong drop from only the third EDM cut. As expected, Figure A.25 shows a substantial change for the peak response as a result of only the third EDM cut. Figures 4.18 through 4.20 compare the 200 kHz healthy and damaged responses from piezo 6 and show how the response changed.

In Figures A.1, A.13, and A.25, a maximum peak amplitude existed at approximately 500 kHx. Looking at the peak amplitude response curves, we are naturally drawn towards the large drop in peak amplitude around 500 kHz. Figure 4.21 shows the large drop between the healthy and damaged response of piezo 6 at 500 kHz when an EDM cut is in the path between sending and receiving sensors. Although operating at large frequency-thickness products makes detailed waveform analysis difficult or impossible, an empirical method appears to have potential for robust crack detection.

This research explored the use of piezoelectric sensors as a means to detect damage in metallic structures. In Chapter 5 the results of the four experiments are summarized and conclusions are drawn. Also, recommendations for future work using Lamb wave SHM are provided.
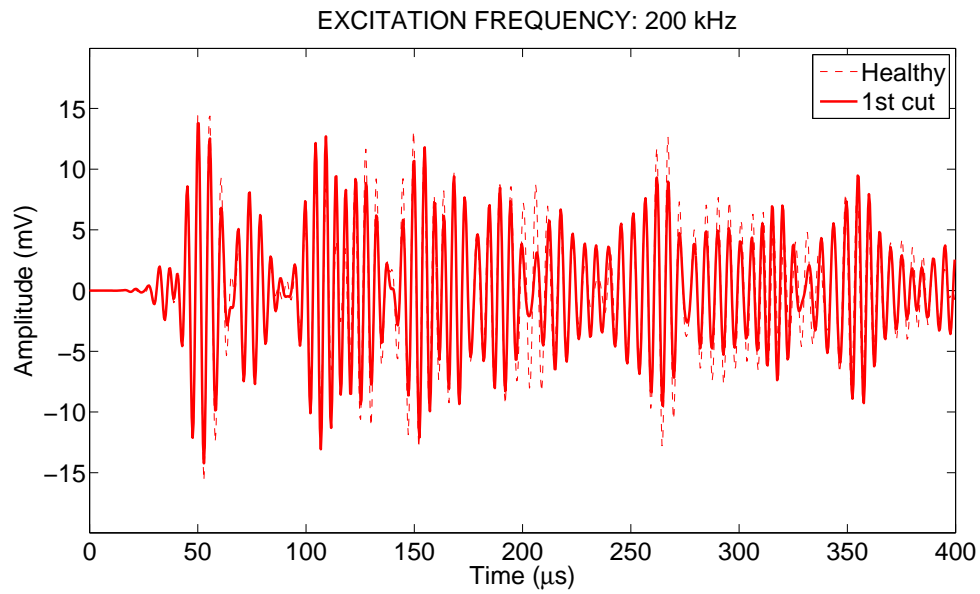
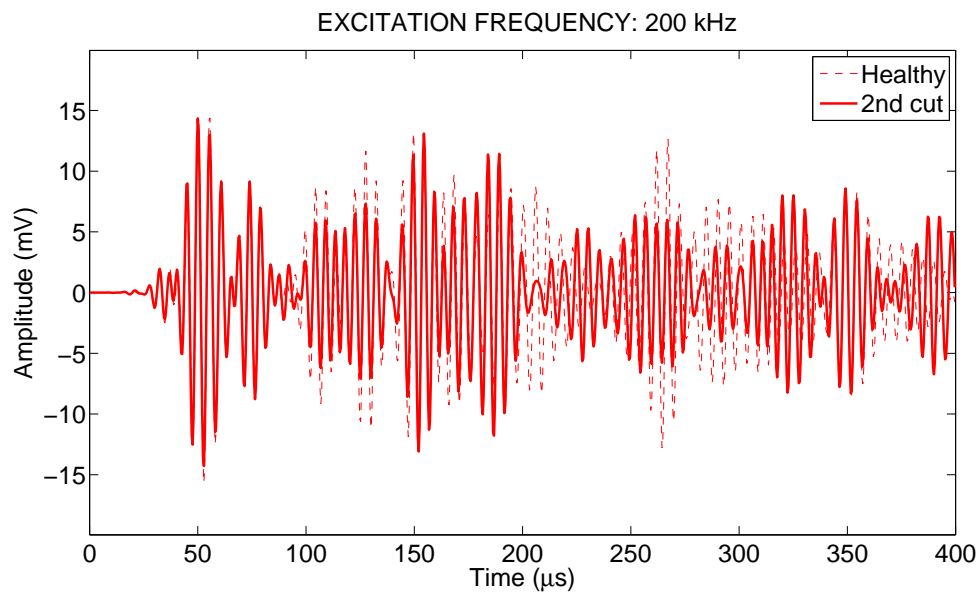Figure 4.18   F-15: healthy compared with 1st cut of piezo 6 response from piezo 5 excitation

Figure 4.19   F-15: healthy compared with 2nd cut of piezo 6 response from piezo 5 excitation
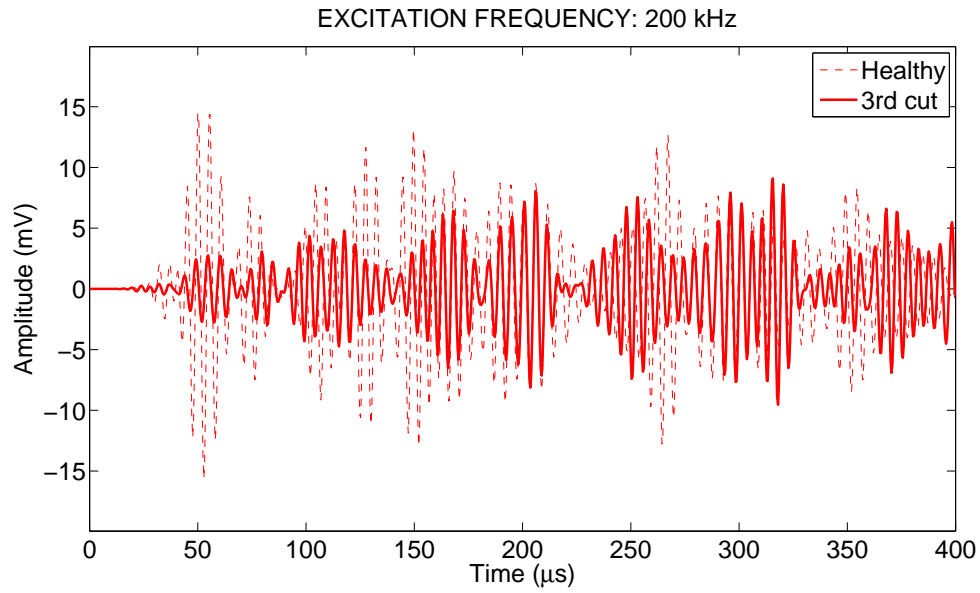
Figure 4.20   F-15: healthy compared with 3rd cut of piezo 6 response from piezo 5 excitation
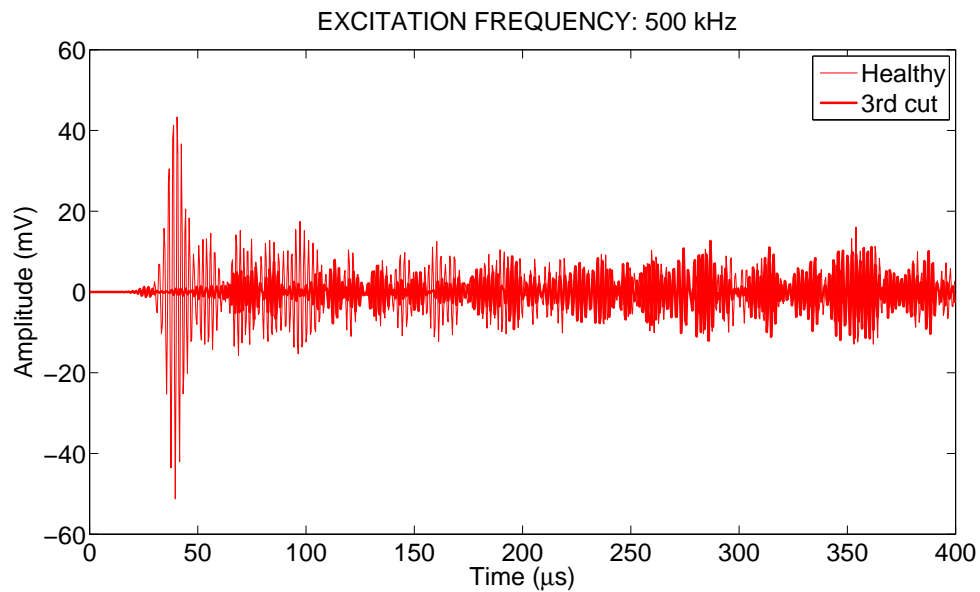

Figure 4.21   F-15: 500 kHz responses at piezo 6 for healthy vs. 3rd cut damaged from piezo 5 excitation

V. Conclusions and Recommendations

5.1 Conclusions

This thesis presented an experimental study of SHM Lamb wave methods using pitch-catch and pulse-echo techniques for damage detection in metallic structures. The goal for this thesis was to evaluate existing Lamb wave methods for damage detection with a realistic USAF SHM issue. The goal was accomplished through extensive testing of four aluminum test specimens using both pitch-catch and pulse-echo SHM techniques for damage detection.

We determined M.E.T.I.-Disk 3's capabilities and identified limitations for implementation into a SHM damage detection system. We were able to generate results consistent with theoretical calculation using the M.E.T.I.-Disk 3 sensor for undamaged structures using low frequencies. Based on our results, the M.E.T.I.-Disk 3 was designed for applications in composite structures where lower frequencies are used. We concluded that the best method for crack damage detection within a constrained geometry is the pitch-catch technique because it reduces the effect of the interference of reflected waves off the boundaries. The M.E.T.I.-Disk 3 was not capable of operating in the pitch-catch mode so another piezoceramic transducer was used, allowing for a broader excitation frequency range with a sufficient amplitude response.

We were able to identify the EDM crack damage in the simulated bulkhead and MPP using the pitch-catch method. Since the excitation transducer was fixed to the structure, the repeatability of the measurements was expected to be excellent. However, we learned that the type of cable used greatly affects the repeatability. After choosing the proper cable, our measurement method provided good accuracy and repeatability.

Most importantly, we were able to successfully transition from large thin plate experiments to implementing the pitch-catch technique on a realistic USAF structure. An experimental demonstration on a simulated bulkhead identified when an

EDM notch cut the path between transducers. Also, operating at higher frequencies provided the most noticeable change in structural integrity leading to our damage detection predictions. With the ability to identify the broken paths from the peak amplitude response, we are able to make a crude prediction of EDM cut length. For crude damage detection, the number of attached sensors directly relates to a more refined damage location prediction.

5.2   Recommendations

Much work still remains before current SHM systems can be relied upon to replace standard maintenance inspections. Further study of Lamb wave SHM should be investigated due to the potential benefit of reducing costly maintenance inspections. Also, a future SHM application well-suited for using Lamb waves is in space borne assets where "hands-on" maintenance is not feasible or possible. One possible topic for future research in the field of Lamb wave SHM includes the natural progression to real crack detection. The EDM cuts removed material from the test specimens, which is drastically different than real cracks that have sharp edges and other effects such as crack closure. We recommend exploring the detection of real cracks in loaded and unloaded cases while identifying crack detection limitations, i.e., crack depth and crack length. Another important damage category to explore using Lamb waves is corrosion.

This study was able to make crude damage location predications; however, with further processing, the ability to accurately locate and pin-point damage within the structure should be possible without attaching an excessive amount of sensors. Our final test specimen involved thicknesses of 3 to 6 mm, and a simple change detection approach was used. The largest amplitude difference between healthy and damaged occurred at high frequency-thickness products. However, at high frequency-thickness products many modes co-exists. Further exploration into the higher Lamb wave modes should be conducted. Also, validation of these results to theoretical

calculations was not approached; thus, our last recommendation is validation of these results with theoretical analysis.

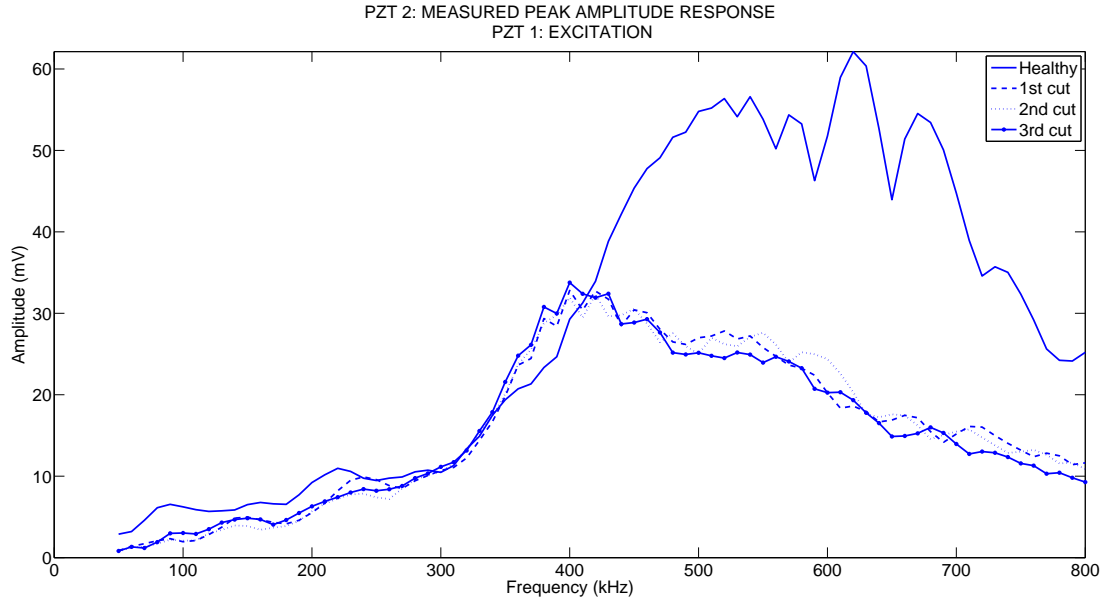## Appendix A. Peak Amplitude Figures for the F-15

PZT 2: MEASURED PEAK AMPLITUDE RESPONSE
PZT 1: EXCITATION

Figure A.1   F-15: peak amplitude comparison of piezo 2 response from piezo 1 excitation

PZT 3: MEASURED PEAK AMPLITUDE RESPONSE
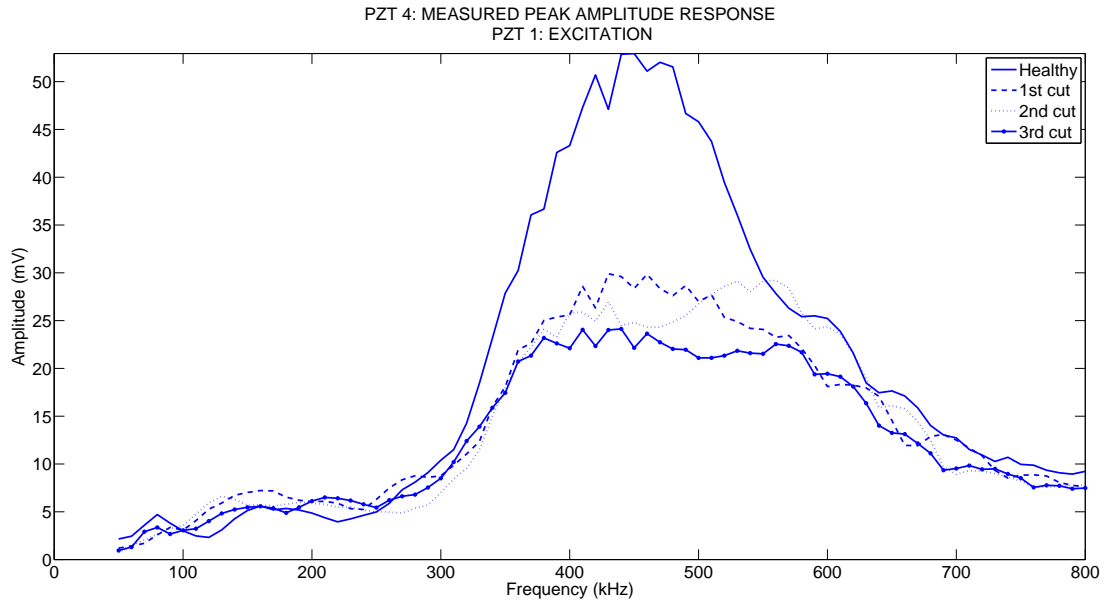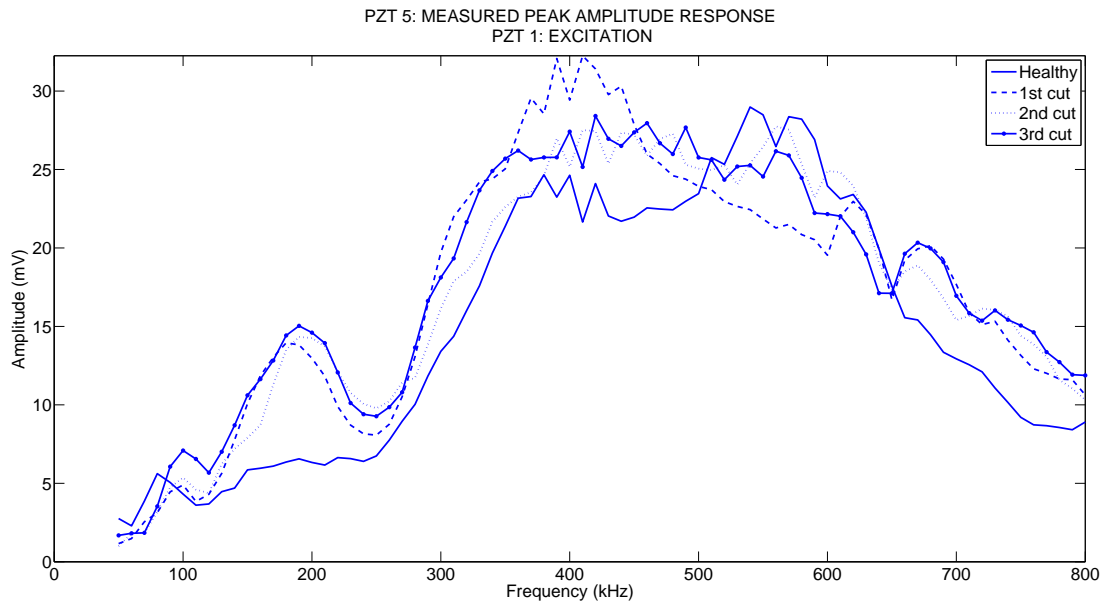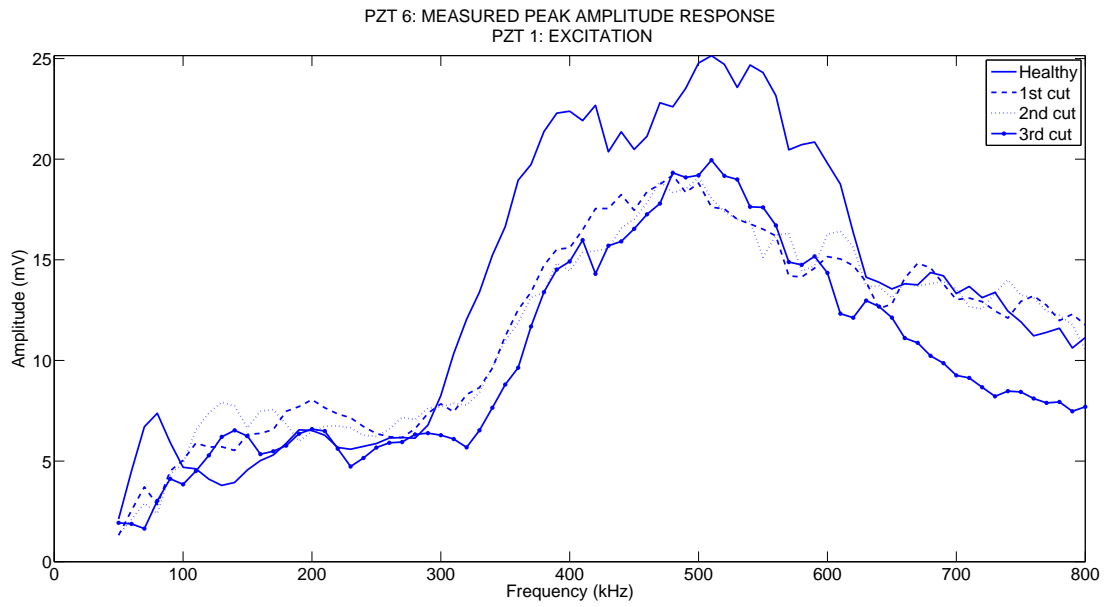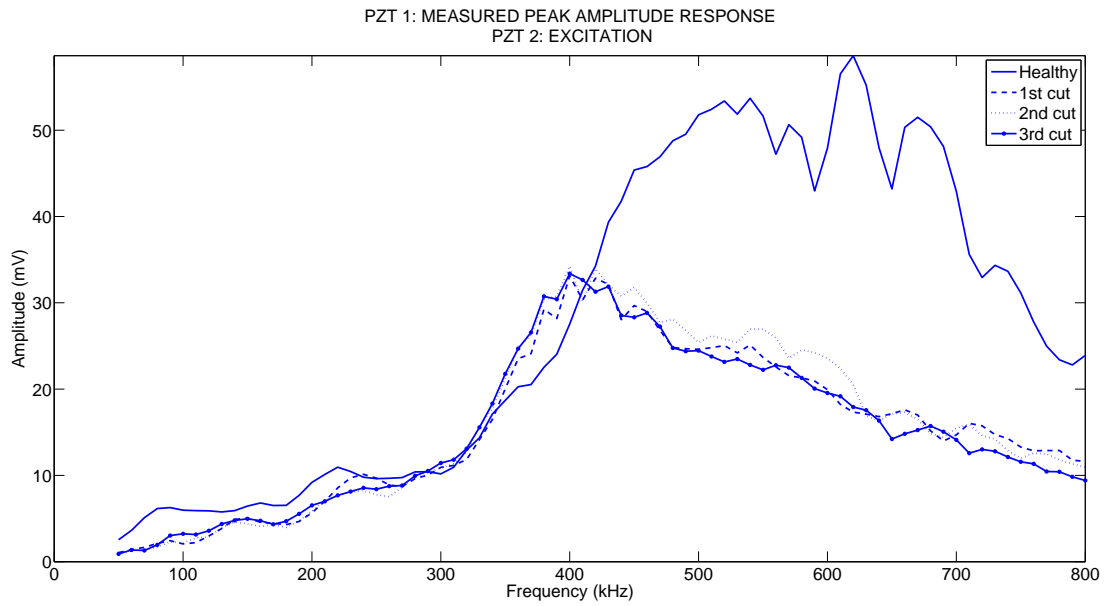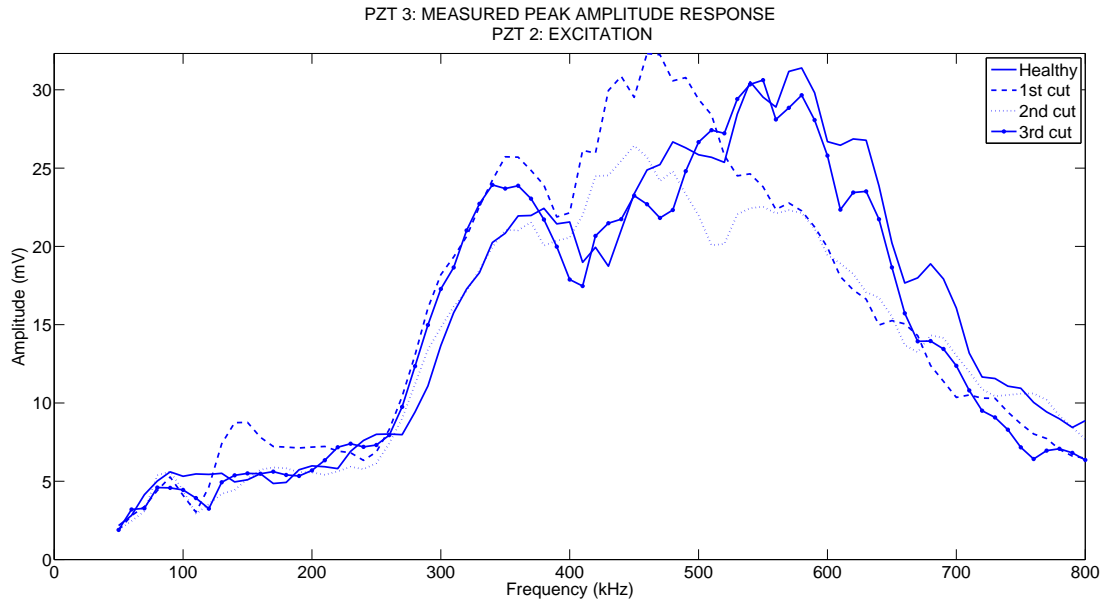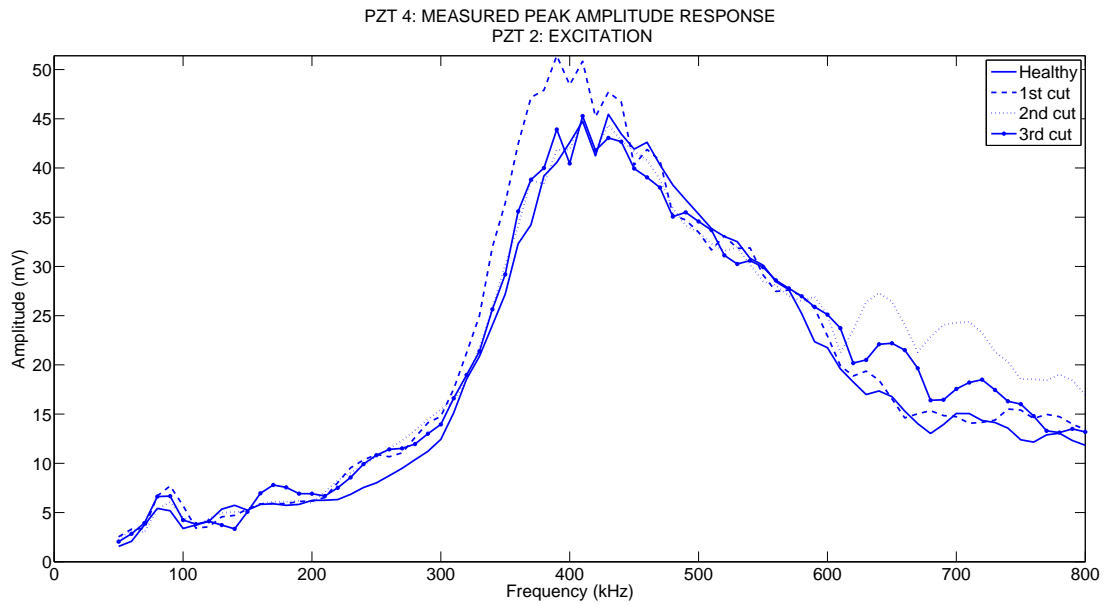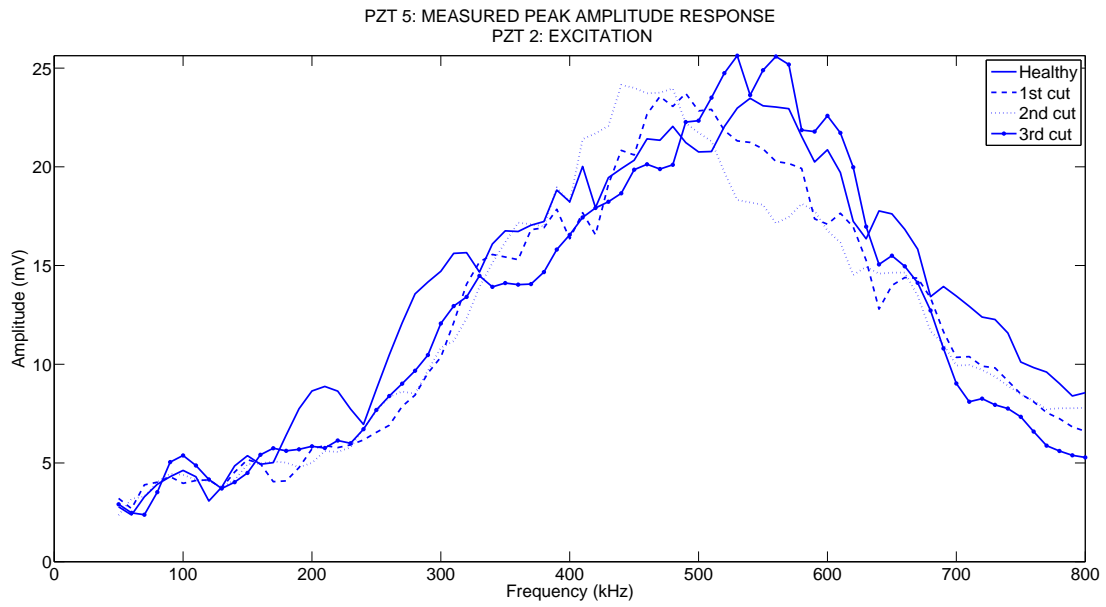PZT 1: EXCITATION
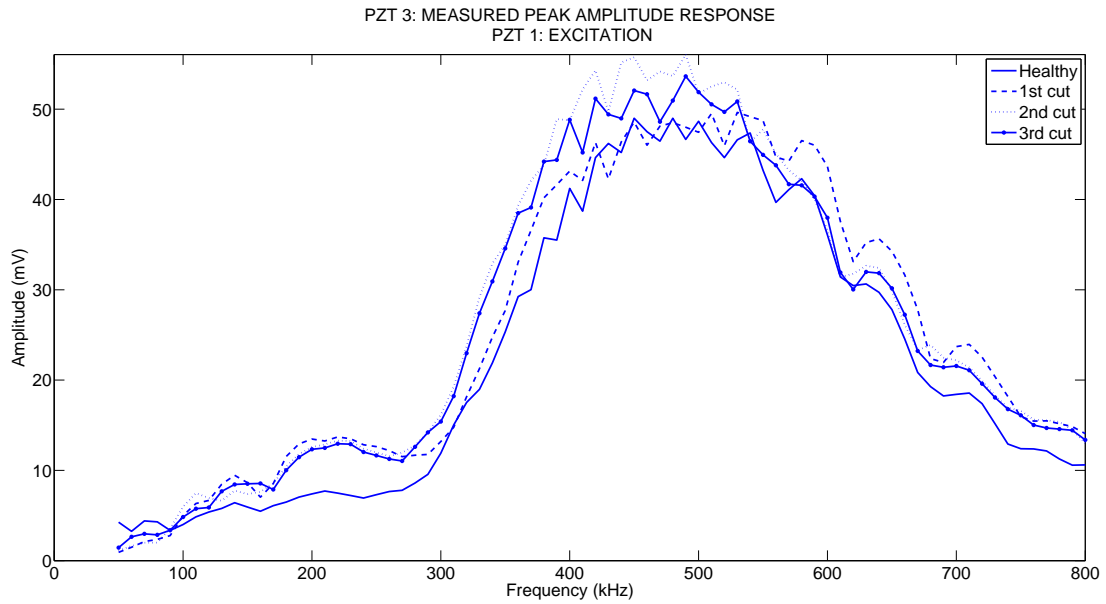
Figure A.2   F-15: peak amplitude comparison of piezo 3 response from piezo 1 excitation

A-1

Figure A.3   F-15: peak amplitude comparison of piezo 4 response from piezo 1 excitation

Figure A.4   F-15: peak amplitude comparison of piezo 5 response from piezo 1 excitation
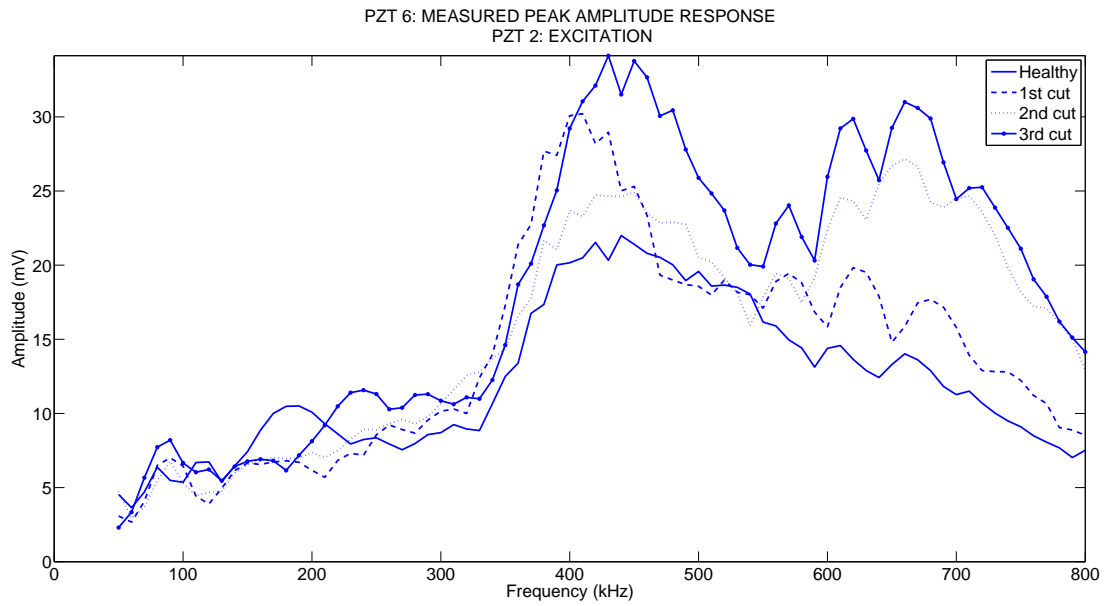
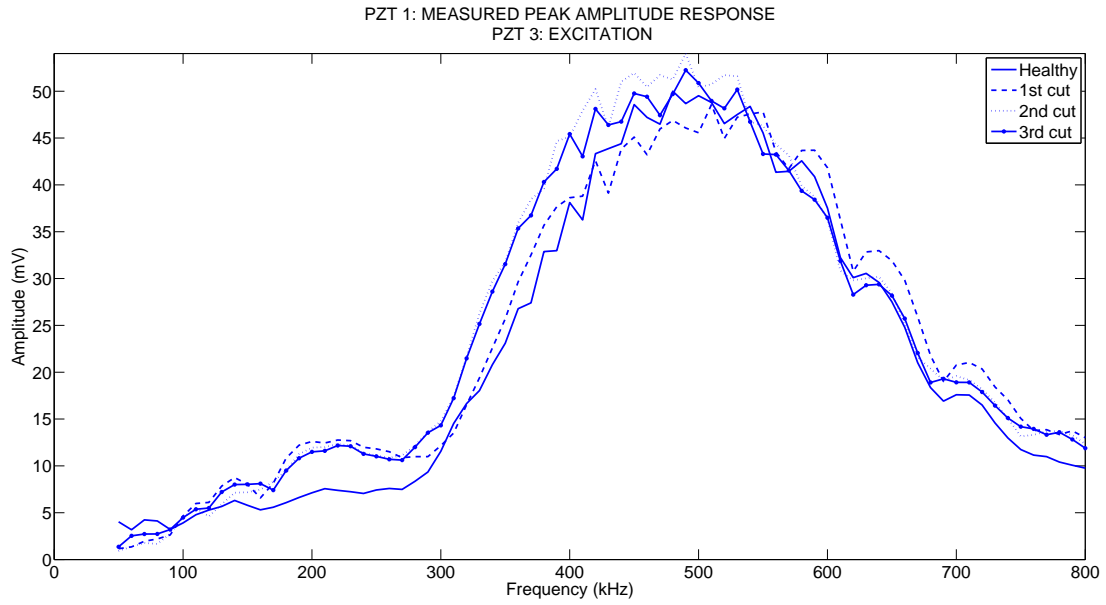Figure A.5   F-15: peak amplitude comparison of piezo 6 response from piezo 1 excitation

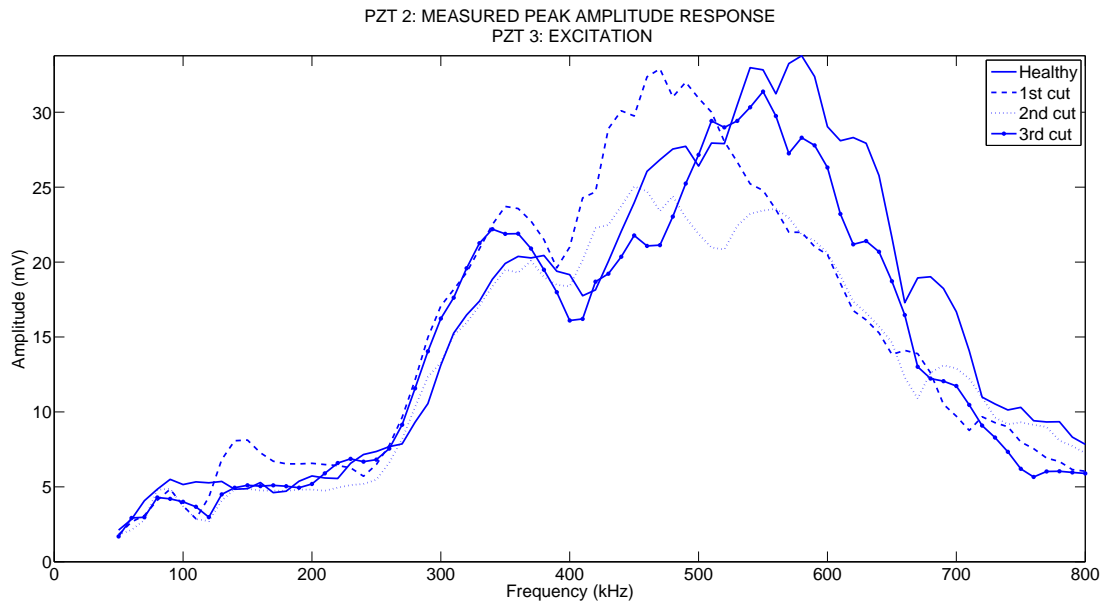Figure A.6   F-15: peak amplitude comparison of piezo 1 response from piezo 2 excitation

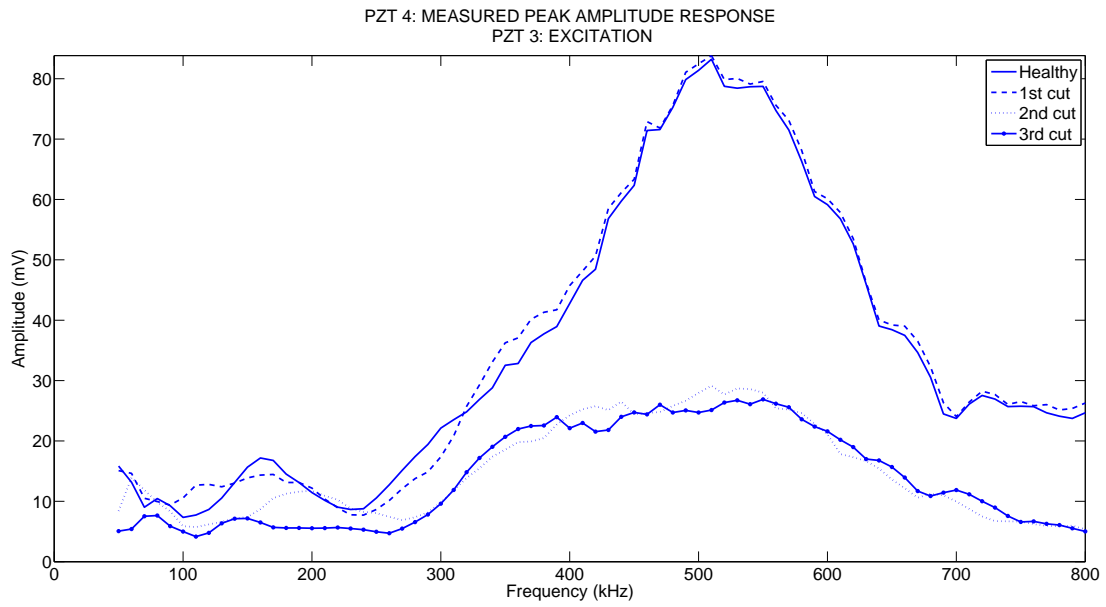Figure A.7   F-15: peak amplitude comparison of piezo 3 response from piezo 2 excitation

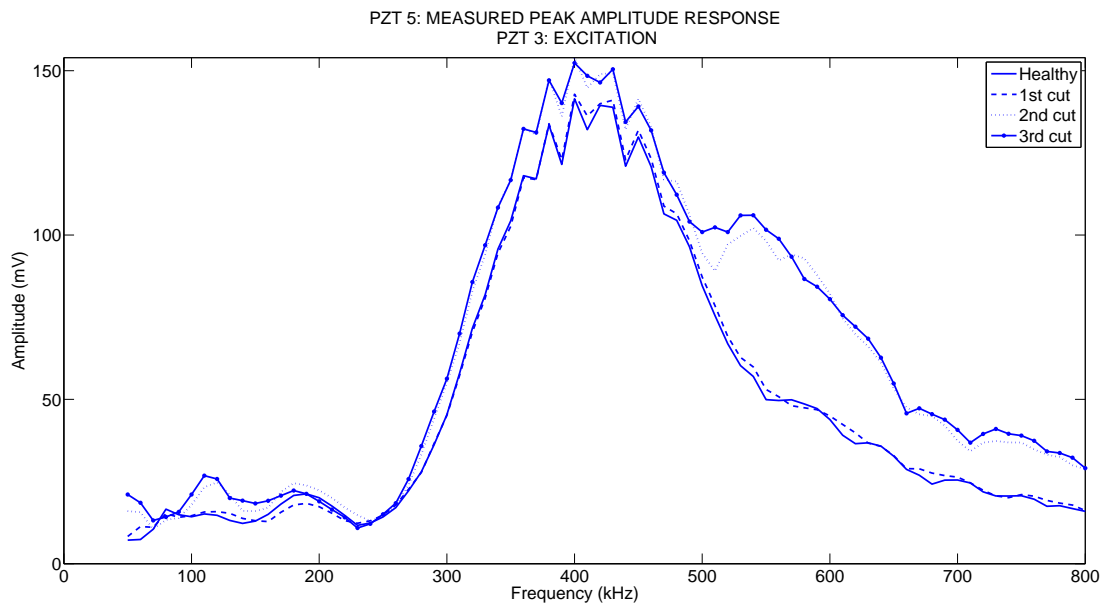Figure A.8   F-15: peak amplitude comparison of piezo 4 response from piezo 2 excitation

PZT 5: MEASURED PEAK AMPLITUDE RESPONSE
PZT 2: EXCITATION

Figure A.9   F-15: peak amplitude comparison of piezo 5 response from piezo 2 excitation

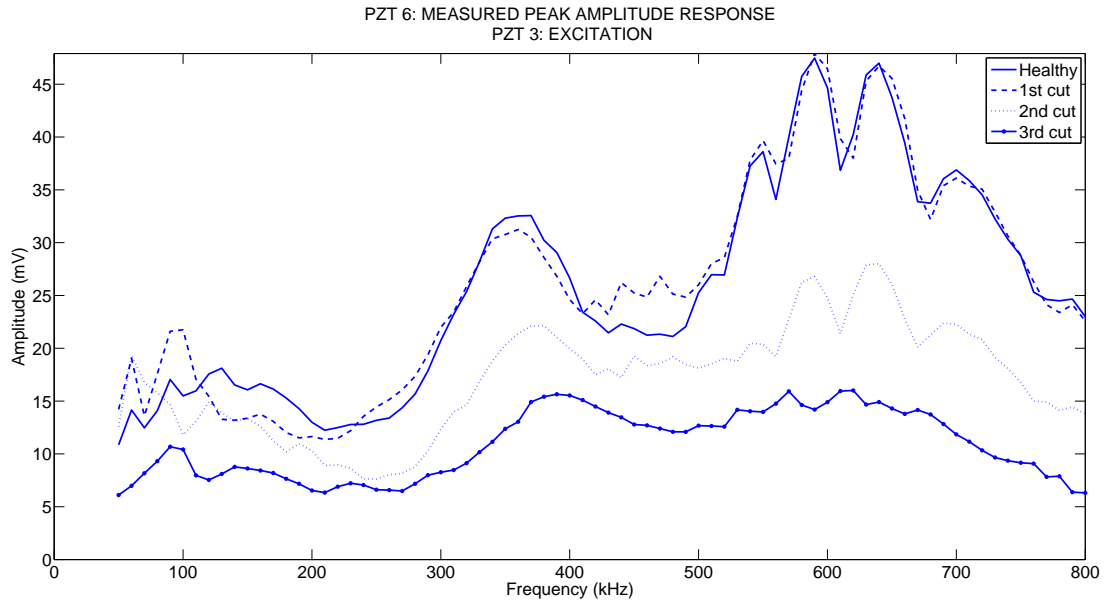PZT 6: MEASURED PEAK AMPLITUDE RESPONSE
PZT 2: EXCITATION

Figure A.10   F-15: peak amplitude comparison of piezo 6 response from piezo 2 excitation
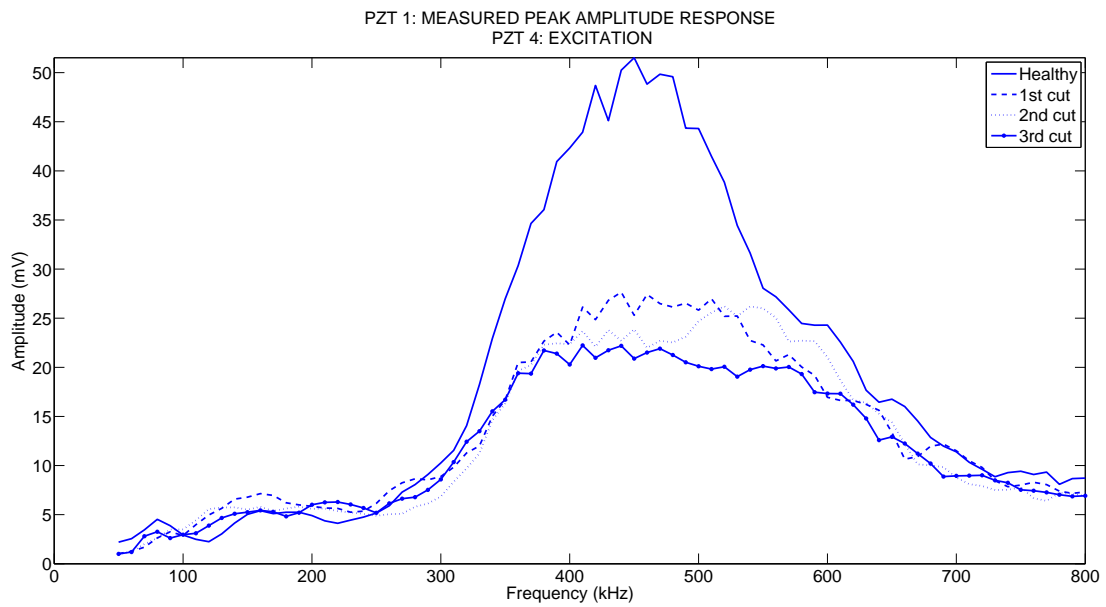
Figure A.11   F-15: peak amplitude comparison of piezo 1 response from piezo 3 excitation
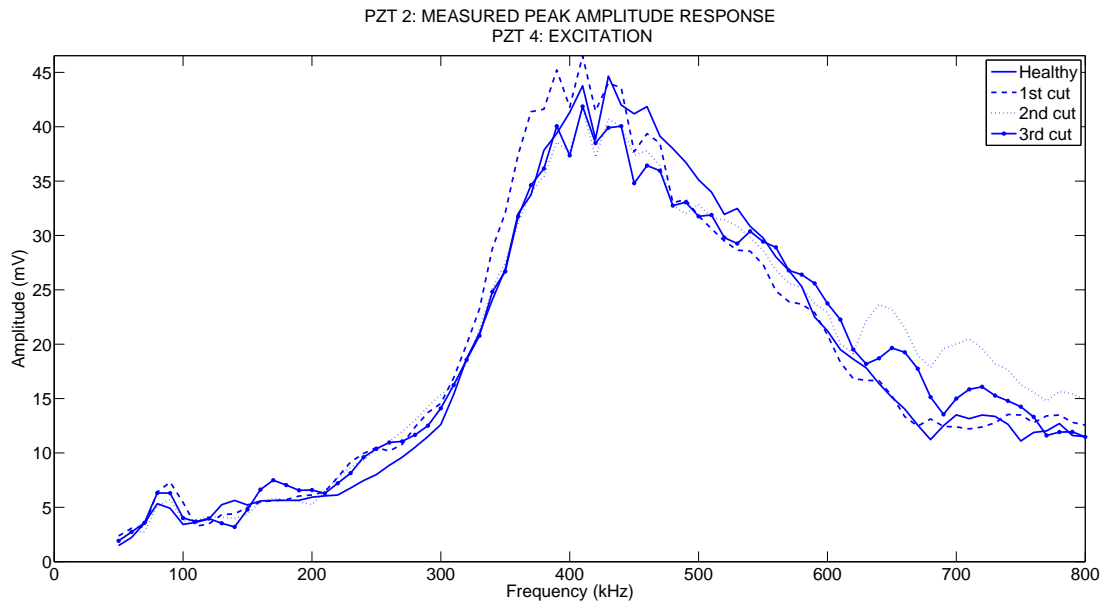

Figure A.12   F-15: peak amplitude comparison of piezo 2 response from piezo 3 excitation

PZT 4: MEASURED PEAK AMPLITUDE RESPONSE
PZT 3: EXCITATION

Figure A.13   F-15: peak amplitude comparison of piezo 4 response from piezo 3 excitation

PZT 5: MEASURED PEAK AMPLITUDE RESPONSE
PZT 3: EXCITATION

Figure A.14   F-15: peak amplitude comparison of piezo 5 response from piezo 3 excitation

A-7

Figure A.15   F-15: peak amplitude comparison of piezo 6 response from piezo 3
excitation

Figure A.16   F-15: peak amplitude comparison of piezo 1 response from piezo 4
excitation

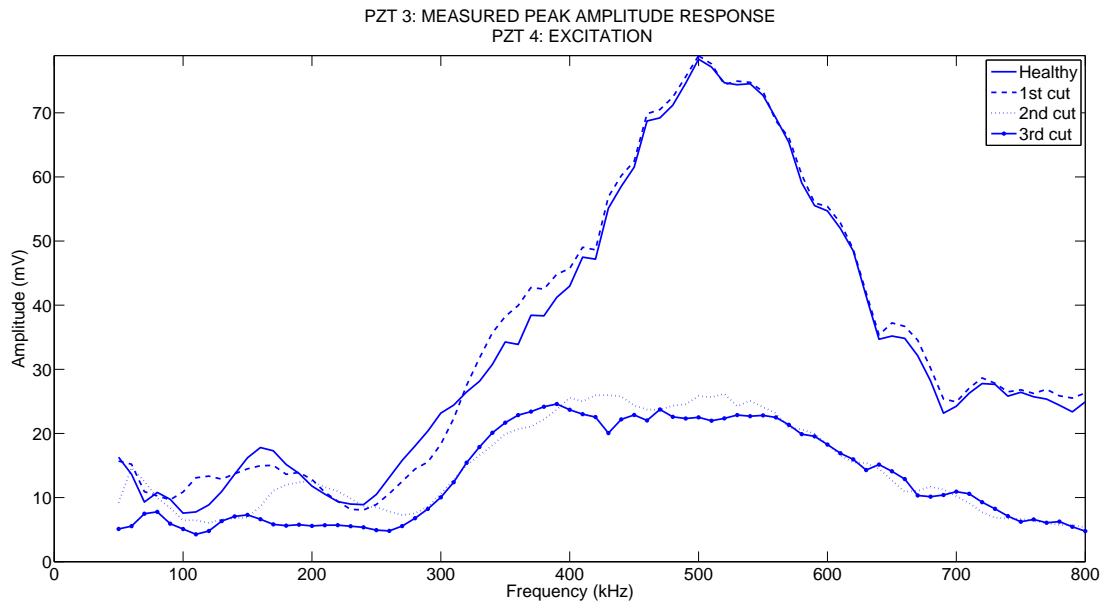Figure A.17   F-15: peak amplitude comparison of piezo 2 response from piezo 4 excitation

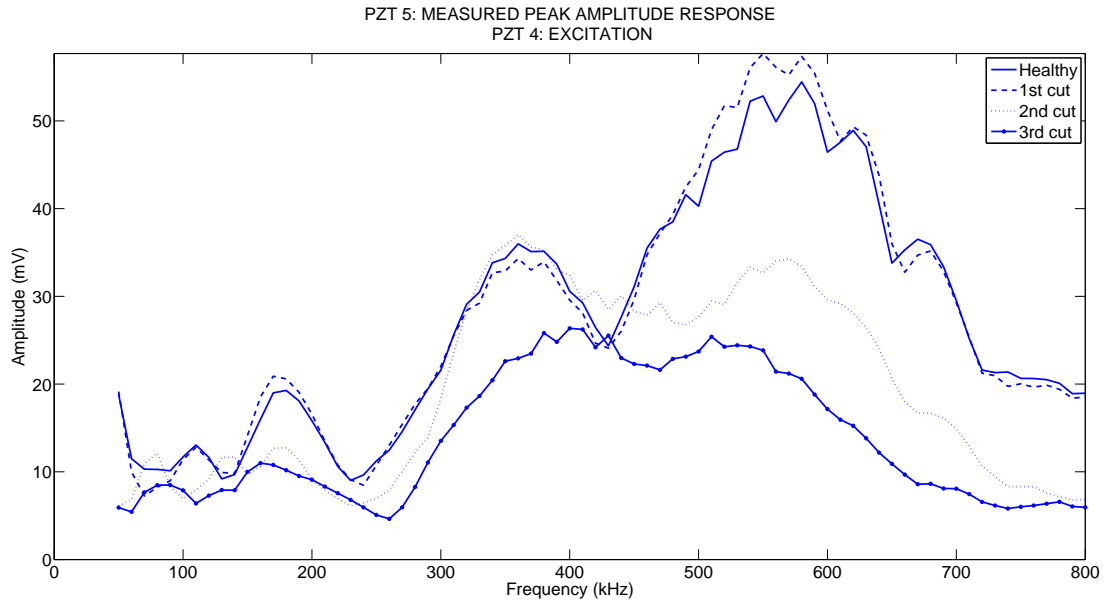Figure A.18   F-15: peak amplitude comparison of piezo 3 response from piezo 4 excitation

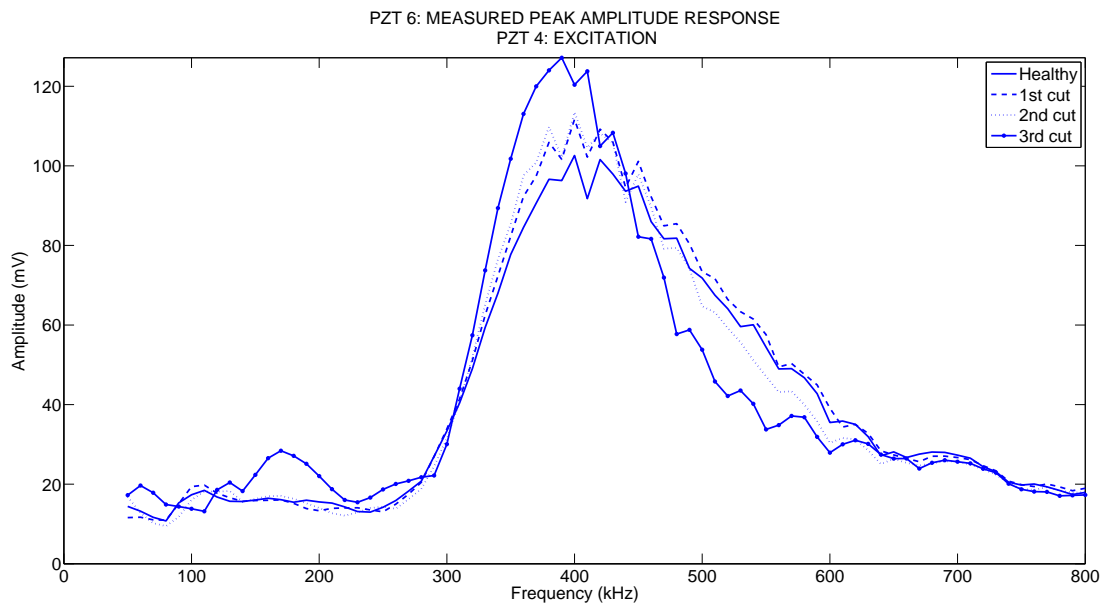Figure A.19   F-15: peak amplitude comparison of piezo 5 response from piezo 4 excitation

Figure A.20   F-15: peak amplitude comparison of piezo 6 response from piezo 4 excitation
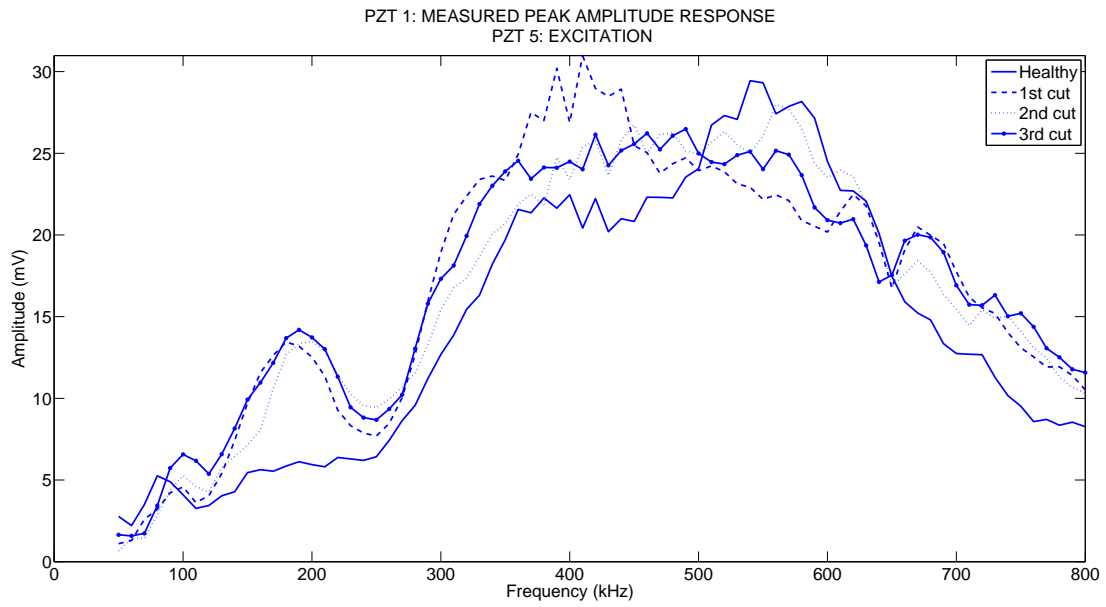
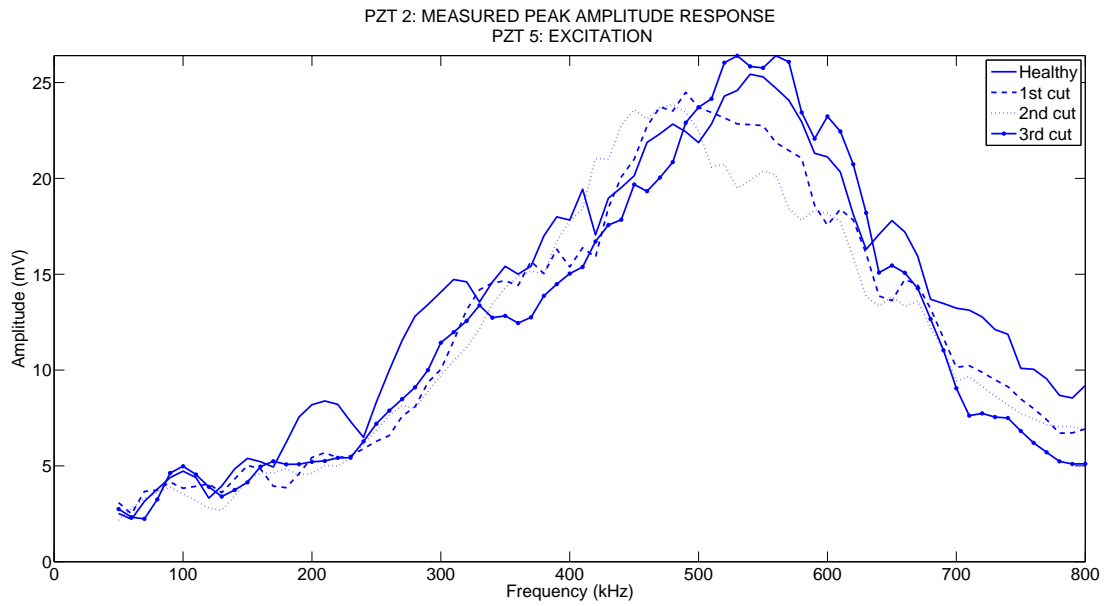Figure A.21   F-15: peak amplitude comparison of piezo 1 response from piezo 5 excitation

Figure A.22   F-15: peak amplitude comparison of piezo 2 response from piezo 5 excitation
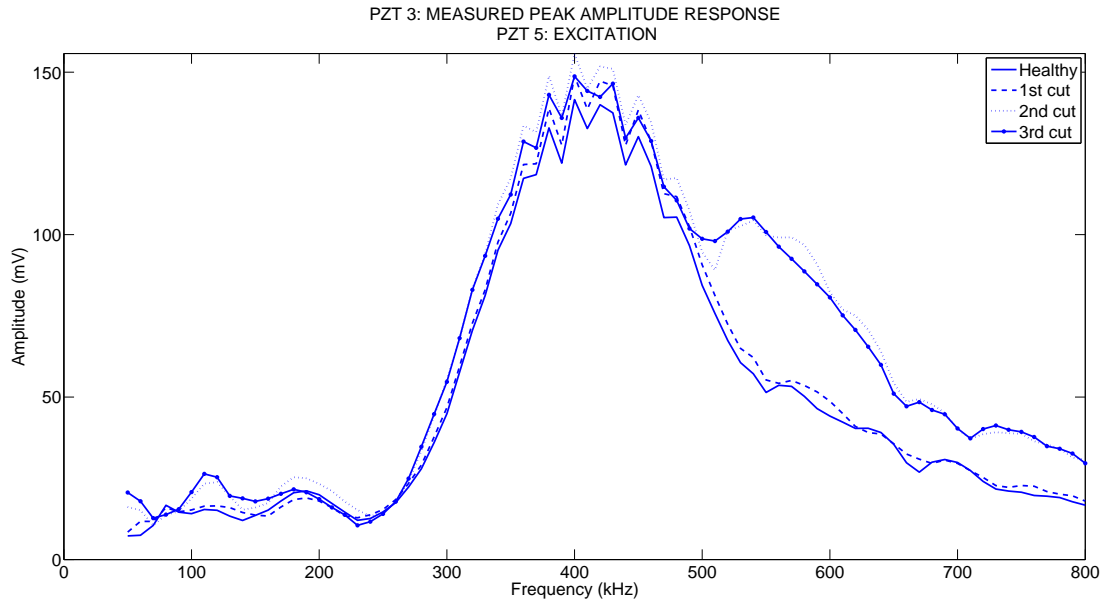
Figure A.23   F-15: peak amplitude comparison of piezo 3 response from piezo 5 excitation

Figure A.24   F-15: peak amplitude comparison of piezo 4 response from piezo 5 excitation

Figure A.25   F-15: peak amplitude comparison of piezo 6 response from piezo 5 excitation
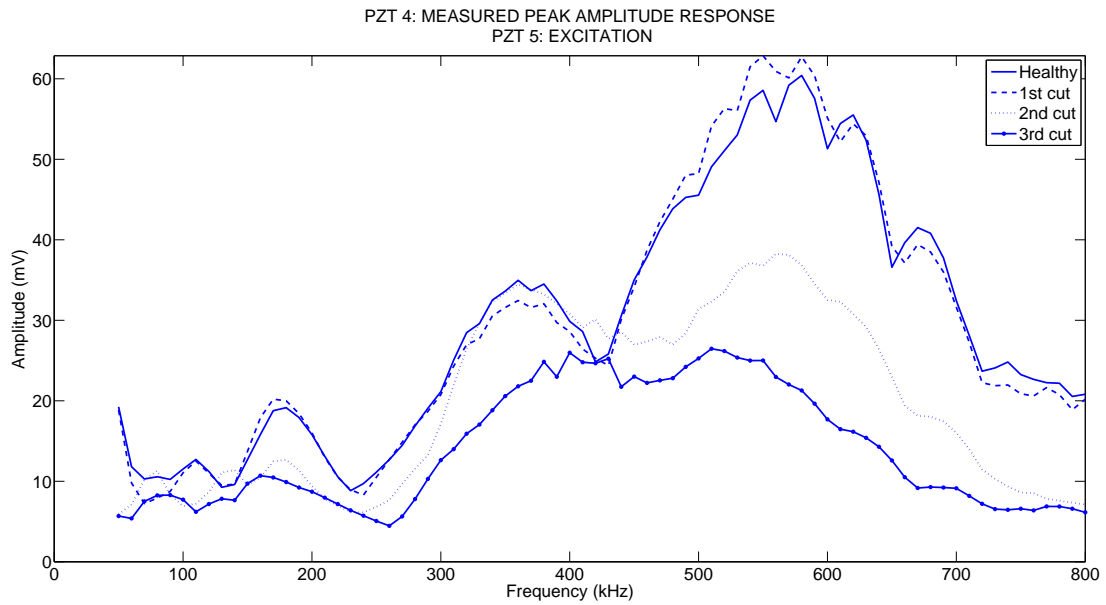

Figure A.26   F-15: peak amplitude comparison of piezo 1 response from piezo 6 excitation
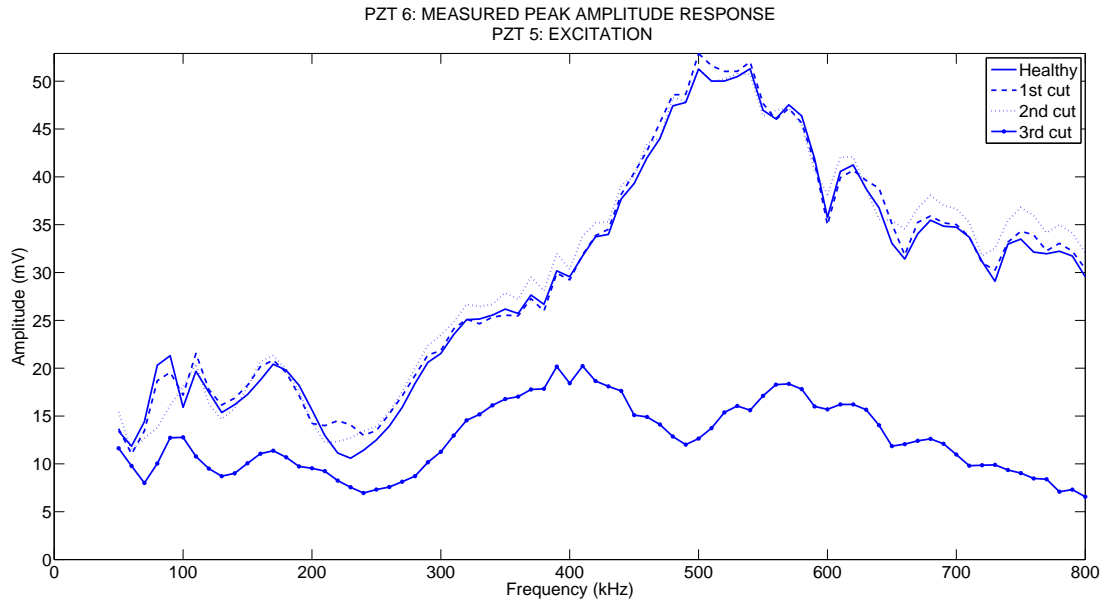
Figure A.27   F-15: peak amplitude comparison of piezo 2 response from piezo 6 excitation

Figure A.28   F-15: peak amplitude comparison of piezo 3 response from piezo 6 excitation
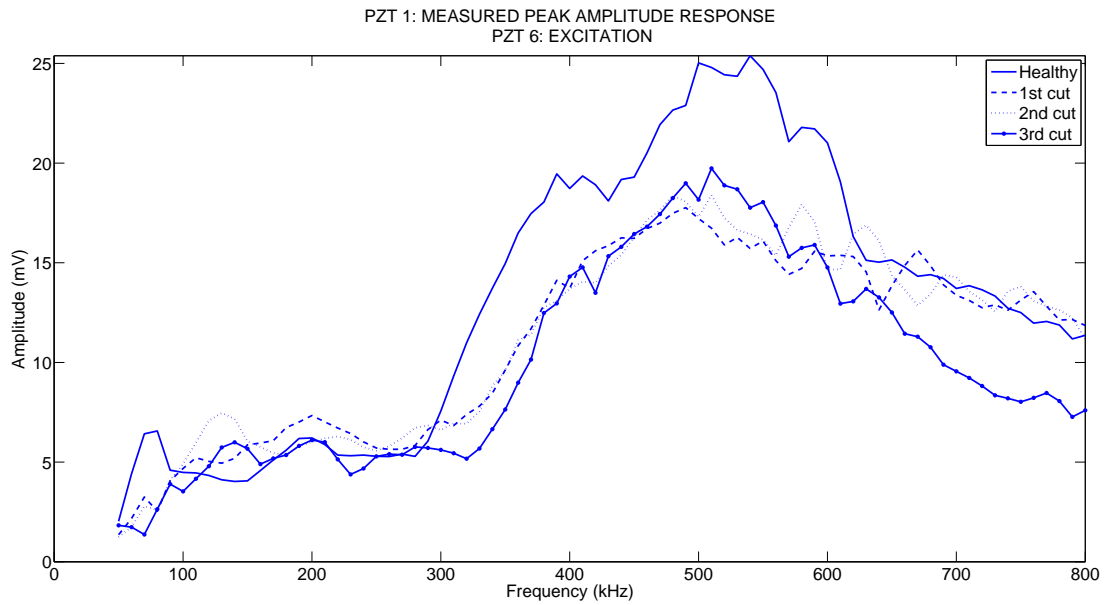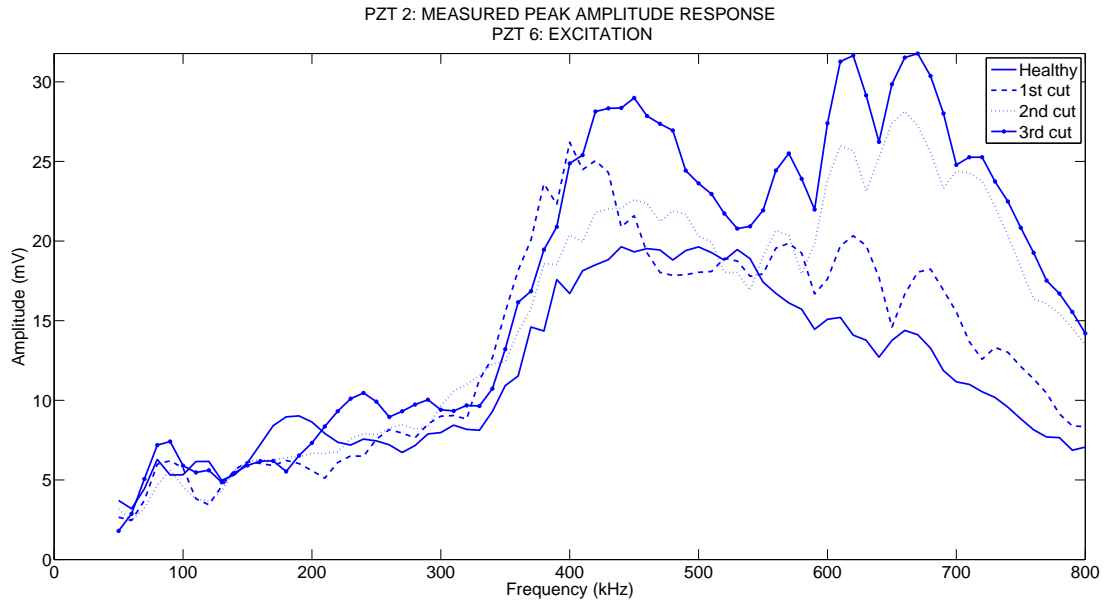
A-14

Figure A.29   F-15: peak amplitude comparison of piezo 4 response from piezo 6 excitation

Figure A.30   F-15: peak amplitude comparison of piezo 5 response from piezo 6 excitation
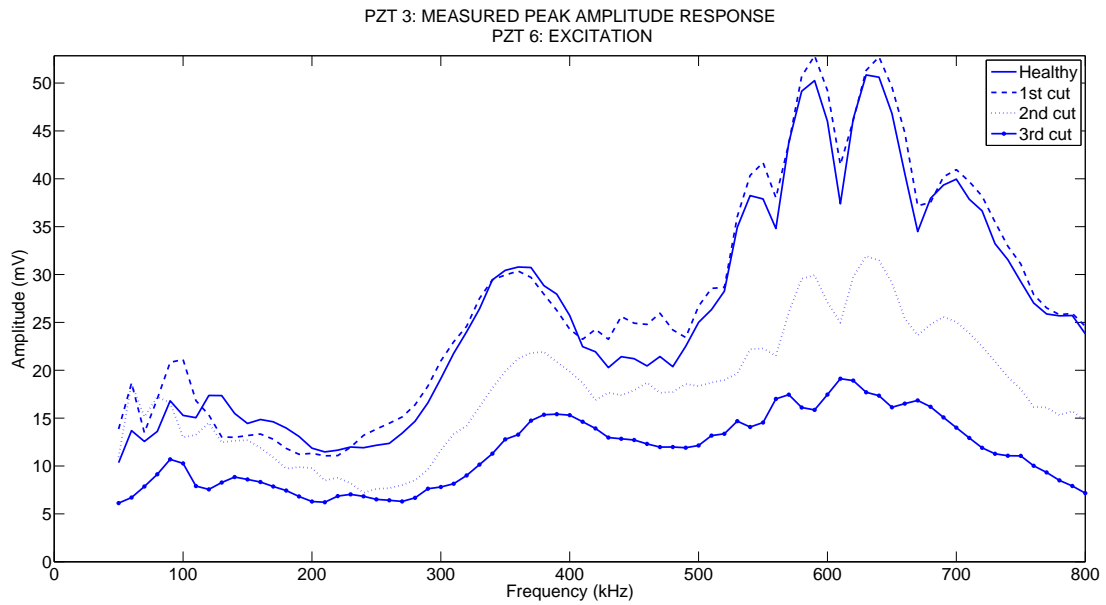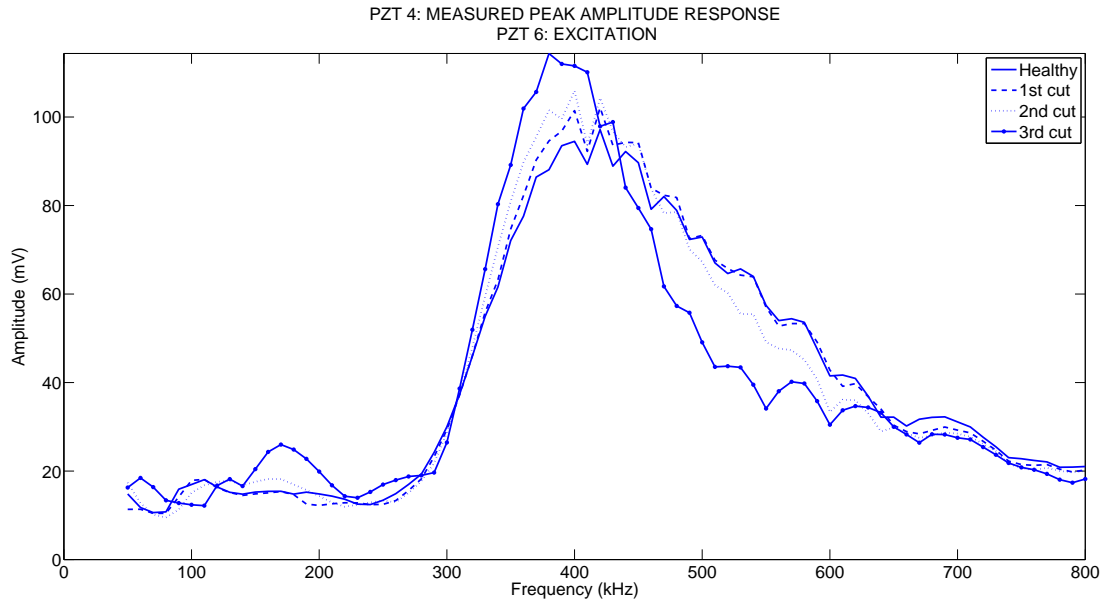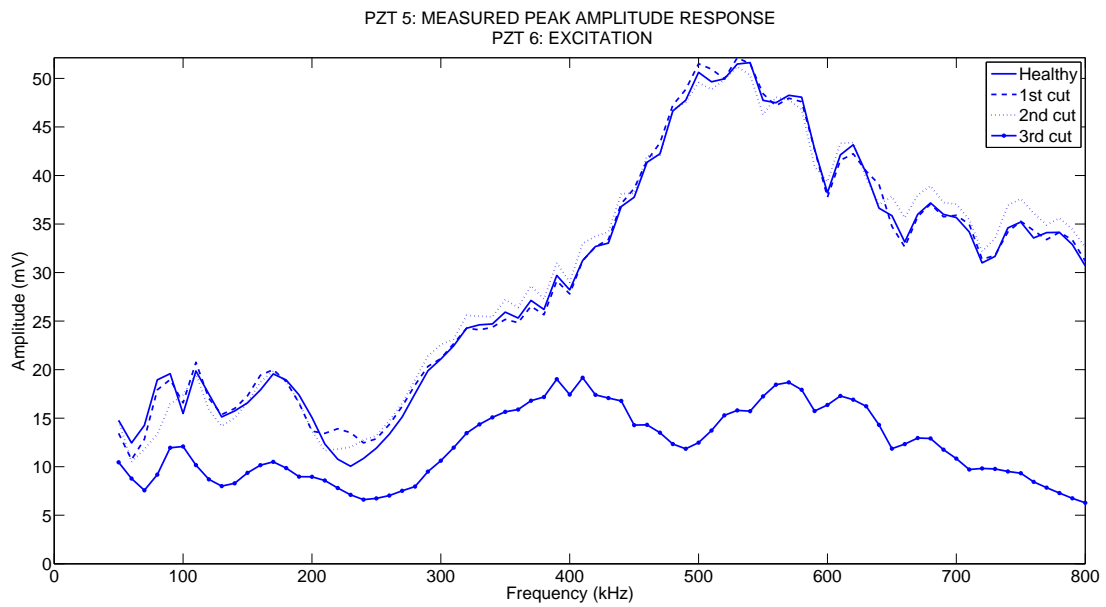
Bibliography

1. APC International Ltd. "Physical and Piezoelectirc Properties of APCI Materials." APC International Ltd. Website, http://www.americanpiezo.com, Accessed: 5 January 2006.

2. Chambers J.T., Wardle B.L. and S.S. Kessler. "Durability Assessment of Lamb Wave-Based Structural Health Monitoring Nodes." Proceedings of the 47th AIAA/ASME/ASCE/AHS/ASC Structures, Structural Dynamics, and Materials Conference. 1–12. May 2006.

3. Drury, John. "Back to Basics - Ultrasonics," *INSIGHT Magazine*, (Chapter 1) (November 2004).

4. Giurgiutiu, Victor. "Tuned Lamb Wave Excitation and Detection with Piezoelectric Wafer Active Sensors for Structural Health Monitoring," *Journal of Intelligent Material Systems and Structures*, 16: 291–305 (April 2005).

5. Giurgiutiu, Victor and Bao, Jingjing. "Embedded Ultrasonic Structural Radar for the Nondestructive Evaluation of Thin-Wall Structures," *Proceedings of the 2002 ASME International Mechanical Engineering Congress*, (IMECE2002-39017) (17-22 November 2002).

6. Kessler, Seth S. *Piezoelectric-Based In-Situ Damage Detection of Composite Materials for Structural Health Monitoring Systems*. Ph.D. thesis, Massachusetts Institute of Technology, January 2002.

7. Kessler, Seth S. "Metis Design Corporation SHM Capabilities." *Aging Aircraft Technical Interchange Meeting*. 20. 18 October 2005.

8. Kessler, Seth S. and Shim, Dong J. "Validation of a Lamb Wave-Based Structural Health Monitoring System for Aircraft Applications." Proceedings of the SPIE's 12th International Symposium on Smart Structures and Materials. 7-10 March 2005.

9. Lamb, Horace. "On Waves in an Elastic Plate," *Proceedings of the Royal Society of London. Series A, Containing Papers of a Mathematical and Physical Character*, *93*(648):114–128 (1 March 1917).

10. Mal, Ajit. "Structural Health Monitoring," *Mechanics*, *33*(11-12):6–28 (November-December 2004).

11. Olson, Steven E., DeSimio, Martin P., and Derriso, Mark M. "Analytical Modeling of Lamb Waves for Structural Health Monitoring." Structural Health Monitoring 2006: Proceedings of the Third European Workshop, edited by A. Guemes. Lancaster, PA: DEStech Publications, Inc., 5-7 July 2006.

12. Olson, Steven E., DeSimio, Martin P., and Derriso, Mark M. "Piezo Generated Lamb Waves for Structural Health Monitoring." Draft, 26 October 2006.

13. Rees, William G. *Physical Principles of Remote Sensing* (2nd Edition). New York: Cambridge University Press, 2001.

14. Rose, Joseph. L. *Ultrasonic Waves in Solid Media*. Cambridge, MA: Cambridge University Press, 1999.

15. Vishay. "M-Bond AE-10." http://www.vishay.com, Document Number 11011, 12 January 2005.

Vita

Captain J. Steve Crider was born in North Carolina and graduated from Anson Senior High School in 1995. He entered undergraduate studies at North Carolina State University in Raleigh, North Carolina where he graduated with a Bachelor of Science degree in Aerospace Engineering in December 2001. He was subsequently commissioned through AFROTC, Detachment 595.

1. REPORT DATE *(DD–MM–YYYY)*	2. REPORT TYPE	3. DATES COVERED *(From — To)*
22–03–2007	Master's Thesis	Sep 2005 – Mar 2007

4. TITLE AND SUBTITLE

Damage Detection Using Lamb Waves for Structural Health Monitoring

5a. CONTRACT NUMBER

5b. GRANT NUMBER

5c. PROGRAM ELEMENT NUMBER

6. AUTHOR(S)

Crider, Jeffrey S., Captain, USAF

5d. PROJECT NUMBER

5e. TASK NUMBER

5f. WORK UNIT NUMBER

7. PERFORMING ORGANIZATION NAME(S) AND ADDRESS(ES)

Air Force Institute of Technology
Graduate School of Engineering and Management
2950 Hobson Way
WPAFB OH 45433-7765

8. PERFORMING ORGANIZATION REPORT NUMBER

AFIT/GA/ENY/07-M05

9. SPONSORING / MONITORING AGENCY NAME(S) AND ADDRESS(ES)

AFRL/VASA
Attn: Mr. Mark Derisso
2790 D Street
WPAFP OH 45433
DSN: 785-8534

10. SPONSOR/MONITOR'S ACRONYM(S)

11. SPONSOR/MONITOR'S REPORT NUMBER(S)

12. DISTRIBUTION / AVAILABILITY STATEMENT

APPROVAL FOR PUBLIC RELEASE; DISTRIBUTION IS UNLIMITED.

13. SUPPLEMENTARY NOTES

14. ABSTRACT

Nondestructive structural health monitoring (SHM) is an evolving technology being developed for monitoring air and space systems. The information gathered on a system's structural integrity through SHM detection methods may result in reduced costly maintenance inspections, enhanced safety, and system failure predictions. This study evaluates Lamb wave approaches used to detect simulated cracks in laboratory experiments on thin plates to detect more realistic damage in a test article representing the complex geometry of an existing aircraft bulkhead. We take a "hot-spot" monitoring approach, where we monitor an area of the structure known to fail. In our experiment, we evaluated the use of piezoelectric generated tuned Lamb waves for crack detection. The use of Lamb waves, guided elastic waves in a plate, has shown promise in detecting highly localized damage due to the relatively short wavelengths of the propagating waves. We evaluated both pitch-catch and pulse-echo approaches for Lamb wave excitation and measurement. Crack detection is accomplished by comparing the responses from the damaged test article to the responses of the healthy test article.

15. SUBJECT TERMS

Lamb Waves, Crack Damage Detection, Structural Health Monitoring, Non-Destructive Evaluation, Dispersion Curves, Group Velocity, Tuning Curves, Pitch-Catch, Pulse-Echo

16. SECURITY CLASSIFICATION OF:			17. LIMITATION OF ABSTRACT	18. NUMBER OF PAGES	19a. NAME OF RESPONSIBLE PERSON
a. REPORT	b. ABSTRACT	c. THIS PAGE			Eric D. Swenson, Maj, USAF (ENY)
U	U	U	UU	97	**19b. TELEPHONE NUMBER** *(include area code)* (937) 255–3636, ext 7479

Standard Form 298 (Rev. 8–98)
Prescribed by ANSI Std. Z39.18